

CHAPTER 6

Recent Progress in Spin Glasses

N. Kawashima¹ and H. Rieger²

Department of Physics, Tokyo Metropolitan University,

¹ *Hachioji, Tokyo 192-0397, Japan*

E-mail: nao@phys.metro-u.ac.jp

² *Theoretische Physik, Universität des Saarlandes,*

66041 Saarbrücken, Germany

E-mail: H.Rieger@mx.uni-saarland.de

We review recent findings on spin glass models. Both the equilibrium properties and the dynamic properties are covered. We focus on progress in theoretical, in particular numerical, studies, while its relationship to real magnetic materials is also mentioned.

The motivation that pulls researchers toward spin glasses is possibly not the potential future use of spin glass materials in “practical” applications. It is rather the expectation that there must be something very fundamental in systems with randomness and frustration. It seems that this expectation has been acquiring a firmer ground as the difficulty of the problem is appreciated more clearly. For example, a close relationship has been established between spin glass problems and a class of optimization problems known to be *NP*-hard. It is now widely accepted that a good (i.e. polynomial) computational algorithm for solving any one of *NP*-hard problems most probably does not exist. Therefore, it is quite natural to expect that the Ising spin glass problem, as one of the problem in the class, would be very hard to solve, which indeed turns out to be the case in a vast number of numerical studies. None the less, it is often the case that only numerical studies can decide whether a certain hypothetical picture applies to a given instance. Consequently, the major part of what we present below is inevitably a de-

scription of the current status of spin glass studies, what is being said and done on the issue, rather than an account of established facts. In what follows, we put an emphasis on the theoretical and the numerical progress achieved in the field in the last decade. We mention older theoretical and experimental works only when it is necessary for readers to be able to follow current topics without reading through many other articles. Many of the important older works and experimental results, therefore, have been left out. For a review on these, the readers are referred to [1], [2], [3], [4], and [5].

The present paper is organized as follows. In section 1, we first give a brief overview of two well-known paradigms on spin glasses and summarize the predictions derived from them. Then, in the subsequent sections 2, 3 and 4, we discuss equilibrium properties of Ising spin glass models. In particular, in section 3, a recent active debate, as to which paradigm is appropriate for realistic short-range spin glass models in three dimensions, is presented. Then, we proceed with the dynamical properties in section 5 to examine these paradigms on a different ground. In this section, an emphasis is put on aging phenomena while some other non-equilibrium properties are also discussed. Models with continuous degrees of freedom as well as the Potts spin glass models are mentioned in section 6. The effects of weak disorder discussed in section 7 provide us with a set of interesting issues quite different from those arising from strong disorder dealt with in the preceding sections. Several exact relations can be found and play an important role in shedding light on the issue under debate. Finally, we see in section 8 what results from the interplay between quantum fluctuations and randomness in spin glasses.

1. Two Pictures

The equilibrium properties of Ising spin-glass models in finite dimensions have been investigated mainly through developments of working hypotheses and numerical techniques. In principle, we can judge which working hypothesis is correct by numerical computations. The working hypotheses are often called “pictures”. Among various pictures, unarguably the most frequently mentioned are the replica-symmetry-breaking (RSB) and the droplet picture. In fact, the dichotomy between these two has been the central issue in the spin glass research for more than a decade. However, it is rather difficult to perform a conclusive numerical test in the three dimensional case. One thing that renders the test so difficult is that the lower critical

dimension appears to be close to three. Another factor is, as mentioned in the introduction, that there is no polynomial algorithm for obtaining the ground state of a given instance in three (and higher) dimension. Therefore, the best we can do at present is to summarize on-going arguments, discriminating what has been established from what has not, and presenting the most important numerical evidences. We try to do these in what follows.

It should also be pointed out that most of the “pictures” are asymptotic theories which are supposed to be correct only for large systems. In contrast to most regular systems the utility of an asymptotic theory for glassy systems cannot be taken for granted. It was pointed out⁶ that in most real spin glass materials the typical length scale of an equilibrated domain within the experimental time scale may not exceed a small number of lattice spacings. If this is the case, considering the numerical evidence of the existence of large corrections to scaling, it can happen that the asymptotically correct theory fails to explain experimental results. The fact that many experiments on spin glasses, those at temperatures below the transition in particular, are not performed in equilibrium implies that an equilibrium theory may not be appropriate. Some attempts to construct a theory for a realistic time and length scales are reviewed in section 5.

1.1. Mean-Field Picture

We start with a brief description of the two pictures mentioned above in the present and the next subsection. We do not, however, intend to repeat the whole history of the development of each picture or discuss every technical detail. The reader may find a complete description of these pictures in a number of review articles.^{1,2,7,8,9,10}

The RSB picture or the mean-field picture is based on Parisi’s solution^{11,12,13,14} of the Sherrington-Kirkpatrick (SK) model¹⁵ and its interpretation in terms of a multitude of thermodynamic states [16,17]. The SK model of N Ising spins, S_i , is defined by the Hamiltonian

$$H = - \sum_{(i,j)} J_{ij} S_i S_j$$

where the summation is taken over all $N(N-1)/2$ pairs of spins (i, j) with $i \neq j$. The coupling constants J_{ij} are quenched Gaussian random variables with zero mean and variance J/N where J is a positive constant of $\mathcal{O}(1)$ that sets the energy scale. In [15], the replica method was used in which n identical copies (replicas) of the system are introduced to perform the disorder average of the free energy: $-\beta F = [\ln Z]_{\text{av}} = \lim_{n \rightarrow 0} ([Z^n]_{\text{av}} - 1)/n$.

They found a solution of the mean-field equations using a replica symmetric Ansatz (see below). This solution has a phase transition and the transition point is located at the temperature $T_c = J$. Below this temperature, the order parameter

$$q_{\text{EA}} = q^{\alpha\beta} \equiv \frac{1}{N} \sum_i S_i^\alpha S_i^\beta \quad (1)$$

has a non-zero value where indices α and β specify replicas. The replica symmetric Ansatz means that only solutions to the mean-field equations with $q^{\alpha\beta}$ being independent of α and β (before taking the limit $n \rightarrow 0$) are allowed. However, this solution did not describe the low temperature phase correctly since the entropy predicted by this solution became negative at low temperatures.

In [18] a different approach was taken for the SK model. They constructed a set of equations (called the TAP equations) that expresses the equation of state for each bond-realization of the SK model in terms of the local magnetization, $m_i = \langle S_i \rangle$. They studied the eigen-modes of the stability matrix of stable solutions of the TAP equations and found that the spectrum of the eigen-values extends down to zero, suggesting that the solutions are only marginally stable in the thermodynamic limit. Furthermore, the stability matrix in the replica space, i.e., the second derivatives of the free energy with respect to the replica order parameters, $q^{\alpha\beta}$, was examined.¹⁹ It turned out that the replica symmetric solution is stable only in the paramagnetic phase and becomes unstable below the phase boundary called the AT line in the T - H plane. Therefore, the SK solution is correct above the AT line whereas it is not below the AT line.

To find the correct solution of the SK model below the AT line the replica symmetry had to be broken. The way the symmetry is to be broken is, however, highly non-trivial. A solution, called the Parisi solution, was proposed^{11,12,13,14} based on a novel metric structure of the replica-index space. It has now been proved with acceptable mathematical rigor that the solution is exact.²⁰ In the Parisi solution, a metric structure is introduced in the replica-index space and it is assumed that the overlap q between two replicas depends only on the distance between the two in this index space. As a result, the order parameter is actually not a single number, in contrast to the EA order parameter q_{EA} , but a function $q(x)$ ($0 \leq x \leq 1$), where x is a suitable parameterization of the distance between two replica indices. A remarkable feature of Parisi's solution below the AT line was that $q(x)$ varies continuously as a function of x .

The order-parameter function $q(x)$ first appeared to be a mathematical artifact, but its physical meaning was later clarified¹⁴ by relating $q(x)$ to the probability distribution $P(q)$ of the overlap q between *pure states*, rather than the replicas. A pure state is defined as an extremal equilibrium distribution in the thermodynamic limit that cannot be expressed as a linear combination of any other distributions. Denoting the inverse function of $q(x)$ as $x(q)$, it was found that

$$x(q) = \int_{-\infty}^q dq' P(q'). \quad (2)$$

Here, the overlap distribution $P(q)$ is formally (and somewhat symbolically) defined as

$$P(q) = \sum_{\alpha, \beta} P_{\alpha} P_{\beta} \delta(q - q^{\alpha\beta}). \quad (3)$$

Here the indices α and β specify pure states, not replicas, $q_{\alpha\beta}$ is the overlap between the two pure states α and β , and P_{α} is the probability for the system to be in the pure state α .

Equation (2) may provide a way to investigate the structure of the space of the equilibrium distributions with the replica method. We can conclude, for instance, that more than one pure state exists and the overlap between two pure states varies depending on the particular pair of states if $q(x)$ is not constant. If $q(x)$ changes continuously in a finite range of x , as in Parisi's solution for the SK model, there must even be an infinite number of pure states. Simply stated, the RSB picture for systems in finite dimensions with short range interactions consists of the hypothesis that there are infinitely many pure states with varying overlaps and various predictions derived from the hypothesis.

The definition (3) of $P(q)$, however, must be taken with caution since the existence of pure states as a well-defined thermodynamic limit is not clear for disordered systems. In fact, it was shown^{16,17} that $P_J(q)$ for a bond realization J depends on J even in the thermodynamic limit. As discussed below, this means²¹ that a unique thermodynamic limit of $P_J(q)$ with fixed bond realization J does not exist. Therefore, the order parameter, $q(x)$, is not self-averaging for the SK model, in striking contrast to homogeneous systems.

Because of this subtle nature of the order parameter, the exact implication of the RSB picture for more realistic spin glass models in finite dimensions is somewhat ambiguous and has been a subject of debates.^{9,10} One focus is the interpretation of the numerical result for finite systems. The

definition of q and $P(q)$ often used in numerical simulations is based on the overlap between two spin configurations, S and S' , independently chosen from the equilibrium distribution of the same bond realization. Namely,

$$q(S, S') \equiv \frac{1}{N} \sum_{i=1}^N S_i S'_i, \quad P(q; L) \equiv [P_J(q; L)], \quad (4)$$

$$P_J(q; L) \equiv \sum_S \sum_{S'} P_J(S; L) P_J(S'; L) \delta(q - q(S, S'))$$

where $P_J(S; L)$ is the normalized Boltzmann weight of the spin configuration S in a system of the linear size L with the bond configuration J . Throughout this article, unless stated otherwise, the angular bracket $[\dots]$ denotes the bond-configuration average with the distribution $P(J) = \prod_{(ij)} P_1(J_{ij})$, where the single-bond distribution P_1 is independent of (ij) . The following link-overlap and its distribution are also often discussed recently:

$$q_l(S, S') \equiv \frac{1}{N_l} \sum_{(ij)} S_i S_j S'_i S'_j, \quad P(q_l; L) \equiv [P_J(q_l; L)], \quad (5)$$

$$P_J(q_l; L) \equiv \sum_S \sum_{S'} P_J(S; L) P_J(S'; L) \delta(q_l - q_l(S, S')) ,$$

where the summation concerning (ij) is over all the pairs of nearest neighbor spins, and N_l is the total number of the pairs in the system.

The following is the list of features that follows from the RSB picture.

- (1) The overlap distribution, $P(q; L)$, converges to a function $P(q)$ that has a continuous part in the limit of $L \rightarrow \infty$. In particular, $P(0; L)$ converges to a finite value $P(0) > 0$.
- (2) Some quantities, such as $P_J(q; L)$, are non-self-averaging, i.e., a unique thermodynamic limit does not exist for a fixed bond realization.
- (3) The bond-averaged link-overlap distribution $P(q_l; L)$ is not $\delta(q_l)$ in the thermodynamic limit, i.e., its width converges to a finite value.
- (4) Global excitations with the energy cost of $\mathcal{O}(1)$ exist.
- (5) A change in the boundary conditions generally affects spins located far away from the boundary.

1.2. Droplet Picture

Another well-known picture^{22,23,24,25,26} is based on a scaling hypothesis on local excitations and produces markedly different conclusion for various

quantities, in particular, $P(q)$. The basic assumption in this picture is that even below the transition temperature in zero magnetic field there are only two pure states that are mapped to each other by the total inversion of spins as in the homogeneous ferromagnets. Then, several scaling properties are assumed for compact excitations with varying size, which are called *droplets*. To be specific, a droplet of the scale l has a typical excitation free energy $\epsilon_l \sim \Upsilon l^\theta$, where θ is called the droplet exponent. Since this exponent relates the energy scale to the length, similar to the stiffness exponent θ_S that relates the domain wall excitation energy to the system size, the simplest assumption is to identify θ with the stiffness exponent θ_S .

Among various results derived from this picture, of particular importance are the scaling forms of the correlation functions.^{24,23} For example, it is predicted for models with a continuous bond distribution and with no magnetic field that the following asymptotic form should apply:

$$[\langle S_i S_j \rangle^2] - [\langle S_i \rangle^2][\langle S_j \rangle^2] \sim T/\Upsilon R^\theta \quad (6)$$

near zero temperature, where R is the distance between site i and site j and the thermal average $\langle \dots \rangle$ is taken in a single pure state (if there are two). It follows that the variance of the distribution function $P(q; L)$ defined in (4) (more strictly, the variance of $P(|q|; L)$) decreases as the system size increases:

$$(\Delta q)^2 \equiv [\langle q^2 \rangle] - [\langle |q| \rangle]^2 \propto L^{-\theta} \rightarrow 0.$$

Therefore, when $P(q)$ is defined as the thermodynamic limit of $P(q; L)$, it consists of a pair of delta peaks at $q = \pm q_{EA}$.

For the models with discrete energy levels, such as the $\pm J$ model, the scaling form of the correlation function near $T = 0$ must be modified. However, it is widely believed that the discretized nature of the energy level is not relevant at finite temperatures and the behavior is qualitatively the same as the one of the models with continuous energy levels.

Below, we list the defining properties of the droplet picture together with some predictions derived from it.

- (1) The distribution of the excitation free energy of droplets of the scale l , $P(\epsilon_l)$, is continuous down to zero energy.
- (2) $P(\epsilon_l)$ has the typical energy scale Υl^θ with Υ being an $\mathcal{O}(1)$ constant. Specifically, $P(\epsilon_l)$ has the scaling form

$$P(\epsilon_l) \sim \frac{1}{\Upsilon l^\theta} \tilde{P}\left(\frac{\epsilon_l}{\Upsilon l^\theta}\right).$$

- (3) $P(q)$ is self-averaging and it consists of a pair of delta peaks below the transition temperature.
- (4) Since $P(0; L)$ is proportional to the excitation probability of a droplet that contains approximately one half of all the spins, for a system with a continuous bond distribution, $P(0; L)$ has the following temperature and size dependence near $T = 0$;

$$P(0; L) \sim [\text{Prob}(\epsilon_L < T)] \sim \frac{T}{\epsilon_L} \propto TL^{-\theta}. \quad (7)$$

- (5) For systems with a continuous bond distribution the bond-averaged link-overlap distribution $P(q_l; L)$ consists of a single delta function in the thermodynamic limit. At low temperature, its width depends on the size and the temperature as²⁷

$$(\Delta q_l)^2 \propto TL^{-\mu} \quad (\mu_l \equiv 2d_S - 2d - \theta) \quad (8)$$

where d_S is the fractal dimension of the surface of droplets.

- (6) For systems with finite temperature spin glass transition, θ is positive. Therefore, a global excitation costs an infinite energy.
- (7) A change in the boundary conditions does not affect spins located far away from the boundary, except for a potential simultaneous inversion of all spins.

2. Equilibrium Properties of Two-Dimensional Ising Spin Glasses

Two-dimensional spin glass models are easier to study than three-dimensional models from a technical point of view. However, there are still some open questions. Among others, the possibility of the existence of a phase transition at non-zero temperatures in the discrete distribution models is important.

2.1. Zero-Temperature Transition?

One of the arguments that supports the zero-temperature phase transition scenario is based on the numerical estimates of the stiffness exponent that characterizes the size dependence of the domain-wall free-energy. The stiffness is simply the difference in the free energy caused by a particular change in the boundary conditions. The most frequent choice in numerical computations is the application of periodic versus anti-periodic boundary

condition. The stiffness exponent θ_S is then determined by the asymptotic size-dependence of the stiffness, ΔF :

$$\Delta F \propto L^{\theta_S}.$$

According to [23], when the distribution of coupling constants is continuous and has a non-zero weight at $J = 0$, whether a phase transition takes place at a finite temperature or not is determined by the sign of the stiffness exponent. If it is positive, the zero temperature phase is strongly ordered, leading to a finite-temperature phase transition, whereas otherwise the order is fragile and infinitesimal thermal fluctuations would destroy it, leading to criticality at zero temperature. Numerical computations of the ground states of finite systems in two dimensions were carried out^{23,28,29} for estimating the stiffness exponent at $T = 0$. For the Gaussian distribution of the bonds, it turned out that $\theta_S \sim -0.3$. At present, one of the most accurate and reliable estimates of the stiffness exponent is given in [30] as $\theta_S = -0.282(2)$ for the Gaussian bond distribution with periodic/anti-periodic boundary condition. Due to the negative value of the stiffness exponent, it is widely believed that there is no finite temperature transition in this model and that the system is critical at zero-temperature.

The stiffness exponent of $\pm J$ model, on the other hand, is much closer to the marginal value, 0. It was estimated,³¹ with the assumption of the power-law dependence of the stiffness on the system size, as

$$\theta_S = -0.060(4),$$

while the possibility of $\theta_S = 0$ was not ruled out. The possibility of the stiffness exponent being zero was strongly suggested by another ground state computation.³⁰

Recently, it was pointed out that the stiffness exponent have to be interpreted differently for $\pm J$ models. Amoruso *et al.*³² carried out a renormalization calculation using the Migdal-Kadanoff method. They found that the stiffness exponent, calculated within this approximation, is zero in any dimension lower than the lower critical dimension. This finding suggests that the stiffness exponent being zero does not necessarily imply that the system is exactly at the lower critical dimension. This type of dimensional dependence of the stiffness exponent was observed only for the class of the bond distribution for which the discretized nature of the coupling constant is not smeared out by the renormalization. Since the $\pm J$ bond distribution falls into this class, the above-mentioned numerical estimates, $\theta_S \sim 0$, may only mean that the lower-critical dimension is two *or above*. For the $\pm J$ model,

however, even the possibility of a finite temperature phase transition was suggested,³³ as we discuss in greater detail further below.

2.2. Droplet Argument for Gaussian-Coupling Models

For two dimensional systems with a symmetric ($P(J) = P(-J)$) and continuous bond distribution, it was argued²³ that there is only one independent critical exponent. In other words, all critical indices are related to the stiffness exponent via scaling laws. We consider the following finite size scaling form of the singular part of the free energy F_s ,

$$\Phi(T, H, L) \equiv \beta F_s = -[\log Z] \sim \phi(TL^y, HL^{y_h}).$$

The condition that the total magnetization $[M] \equiv \lim_{H \rightarrow 0} \partial F_s / \partial H$ is proportional to $L^{d/2}$ at $T = 0$ relates y to y_h via

$$y_h = y + \frac{d}{2}.$$

Then, by differentiating Φ with respect to T and H , we can express any critical index by y . For example, the magnetization per spin depends on the magnetic field as $m = L^{-d} M \sim L^{-\frac{d}{2}} \sim H^{\frac{d}{2y_h}}$, which means that the exponent δ appearing in the scaling of the magnetization with the magnetic field is $\delta = 1 - 2y/d$. The non-linear susceptibility $\chi_2 \equiv L^{-d} \partial^3 M / \partial H^3$ at $H = 0$ depends on the temperature as $\chi_2 \sim T^{-\gamma_2}$ with $\gamma_2 = 3 + \frac{d}{y}$. Since the spin glass susceptibility χ_{SG} at $H = 0$ is related to χ_2 as $\chi_{SG} \equiv L^{-d} \sum_{i,j} [\langle S_i S_j \rangle^2] = T^3 \chi_2$, the corresponding exponent is $\gamma_{SG} = d/y$. Similarly, the specific heat exponent can be expressed as $\alpha = -d/y$. As for the exponent η_{SG} , that characterizes the asymptotic form of the two-point spin glass correlation function $[\langle S_i S_j \rangle^2] \sim R_{ij}^{d-2+\eta_{SG}}$, we have $2 - \eta_{SG} = y\gamma_{SG}$, which yields $\eta_{SG} = 2 - d$. This is consistent with the fact that the correlation function does not decay at zero-temperature.

2.3. Droplets in Gaussian-Coupling Models: Numerics

As mentioned above, one naturally expects²⁴ that the exponent $-y$ is identical to the stiffness exponent θ_S since both the exponents relate the energy scale to the length scale. However, the estimates of various critical exponents^{34,35,36,38,39} based on the system size up to $L \sim 50$ seem to satisfy the scaling relation with $y \sim 0.5$ rather than $y = -\theta_S \sim 0.3$.

In order to check if y coincides with $-\theta$, a direct numerical estimate of the droplet excitation exponent θ was carried out using a heuristic op-

timization procedure^{40,41} applied to the EA model with a Gaussian bond-distribution in two dimensions. For each realization of the model, the ground state spin-configuration was computed with free boundary condition. Then, the spins on the boundary were fixed as they were in the original ground state whereas the spin at the center was fixed in the opposite direction. These constraints lead to a new ground state that is identical to the old one on the boundary but differs from it in the vicinity of the central spin by a droplet of flipped spins around the center. The droplet is typically as large as the system itself. The system-size dependence of the droplet volume V and the droplet excitation energy E could be described well by the scaling law

$$V(L) \propto L^{d_D}, \quad \text{and} \quad E(L) \propto (V(L))^{\theta/d_D}$$

with

$$d_D = 1.80(2), \quad \text{and} \quad -\theta = 0.47(5)$$

for the range of the system size $5 \leq L \leq 49$. In particular, the value of $-\theta$ agreed with most of the previous estimates of y . This can be understood also within the droplet theory because all scaling forms derived by droplet arguments are identical to what one can get via the ordinary finite size scaling by identifying θ and $-y$.

However, a recent computation⁴² demonstrates the presence of a cross-over in the droplet excitation energy. They performed essentially the same calculations as the one described above for larger systems (up to $L = 160$), and argued that there may be a correction term due to the self-interaction of the surface of the droplets and that the droplet excitation energy has the form

$$\Delta E(L) \sim AL^\theta + BL^{-\omega}$$

with $\omega > |\theta_D|$. The numerical data could be well fitted by

$$-\theta_D = 0.29, \quad \text{and} \quad \omega = 0.97(5).$$

as is shown in Fig.1(a). The fact that the estimate of the droplet exponent now becomes close to the stiffness exponent indicates the validity of the simplest scenario. However, the result on the fractal dimension of droplets seems to suggest the contrary; their result appears to confirm the previous result $d_D \sim 1.8$ (Fig.1(b)). While this may be another transient behavior, the problem of compactness of the droplets remains open in the two-dimensional system.

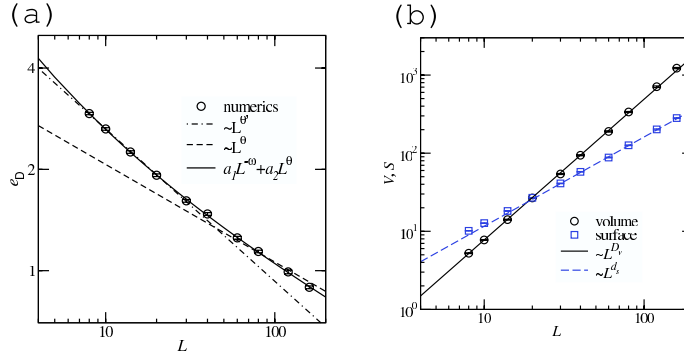


Fig. 1. (a) The droplet energy as a function of the system size. The two dashed straight lines represent the algebraic dependences $L^{-0.47}$ for smaller systems and $L^{-0.29}$ for larger ones, respectively. The solid curve is a fitting function (see text). (b) The volume and surface of the droplets. (From [42].)

The same model was studied in [43] and then in [44] at zero-temperature using a different approach. For each realization of the model, the ground state for periodic boundary condition was compared with the ground state for another set of boundary conditions, such as anti-periodic and random boundary conditions. (In the latter, half of the bonds across the boundary are chosen at random and inverted while the other half are kept unchanged.) The authors of [44] argued that in the RSB picture the change in the boundary condition would induce an excitation whose surface-to-volume ratio should not diminish as the system size increases, whereas in the droplet picture it should decrease down to zero. Therefore, we can differentiate between the two pictures by applying a boundary condition that induces a domain wall in the system and focusing on a small box located at the center of the system. If the probability of having the domain wall crossing this part is finite even in the thermodynamic limit, it would indicate the validity of the RSB picture. On the other hand, it should decrease to zero if the droplet picture is valid.

They performed a calculation of exact ground states of many instances of the EA model in two dimensions with the Gaussian bond distribution. The system size explored was up to $L = 30$. They considered a box of the linear size of $L_{\text{box}} = 2$ located at the center of the system, and measured the distribution of the overlap q_{box} on this box:

$$q_{\text{box}}^{\alpha\beta} \equiv \frac{1}{L_{\text{box}}^d} \sum_{i \in \text{"box"}} S_i^\alpha S_i^\beta$$

where α and β are the indices specifying real replicas. If the boundary passes the box with a finite probability, the distribution of $q_{\text{box}}^{\alpha\beta}$ should have a finite weight around $q_{\text{box}}^{\alpha\beta} = 0$. This weight turned out to be decreasing with the power of -0.7 as a function of the system size. Based on this result, they concluded that the zero-temperature structure of the two-dimensional EA model is trivial, i.e., only two pure states exist. (See Fig.4.)

2.4. Finite-Temperature Transition?

There are some numerical results³³ of Monte Carlo simulation on the $\pm J$ model that suggest the existence of a phase transition at a finite temperature. Specifically, the overlap distribution $P(q; L)$ and the binder parameter g were computed. The estimates of the Binder parameter

$$g_q \equiv \frac{1}{2} \left(3 - \frac{[\langle q^4 \rangle]}{[\langle q^2 \rangle]^2} \right) \quad (9)$$

as a function of the temperature for various system sizes appeared to have a common crossing point. The finite-size-scaling plot seems better when a finite transition temperature $T_c \sim 0.24J$ was assumed in stead of zero transition temperature. Their estimate for the critical indices of this finite temperature transition are $\nu \sim 1.8$ and $\eta \sim 0.2$. The overlap distribution $P(q; L)$ could be nicely scaled with the same η but with a slightly higher temperature $T_c \approx 0.29J$. Similar results were obtained⁴⁵ for an asymmetric bond distribution.

Numerical evidences suggest that the stiffness exponent of the two-dimensional $\pm J$ model is non-positive, as discussed in subsection 2.1, which indicates that the lower critical dimension of the $\pm J$ model is equal to or greater than two. Now, if a spin-glass transition takes place at a finite temperature as suggested, it means that the lower critical dimension is not greater than two. Therefore the only scenario consistent with all the available numerical and analytical results is that the lower-critical dimension is exactly two and that the stiffness exponent is exactly zero in two dimensions. More evidences, however, appear to be necessary to settle this issue beyond reasonable doubts.

3. Equilibrium Properties of Three-Dimensional Models

The problem of spin glasses in three dimensions is the central topic of the field. Whereas the RSB nature of the low-temperature phase in four dimensions is much less controversial, the nature of the low-temperature phase in three dimensions still remains the subject of an active debate.

Below we present a number of numerical results. Because of the severe technical limitations for three dimensional cases, all the results obtained are for small systems, typically up to the linear size of about 10 lattice spacings or slightly more. Therefore, many important issues are left open, in particular the question as to what picture yields the correct description of the low-temperature phase of the EA model, which is the main subject of subsection 3.3 through subsection 3.8.

3.1. Finite Temperature Transition?

Even the very existence of a phase transition at finite temperature was not easy to establish. An evidence of the existence was obtained through the calculation of the domain wall energy at zero-temperature,²⁹ in which a positive estimate for the stiffness exponent was obtained. However, the system size was rather limited ($L \leq 8$) and the estimated value of the stiffness exponent was small ($\theta \sim 0.2$). Therefore, this finding about the stiffness exponent alone was not sufficient to establish the existence of a finite-temperature phase transition. Finite temperature approaches could not settle the issue, either. For example, while Monte Carlo simulations^{46,47} strongly suggested the existence of a transition at a finite temperature, they could not rule out the possibility of zero-temperature singularity with an exponentially diverging correlation length; it was suggested⁴⁸ that all existing data at that time (namely 1994) were consistent with both hypotheses: $T_c > 0$ and $T_c = 0$. In particular, the simulation results of [48] for the spin-glass susceptibility could be fitted by a functional form consistent with a zero-temperature singularity, $\chi_{\text{SG}} = 1 + A/(T - T_c)^\gamma$, just as well as the one consistent with a finite-temperature transition $\chi_{\text{SG}} = A(e^{(B/T)^p} - 1) + C$.

However, another set of Monte-Carlo results⁴⁹ showed beyond reasonable doubts the existence of a finite temperature transition in the $\pm J$ model in three dimensions. Specifically, it demonstrated that the Binder parameter curves for different system sizes cross at the same point (Fig.2) near

$$T \sim 1.1, \quad \text{and} \quad g_{\text{sg}} \sim 0.75.$$

With the assumption of the algebraic singularity at the critical point, the critical temperature and the critical indices were estimated as

$$T_c = 1.11(4), \quad \nu = 1.7(3), \quad \text{and} \quad \eta = -0.35(5).$$

These estimates were consistent with previous ones⁴⁶ and confirmed by other simulations as presented in Table 1.

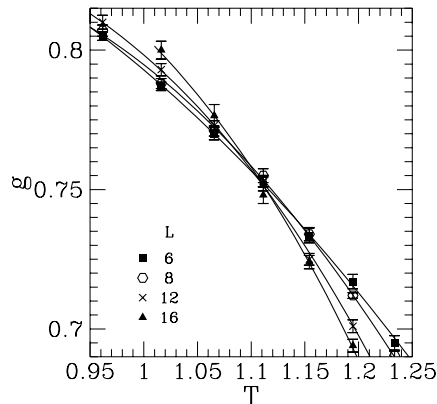


Fig. 2. The Binder parameter vs temperature for the $\pm J$ model in three dimensions. (From [49].)

A Monte Carlo simulation for larger system sizes⁵⁰ clarified the issue further. The results of the correlation length and the spin-glass susceptibility were extrapolated to the infinite system-size limit via finite size scaling, and were well fitted by a curve representing an algebraic divergence at a finite temperature. While the existence of a finite temperature phase transition could be concluded from this result, the nature of the singularities at the critical point could not unambiguously be settled. (The singularity could be an essential rather than an algebraic singularity.) In the next subsection, we present other numerical results concerning the nature of the critical point.

3.2. Universality Class

Early Monte Carlo simulations such as [46] indicated a scenario that the system stays critical in the whole low temperature region. Namely, these data could be explained by a line of critical points terminating at $T_c = 1.2$, similar to the Berezinskii-Kosterlitz-Thouless transition in the two-dimensional XY ferromagnet. The conclusion of [50] on this issue was similar, while it was suggested that a finite-temperature transition with an algebraic divergence is most likely. With the assumption of the algebraic divergence, the critical parameters were estimated to be consistent with previous ones mentioned above. However, the data were also consistent with an exponential divergence as in the BKT transition.

A large-scale Monte Carlo simulation⁵¹ clarified the issue of the nature of the phase transition. Using special purpose machines and parallel tempering method^{52,53} the authors succeeded to equilibrate the $\pm J$ model of sizes up to $L = 20$ down to a temperature low enough to cover a sufficiently large region around the transition point. They obtained various results consistent with an ordinary second order phase transition. For example, they observed a clear crossing in the effective correlation length⁵⁴ $\xi(L)$ divided by the system size L . (They defined the effective correlation length as $\xi^2(L) \equiv \tilde{k}_m^{-2}(C_q(0)/C_q(\mathbf{k}_m) - 1)$, where $C_q(\mathbf{k})$ is the static structure factor, \mathbf{k}_m is the smallest non-zero wave number compatible to the boundary condition, and $\tilde{k}^2 \equiv 4(\sin^2(k^x/2) + \sin^2(k^y/2) + \sin^2(k^z/2))$.)

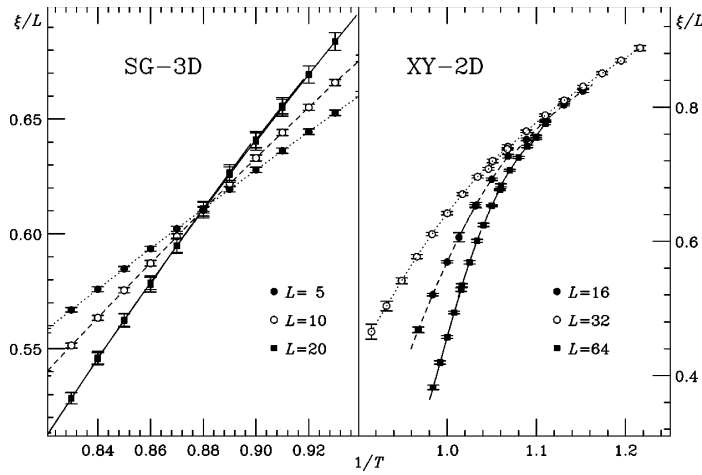


Fig. 3. The effective correlation length divided by the system size. The left panel is for the $\pm J$ model in three dimensions whereas the right panel is for the XY model in two dimensions. (From [51].)

The scaling dimension of the effective correlation length is zero; the curves for various system sizes should intersect at the same point similar to the Binder parameter. Indeed, it shows a common intersection point as in the right panel of Fig.3. This is in marked contrast to what we typically see in a BKT type transition, which is shown in the right panel of Fig.3 for comparison. From this result one concludes that the phase transition is an ordinary second-order one. For the critical temperature and the indices, again, see Table 1.

The results of [51] provided also indications in favor of an RSB nature of the system below the critical temperature. Namely, the estimates of a quantity called the G -parameter seems to have a finite value even below the critical point. The G -parameter is defined⁵⁵ as

$$G \equiv \frac{[\langle q^2 \rangle^2] - [\langle q^2 \rangle]^2}{3[\langle q^2 \rangle]^2 - [\langle q^4 \rangle]}.$$

The numerator is finite only if the sample-to-sample dependence of $P(q)$ does not vanish, while the denominator can be finite even if there is no sample dependence. Therefore, a observed non-vanishing value of G implies that $P(q)$ is not self-averaging.

However, there are a number of evidences by other groups that can be interpreted otherwise, namely, in favor of the absence of an RSB nature of the low temperature phase, as we discuss below.

3.3. Low-Temperature Phase of the $\pm J$ Model

There is a very active debate on the nature of the low-temperature phase of three dimensional spin glass models. In the following few subsections, we review various theories, arguments and numerical calculations that were made or done with the ultimate aim to clarify the issue. But none of the pictures, RSB, droplet, or others, could be established so far. Nonetheless, the debate itself is interesting and each picture is worth being scrutinized with detailed numerical calculations. While the common belief is that the $\pm J$ model and the Gaussian-coupling model show essentially the same physics at finite temperature, we present them separately since many of the computations are done at zero temperature where the two may differ. The $\pm J$ model is discussed in the present subsection and the Gaussian-coupling model in the next.

A finite temperature simulation on the $\pm J$ model was performed⁷⁷ using the replica exchange Monte Carlo simulation⁵³ for $\pm J$ model reaching down to $T = 0.2$ for the system size up to $L = 10$. The integrated overlap probability distribution

$$x(1/2) \equiv \int_0^{1/2} dq P(q)$$

was computed as a function of the temperature and the system size. Inspired by [78], the scaling — $x(1/2)$ being proportional to L^λ for small L and to L^θ for larger L — was assumed. In other words,

$$x(1/2) = TL^{-\theta} f(TL^\lambda)$$

Table 1. The estimates of the critical temperature and the exponents for the three dimensional spin glass models. The entries are categorized into three groups according to the anisotropy; easy-axis (top), isotropic (middle), and easy-plane (bottom). The entries with “*” are not quoted in the original paper but estimated through the scaling relations by the present authors. The entries with “c” are for the chiral glass transition. .

Authors	Material/Model	T_c/J	ν	η	β	γ	z
Gunnarsson <i>et al.</i> ⁵⁶	FeMnTiO	—	1.7	-0.35	0.54	4.0(3)	6.2
Ogielski ⁴⁷	Ising, $\pm J$	1.175(25)	1.3(1)	-0.22(5)	0.5	2.9(3)	6.0(5)
Bhatt-Young ⁴⁶	Ising, $\pm J$	1.2 ^{+0.1} _{-0.2}	1.3(3)	-0.3(2)	0.46*	3.2	—
Singh-Chakravarty ⁵⁷	Ising, $\pm J$	1.2(1)	—	—	—	2.9(5)	—
Bhatt-Young ⁵⁸	Ising, Gaussian	0.9	1.6(4)	-0.4(2)	—	—	—
Kawashima-Young ⁴⁹	Ising, $\pm J$	1.11(4)	1.7(3)	-0.35(5)	0.55*	4.0*	—
Iñigues <i>et al.</i> ⁵⁹	Ising, Gaussian	1.02(5)	1.5(3)	—	—	—	—
Marinari <i>et al.</i> ⁶⁰	Ising, Gaussian	0.98(5)	2.00(15)	-0.36(6)	0.64*	4.72*	—
Berg-Janke ⁶¹	Ising, $\pm J$	0.88	—	-0.37(4)	—	—	—
Palassini-Caracciolo ⁵⁰	Ising, $\pm J$	1.156(15)	1.8(2)	-0.26(4)	0.65*	4.1(5)	—
Mari-Campbell ⁶²	Ising, $\pm J$	1.19(1)	1.33(5)	-0.22(2)	0.52*	2.95(15)	—
Ballesteros <i>et al.</i> ⁵¹	Ising, $\pm J$	1.138(10)	2.15(15)	-0.337(15)	0.73*	5.0*	—
Mari-Campbell ⁶³	Ising, $\pm J$	1.195(15)	1.35(10)	-0.225(25)	0.55*	2.95(30)	5.65(15)
Nakamura <i>et al.</i> ⁶⁴	Ising, $\pm J$	1.17(4)	1.5(3)	-0.4(1)	0.45*	3.6(6)	6.2(2)
de Courtenary <i>et al.</i> ⁶⁵	CuMn,AgMn	—	1.4*	0.4*	1.0(1)	2.2(1)	—
Bouchiat ⁶⁶	AgMn	—	1.4*	0.4*	1.0(1)	2.2(2)	—
Levy-Ogielski ⁶⁷	AgMn	—	1.3(2)	0.4*	0.9(2)	2.1(1)	5.5
Simpson ⁶⁸	CuAlMn	—	1.3*	0.5*	1.0*	1.9*	—
Coles-Williams ⁶⁹	PdMn	—	1.3*	0.4*	0.90(15)	2.0(2)	—
Vincent-Hamman ⁷⁰	CdCrInS	—	1.25(25)	0.2*	0.75(10)	2.3(4)	5.5
Kawamura ⁷¹	Heisenberg, Gaussian	0.157(10) ^c	—	—	1.1(1) ^c	—	—
Hukushima-Kawamura ⁷²	Heisenberg, Gaussian	0.160(5) ^c	1.2 ^c	0.8 ^c	1.1(1) ^c	1.5(3) ^c	—
Matsubara <i>et al.</i> ⁷³	Heisenberg, $\pm J$	0.18	—	—	—	—	—
Nakamura-Endoh ⁷⁴	Heisenberg, $\pm J$	0.21 ^{+0.01} _{-0.03}	1.1(2)	0.3*	0.72(6)	1.9(4)	4.5
Lee-Young ⁷⁵	Heisenberg, Gaussian	0.16(2)	1.1(2)	—	—	—	—
Nakamura <i>et al.</i> ⁶⁴	Heisenberg, $\pm J$	0.20(2)	0.8(2)	-0.3(3)	—	1.9(5)	6.2(5)
Kawamura-Li ⁷⁶	XY , $\pm J$	0.39(3) ^c	1.2(2) ^c	0.15(20) ^c	—	—	7.4(10) ^c
Lee-Young ⁷⁵	XY , Gaussian	0.34(2)	1.2(2)	—	—	—	—
Nakamura <i>et al.</i> ⁶⁴	XY , $\pm J$	0.43(3)	—	-0.4(2)	—	—	6.8(5)

was assumed. The fitting to the numerical results worked nicely with $\theta = 0$ yielding

$$\lambda = 0.9(1),$$

whereas a fitting with $\theta = 0.2$, the droplet prediction, turned out to be significantly worse. The estimate of λ is considerably smaller than a preceding estimate⁷⁹ while consistent with the value $\lambda = 0.72(12)$ in [80].

Zero-temperature calculations offer a powerful alternative to the finite temperature approach with Monte Carlo simulations, because one might expect that the differences between the two scenarios should be more prominent at lower temperature, and much better methods are available for systems at zero-temperature than for a very low but finite temperature. For three dimensional models, most methods for solving zero-temperature problems are based on heuristic optimization since no good exact method is available due to the NP-hardness of the problem. A computation of the ground states of the $\pm J$ Ising model up to $L = 14$ was done^{81,82} with a heuristic algorithm called the cluster-exact approximation method.⁸³ Later the computation was redone,^{79,84} in order to fix the problem of the biased sampling.⁸⁵ It was found that the width of the overlap distribution, $P(q)$, decreases as the system becomes larger, indicating the triviality of $P(q)$. The validity of the ultra-metric relation, $q_{12} = q_{23} < q_{31}$, was also examined, where q_{ij} 's are the overlaps among three randomly chosen ground states. The numerical results indicated that the ultra-metric relation holds for a typical triplet of ground states with relatively large mutual distances. However, it was also found that the contribution from these triplets to $P(q)$, which constitutes the “non-trivial” (i.e., continuous) component of $P(q)$, decreases as the system becomes larger. In fact, the integrated weight of $P(q)$ systematically decreased toward zero as

$$x(q) \equiv \int_{-q}^q dq P(q) \propto L^{-\lambda}$$

with $\lambda = 1.25(5)$ for $q = 0.5$. This indicated a trivial structure of $P(q)$ at zero temperature. As for the exponent λ , a different estimate was obtained⁷⁷ as mentioned below.

The authors of [78] considered $P(q)$ for the $\pm J$ model at $T = 0$, and pointed out that the ground state space may be dominated by a single valley or a single pure state no matter which picture is valid. They argued that even if there are multiple valleys in the energy landscape of the discrete energy model, the distribution of the overlap $P(q)$ may still be trivial,

indicating that it is impossible to discriminate between the two scenarios by a computation of $P(q)$ such as the one mentioned above.

The underlying assumption of the argument is the many-valley structure in the phase space and the sponge-like structure of low-lying excitations in the real space. (The latter is further discussed below in subsection 3.6 and subsection 3.7.) A droplet typically has a finite volume and when flipped it takes a state in a valley to another state in the same valley. In contrast, a typical sponge-like cluster is supposed to occupy a finite fraction of the whole system and flipping it generally causes a transition from one valley to another.

This argument is based on an estimate of the entropy by counting zero-energy excitations from a particular ground state. In general, the continuous part of $P(q)$, if any, is caused by excitations of various scales whose excitation free energies are smaller than the temperature. In particular, at zero temperature, it is caused by zero-energy “excitations”. They argued that $P(q)$ has a trivial structure even if there are multiple valleys. To see this, it suffices to consider the case of two valleys. Each valley contributes to $P(q)$ according to its weight that is the number of distinct spin configurations in the valley. This number is roughly the same as the number of zero-energy droplets. We can choose two representative configurations, one from each valley, that can be transformed to each other by flipping a sponge-like cluster. Then, the zero-energy droplet excitations in one configuration differ from those in the other configuration only on (or near) the boundary of the sponge-like cluster. Therefore, if A is the area of the surface of the sponge-like cluster, the droplets differ only at A positions. This difference results in the entropy difference of $\mathcal{O}(A^{1/2})$. (The power 1/2 comes from the assumption that the number of the droplet-like excitation located on the surface is a random variable.) It follows that the contribution (to the continuous part of $P(q)$) from one valley differs from that from the other typically by a factor $e^{\pm(\text{const}) \times A^{1/2}}$. We now see that almost certainly $P(q)$ is dominated by a contribution from a single valley in the thermodynamic limit where $A \rightarrow \infty$, leading to a trivial structure in $P(q)$. It is clear that the presence of more than two valleys does not affect the result as long as the number of valleys does not grow too fast as the system size increases. Based on this result, they argued that a trivial $P(q)$ for the $\pm J$ model in three dimensions at $T = 0^{84}$ does not necessarily indicate the absence of the RSB.

However, it is not known how the number of valleys depends on the system size. It is not too unrealistic to assume that the number of valleys

grows faster than or proportional to the number of spins, N . If so, a typical minimum entropy difference between two valleys would be less than $A^{1/2}/N < N^{-1/2} \rightarrow 0$. Therefore, it is not clear if this argument really invalidates the numerical evidence in [84] for triviality of the energy landscape structure.

3.4. Low-temperature Phase of the Gaussian-Coupling Model

The ground state of models with the Gaussian bond distribution, is unique up to a trivial degeneracy due to the Z_2 symmetry. However, it is still possible to extract useful information about low-lying excitations from zero-temperature computations. The authors of [86] attempted to use the same strategy that they used for two dimensional models with the Gaussian bond distribution⁴⁴ (see subsection 2.3) to discriminate between the two scenarios in three dimensions. They estimated the probability of a domain-wall passing through a small imaginary box placed inside the system. A clear decreasing behavior as a function of the system size was found, in favor of the droplet picture. However, the amount of the total decrease that they could observe by changing the system size was only of a factor of 1.3 or 1.4, due to a severe system size limitation. (In the case of two dimensions, the same quantity varies by almost an order of magnitude as can be seen in Fig.4.)

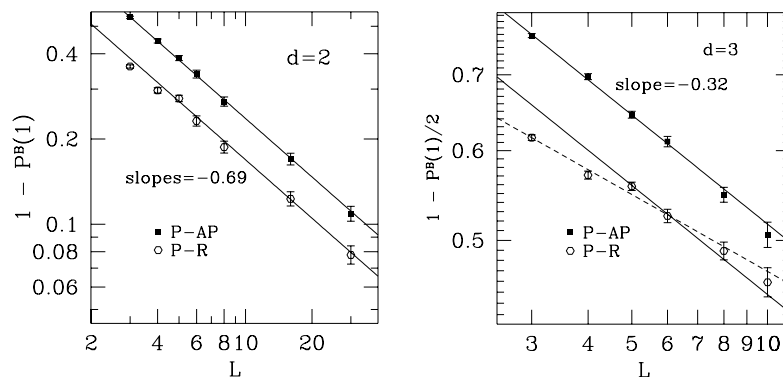


Fig. 4. The probability of a domain wall passing through the box. The left panel is for the EA model with the Gaussian bond distribution in two dimensions at $T = 0$ and $H = 0$, whereas the right panel is for the same model in three dimensions. (From [86].)

In addition to the response to the boundary condition, the effect of a weak perturbation applied to the whole system was also examined.⁸⁷ The perturbation was chosen in favor of the excited states against the ground state. For each bond realization, they first obtained the ground state, which we denote $\{S_i^{(0)}\}$. Then to each coupling constant J_{ij} the following perturbation was added

$$\Delta J_{ij} \equiv -\Delta J S_i^{(0)} S_j^{(0)}.$$

where $\Delta J \equiv \epsilon/N_{\text{bond}}$ was chosen to be of $\mathcal{O}(L^{-d})$. With this perturbation the ground state energy is increased, exactly, by ϵ , whereas excited state energies are changed according to its similarity to the ground state. Therefore by adjusting the amplitude of the perturbation and examining the overlap between the original ground state and the ground state of the perturbed system, one may obtain some information about the excitations.

The RSB picture predicts the existence of many spin states that are local minima of the Hamiltonian. These states differ from the ground state by only an infinitesimal amount of energy per spin but differ by a macroscopic number of spins such that the average Hamming distance between them (normalized by the system size) converges to some finite value in the large system size limit. This means for the bulk perturbation considered in [87] that the overlap between the two such minima, the one with the perturbation and the other without, should be truly smaller than unity in the thermodynamic limit, no matter how small the perturbation may be. Therefore in the RSB picture, $1 - [q]$ should be finite where q is the overlap between the two minima. On the other hand, in the droplet picture, $1 - [q]$ should depend on the system size by a power-law being characterized by the droplet energy exponent θ and an exponent related to the geometrical properties of the excitations. To be specific, since $1 - [q]$ is dominated by the contribution from droplets whose linear size is comparable to the system size L , it is roughly equal to the volume fraction of a typical droplet of size L multiplied by the probability of such a droplet being excited. Namely,

$$1 - [q] \propto \frac{L^{d_v}}{L^d} \times \frac{\Delta_L}{\epsilon_L} \quad (10)$$

where Δ_L is the energy gain by the droplet excitation due to the perturbation and ϵ_L is the droplet excitation energy without the perturbation. If the droplets are compact, as assumed in [87], only the second factor matters since $d_v = d$. For Δ_L , the authors of [87] assumed that $\epsilon \sim \mathcal{O}(1)$ when integrated over the whole system, which is equivalent to setting $\Delta_L \propto L^{-d+d_s}$

where d_s is the fractal dimension of the boundary of droplets. Based on this, the following scaling form for the overlap was proposed [87]:

$$v(\epsilon, L) \equiv 1 - [q] \sim \tilde{V}(\epsilon/L^{d-d_s-\theta}). \quad (11)$$

For the link overlap q_l , a similar argument yields

$$s(\epsilon, L) \equiv 1 - [q_l] \sim L^{-(d-d_s)} \tilde{S}(\epsilon/L^{d-d_s-\theta}). \quad (12)$$

In the system size range that could be explored, (namely, $L \leq 8$), the numerical results for $[q]$ and $[q_l]$ shows that $v(\epsilon, L)$ and $s(\epsilon, L)$ obeys the power law and decreases to zero as the system size increases, contradicting the RSB picture. However, fitting the numerical results to the forms (11) and (12) yielded

$$d - d_s = 0.42(2), \quad \text{and} \quad d - d_s + \theta = 0.44(2).$$

This implies

$$\theta = 0.02(3).$$

The difference between the value and the stiffness exponent (~ 0.2) obtained from the domain wall calculation is statistically significant, i.e., the result contradicts not only to the RSB picture but also to the droplet picture unless this seeming contradiction is caused by a large correction to scaling.

Concerning the possible source of the correction, two arguments^{88,89,42} were presented to explain the inconsistency observed in numerical results within the framework of the droplet argument. It was pointed out⁸⁸ that if one assumes a “clean” scaling with no correction for the droplet excitation energy, the contribution from small droplets gives rise to a correction to scaling in quantities such as the spin-glass susceptibility and the magnetic susceptibility. The droplet excitation energy computed with the condition used in [40,41] and the link overlap computed in [87] may have been affected by such a correction to scaling. Another possible source of a correction to scaling is the interaction between domain walls. It was argued^{89,42} that the energy of a domain wall may be increased by the presence of another domain wall and that the energy shift due to this interaction may have the form $l^{-\omega'}$ where l is the distance between two domain walls. Similarly, a “self-interaction” of the domain wall may give rise to a correction to scaling in the droplet excitations as $E = Al^\theta + Bl^{-\omega}$. In this case l stands for the size of the droplets. As the correction-to-scaling exponent due to this mechanism, the authors of [89] quoted the value $\omega \sim 0.13(2)$ ⁹⁰.

In response to some reports (see the following paragraphs in the present section) contradicting to their conclusion, the authors of [91] further pursued the ground state nature of the three dimensional system with the Gaussian bond-distribution, along the same line as their own preceding calculation.⁸⁷ This time, however, larger systems ($L = 12$) were dealt with the branch-and-cut algorithm.⁹² This algorithm guarantees that the states found are the true ground states. In addition, a greater care was taken for various possibilities of fitting functions and different sources of corrections to scaling. Specifically, they considered a few different fitting functions for size dependent quantities such as the link overlap and the box overlap. Fitting functions consistent with the droplet, the TNT, and the RSB scenario, respectively, were considered. (For the TNT scenario, see subsection 3.6 and subsection 3.7 below.) It was found that the size dependence of the surface-to-volume ratio, i.e., $1 - q_1$, could be explained by any one of three pictures, and also that the size dependence of the box overlap could be explained by any one of three pictures. The estimates of the exponent $\mu \equiv d - d_s + \theta$ turned out to depend on the boundary condition. With the free boundary condition, the estimates are $d - d_s = 0.44(3)$, $\mu = 0.63(3)$, and $\theta = 0.19(6)$, whereas for the periodic boundary condition, they are $d - d_s = 0.43(2)$, $\mu = 0.42(3)$, and $\theta = -0.01(3)$. The latter set of values are consistent with their preceding estimates⁸⁷ whereas the former are not.

Another set of numerical results, presented in [93,94,95] seems to contradict to the results of [87,86] presented above. As for the calculation based on the small imaginary box placed at the center of the system, it was argued⁹³ that the probability of the state inside the box being affected by the change in the boundary condition should obey the scaling

$$P_{\text{change}}(L_{\text{box}}, L) \sim g(L_{\text{box}}/L), \quad (13)$$

if the droplet argument is correct. However, the numerical results in [93] for $L_{\text{box}} = 2, 3, 4$ and $L = 12$ did not fit in this scaling.

In [93], the scaling property of the domain wall induced by the anti-periodic boundary condition in the x -direction was also examined. In particular, the probability of the domain wall not intersecting a plane perpendicular to the x axis was measured. It was found that the non-intersecting probability approaches zero as the system size increases:

$$P_L(\text{"The domain wall does not intersect the plane."}) \propto L^{-\gamma},$$

with $\gamma = 1.5 - 2.0$. Based on this observation they suggested that the domain wall is space filling, i.e., $d = d_s$.

In [94,95], zero-temperature calculations were performed with the conditions analogous to the ones in [86] and [87]. In [94], the effect of the anti-periodic boundary conditions, which were imposed in the x direction, was compared with the periodic one. The links perpendicular to the yz plane were treated separately from those parallel to the yz plane. The result of the link overlap for the perpendicular links, q_P , and that for the transverse ones, q_T , are shown in Fig.5(a). Both kinds of the link overlap can be fitted

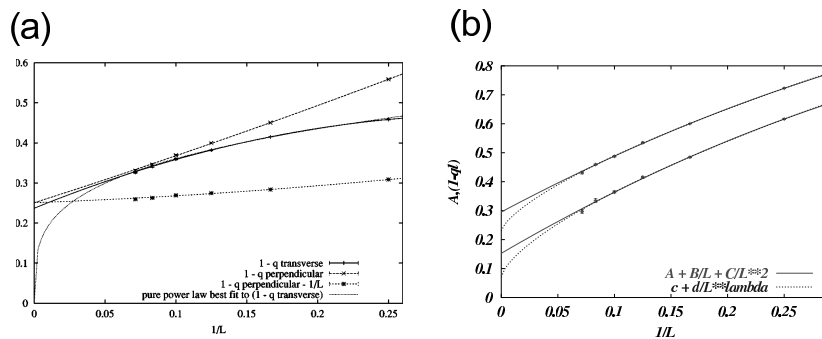


Fig. 5. (a) The link-overlap for the perpendicular links, q_P , and that for the transverse ones, q_T , between the two ground states with and without a twist in the boundary, and (b) the link-overlap (subtracted from unity) between the two ground states with and without a bulk perturbation. (The lower set of data is for the average link-overlap, whereas the upper one is for the link-overlap restricted to those pairs of states which have zero mutual overlaps. For each set of data, the upper fitting curve is a second order polynomial in $1/L$ and the lower one is a fractional power in $1/L$ with an additional constant term.) For both (a) and (b), the model is the three-dimensional EA model with the Gaussian bond distribution at zero temperature. (From (a) [94] and (b) [95].)

well by second order polynomials in $1/L$ as shown in the figure. From the zero-th order term, they concluded that

$$\lim_{L \rightarrow \infty} 1 - q_l = 0.245(15),$$

in contrast to the droplet prediction $1 - q_l \rightarrow 0$.

In [95], the effect of the bulk perturbation at zero temperature was studied. The perturbation was the same as the one considered in [87]. The link overlap, $q_l(q)$, was computed as a function of the bulk overlap, q . In addition to the average link-overlap, $q_l(L)$, attention was paid to the quantity $A(L) \equiv 1 - q_l(q = 0)$, where $q_l(q = 0)$ is the link overlap between two states that have zero overlap. In the droplet picture, both quantities should converge to 0 as L goes to infinity. The numerical results are shown in Fig.5(b).

It was found that in both cases of the boundary and the bulk perturbations, the size dependence of the surface-to-volume ratio of the domain wall, i.e., $1 - q_l$ can be fitted by a polynomial in $1/L$ with a finite constant term, consistent with the RSB picture.

Concerning the results presented in [93], it was pointed out⁹⁶ that the probability P_{change} is subject to a strong correction to scaling and that, taking such a correction term into account, the data presented in [93] can be fitted reasonably well with the scaling form (13). It was also pointed out that even the two dimensional data, which is believed to obey (13), could not be fitted by this scaling form without a similar correction term. As for the non-intersecting probability of the domain wall with the plane, it was simply pointed out that the observation in [93] does not necessarily imply $d = d_s$ because the observed behavior can be caused by domain walls that are rough but not space filling. In addition, as already mentioned above, their latest calculation⁹¹ suggests that we have not yet accumulated numerical evidences sufficient to decide between the possible scenarios.

Before concluding this subsection, let us mention what is known about the geometrical nature of droplets. For this issue, a zero-temperature calculation was performed.⁹⁰ Using an efficient heuristic algorithm, the authors of [90] obtained ground states of three dimensional systems of the size $L = 6$ and $L = 10$. For each sample, they first obtained the ground state. Then, a center of the excitation is chosen randomly. They searched for the droplets of various sizes including the central spin. In their calculation, a droplet was defined as the cluster of spins of the smallest excitation energy among those which have a given volume. In spite of the limited system size, they succeeded in obtaining system-size independent numerical results. They found that the linear scale of the droplets is described by

$$R(v) \propto v^b \quad (b \sim 0.5),$$

whereas the volume dependence of the excitation energy obeys

$$E(v) \propto v^a \quad (a \sim -0.06).$$

The first relation means that the droplets are roughly two dimensional fractal objects rather than compact ones. The second relation is rather surprising, since at first glance it might seem to contradict the existence of the finite-temperature phase transition. They claimed that this does not necessarily mean the absence of the phase transition because the basic assumption of the droplet argument may not be valid. Another possible source of the discrepancy may be the definition of the droplet with the very restrictive fixed-volume constraint.

3.5. Effect of Magnetic Fields

Whereas the RSB picture predicts the persistence of the spin glass phase against a small but finite magnetic field, the droplet-picture predicts the contrary — the absence of the spin glass phase at any finite magnetic field. Therefore, one of the possible ways to distinguish between the two scenarios may be found in the behavior of short-range models in a finite magnetic fields. However, it is rather hard to perform this task near the critical temperature (of the zero-field case). This difficulty is not only because the dynamics near the critical point is slow but also because the critical value of the magnetic field predicted by the mean-field type argument is small. To avoid at least the latter difficulty, a zero-temperature calculation was performed.⁹⁷ Using a heuristic optimization algorithm, the ground state of the three dimensional EA model was computed with the Gaussian bond distribution up to $L = 12$ with various uniform magnetic fields.

In addition to the magnetic field, also some constraints were imposed at the same time to probe low-lying excitations. For example, a spin may be forced to be opposite to its natural direction in the original ground state with no constraint. Then, the lowest-energy excitation among those which include the chosen spin is excited. In the RSB picture, where there are infinite number of states different from each other by a finite fraction of spins within an $\mathcal{O}(1)$ window of excitation energy, such a excitation should typically contain a finite fraction of all spins. (See also subsection 3.6 and subsection 3.7 below.) Therefore, the volume of excited cluster tends to infinity with increasing system size. On the other hand, in the droplet scenario, the influence of the forced spin cannot reach beyond the distance determined by the magnetic field H as

$$l(H) \propto H^{-2/(d-2\theta)}.$$

Therefore, when the system size is increased beyond this length, the size of the excited clusters should stay constant independent of the system size. Some results of computation along this line of consideration were presented in [97]. They demonstrate the fragility of the ground state in a magnetic field. For example, the forced spin-flip typically drags as much as 30 percents of all spins at $H = 0.2$ for $L = 12$. The size of the excited cluster generally increases as the system size increases. However, neither a saturation nor a proportionality to L^d could be identified clearly.

Therefore, they tried another constraint where signs of an array of bonds along a plane are switched. This corresponds to imposing the anti-periodic boundary condition to the system. In the RSB picture, the resulting ex-

citation again should extend to the whole system, whereas in the droplet scenario, it should not for systems larger than $l(H)$. They measured the probability of the excitation wrapping around the system. It was found that the wrapping probability increases for $H \leq 0.6$ as the system becomes larger whereas it decreases for $H \geq 0.7$. Based on this result they suggested that H_c is finite and is close to 0.65 at $T = 0$. While they did not exclude the possibility of $H_c = 0$ considering the finite size corrections that may be present, their approach seems promising and it is probably worth putting more effort in this direction.

3.6. *Sponge-Like Excitations*

While the droplet picture presents a clear “real-space” image for the low-lying excitations, we have not discussed how low-lying excitations should look in the RSB picture. The authors of [98] discussed geometrical properties of low-lying excitations that are compatible with the RSB picture. They proposed that low-lying excitations may have a “sponge”-like shape. A sponge-like cluster has a characteristic length scale l_c . They argued that excitations smaller than this scale obey the droplet scaling whereas beyond this scale the droplet predictions do not apply. A sponge-like object is defined by the following properties.

- (1) It is a connected object, and so is its complement.
- (2) It occupies a finite fraction of the whole system’s volume.
- (3) It spans the whole system, and so does its complement.
- (4) It has a characteristic length scale different from the system-size and the lattice constant. When coarse-grained beyond this length scale, the object occupies the space uniformly whereas below this scale non-uniformity can be seen.
- (5) Its surface contains a finite fraction of its volume, i.e., the surface-to-volume ratio is finite and independent of the system size up to a finite size correction.

They argued that in finite dimensions, three for instance, there may be excitations of sponge-like clusters with excitation energy of $\mathcal{O}(1)$, independent of the system size. At the same time, the energy barrier that must be overcome in order to excite such a cluster diverges as the system size increases. Namely, two pure states in the RSB picture can be transformed into one another by flipping spins in one or more of the sponge-like clusters. Since they occupy a finite fraction of the whole system, as soon as thermal

fluctuations are introduced, they give rise to the non-trivial structure in the overlap distribution function, $P(q)$. In addition, because of the property (5), such excitations yield a non-trivial functional form for the link overlap distribution $P(q_l)$.

Obviously, the last two properties (4) and (5) above are closely related to each other, because the surface-to-volume ratio may be determined by the characteristic length scale as $S/V \sim l_c^{-1}$. It is important to estimate the length scale, l_c , in order to check the applicability of the picture to individual cases. An attempt was made⁹⁹ to estimate this ratio numerically by considering the EA spin glass model with a Gaussian bond distribution. For each bond realization, the ground state was obtained using a heuristic optimization technique. Then, the ground state search was performed once more, this time under the constraint that a pair of spins (chosen randomly) have the opposite relative orientation as compared to the one in the first ground state.

In the droplet picture, the difference of two ground states is supposed to be a droplet of a size that is smaller than the distance of the two chosen spins, whereas in the sponge picture it should be identified with a sponge if one of the chosen spin is included in the sponge and the other is not. In the sponge picture, such an event should happen with a pfinite and system-size-independent probability because at the scale larger than l_c the sponge is uniform and the fraction of the sponge is system-size-independent.

Calculations of the system up to $L = 11$ were performed.⁹⁹ In order to check the property (3), the authors measured the probability of the event that the excited cluster spans the whole system. It was found that the probability does not show a strong system size dependence, indicating that large excitations with $\mathcal{O}(1)$ excitation energy exists.

3.7. TNT Picture — Introduction of a New Scaling Length

However, their other findings⁹⁹ indicated that the sponge picture defined above does not exactly describe the model, either. Particularly disturbing was the result of the surface-to-volume ratio of the system-spanning clusters obtained by the procedure mentioned in subsection 3.6; the ratio decreases as a function of the system size. A power-law yielded a reasonable fit, i.e. $S/V \propto L^{-0.3}$, suggesting l_c (defined as the V/S) tends to infinity in the limit $L \rightarrow \infty$. If one compares the ground state with the (sponge) excited state and focus on a small box located around the center of the system, the domain boundary S would never pass through this box in the infinite system

size limit. The link-overlap is therefore always complete (i.e., 1) within the box. This is in agreement with the result^{86,87} mentioned in subsection 3.4. The increase of the characteristic length l_c was also confirmed in [100]. It follows that the distribution of the link overlap should have a trivial delta-peak structure while that of the ordinary overlap may have a non-trivial structure. This new scenario with the new system-size-dependent scaling length $l_c(L)$ is called⁹⁹ the ‘TNT’ scenario, an abbreviation of “Trivial $P(q_l)$ and Non-Trivial $P(q)$ ”.

A closely related calculation was done by the authors of [101], who performed a Monte Carlo simulation of the EA model with the Gaussian bond distribution. They reached rather low temperatures ($T \sim 0.2J$) employing the exchange Monte Carlo method.⁵³ The overlap distribution $P(q)$ was measured. The zero-overlap probability $P(0)$ stays constant, in contrast to the prediction of the droplet picture ($P(0) \propto L^{-\theta}$ with $\theta \sim 0.2$), consistent with the RSB picture and the TNT picture. However, the temperature dependence of $P(0)$ at a fixed system size agreed with the droplet picture, i.e., $P(0) \propto T$. They also obtained the link-overlap distribution. Its width turned out to be proportional to $L^{-\mu_l}$ where μ_l was estimated as

$$\mu_l = 0.76(3)$$

from an extrapolation to $T = 0$. The TNT picture discussed above assumes the presence of excitations with size-independent energy, i.e., $\theta = 0$ whereas the surface-to-volume ratio of excited clusters goes to zero. Based on this picture together with the above estimate of μ_l , they obtained (by setting $\theta = 0$ in (8))

$$d - d_S = 0.38(2)$$

which is consistent with the zero-temperature calculation⁸⁷ $d - d_S = 0.42(2)$.

3.8. Arguments Supporting the Droplet Picture

In [102], the notion of pure states was re-examined for the disordered systems. The relationship between the appearance of $P_J(q)$ and the number of pure states was discussed. It was suggested that $P_J(q)$ is an erroneous indicator of the multiplicity of pure states. In the ferromagnetic two-dimensional Ising model below the critical temperature, one has an example of $P(q)$ being non-trivial while there are only two pure states. Namely, when the anti-periodic boundary condition is imposed in both the directions, because of the arbitrariness of the position of domain boundaries, $P(q)$ includes a continuous part. On the other hand, in the three-

dimensional random field model, one can see the case where $P_J(q)$ consists of a single delta peak although there are two pure states. This is because the free-energy difference between the two pure states, one with $\langle S_i \rangle = m > 0$ and the other with $\langle S_i \rangle = -m$, diverges being proportional to $N^{1/2}$. Therefore $P_J(q)$ for a given sample consists of only one delta peak.

The argument was elaborated in [21,10], in which the authors exploited the translation ergodicity. They proved that any translationally invariant quantity measured for a particular bond realization J is equal to its bond configuration average, provided that the distribution of each bond is independent and spatially uniform. Since $P_J(q)$ is obviously translationally invariant, it follows that $P_J(q)$ is self-averaging, i.e., does not depend on J . This result is in contrast with what we know for the SK model. Furthermore, they argued that since $P_J(q)$ is self-averaging it would be improbable that $P_J(q)$ has a continuous part. The reason for this is that there are only countably many pure states and therefore $P(q)$ consists of countably many delta peaks. Consequently, we would have to choose many but only countably many numbers from the interval $-1 \leq q \leq 1$ to locate these delta functions. They argued that existence of such countably many “preferred” locations, yet independent of J , are very implausible. Their argument made it clear that we must be careful about using the notion of the pure state in the disordered systems.

However, it was pointed out¹⁰³ that the very existence of the pure states that was implicitly assumed in [21] is questionable. This means that the pure states that appear in (3) may have only a metaphoric meaning, and should not be taken too strictly for disordered systems. From this point of view, one may say that the non-existence of the unique thermodynamic limit, or, more specifically, a chaotic system-size dependence of various quantities may signify the RSB nature of the spin glass systems.

4. Models in Four or Higher Dimensions

Numerical simulations are easier in four or higher dimensions than in three. This is presumably because $d = 4$ is well separated from the lower critical dimension. The existence of a finite-temperature phase transition in four dimensions was established already in an early numerical study⁵⁸ where a clear crossing in the Binder parameter, defined in (9), could be observed. The critical point was located at $T_c = 1.75(5)$ and the critical exponents were estimated to be $\nu = 0.8 \pm 0.15$ and $\eta = -0.3 \pm 0.15$ for the Gaussian bond distribution. The scaling relation $\gamma/\nu = 2 - \eta$ yields $\gamma = 1.8(4)$

which agrees well with the result $\gamma = 2.0(4)$ of a high-temperature series expansion¹⁰⁴ for the $\pm J$ bond distribution. More precise estimates of the critical indices were obtained in [105]:

$$T_c = 1.80(1), \quad \nu = 0.9(1), \quad \eta = -0.35(5), \quad \text{and} \quad \gamma = 2.1(2).$$

Based on an off-equilibrium simulation, they also obtained an estimate of the EA order parameter below the critical point as a function of the temperature. A non-vanishing order parameter excludes the possibility that the transition is of the BKT-type. As for the nature of the low-temperature phase, the observation made in [106] that $P(0)$ is system-size independent below the critical temperature indicates that the droplet picture is inappropriate for the four-dimensional spin glass. For a detailed discussion on other results obtained before 1997, the readers are referred to the review [103]. Here we only mention one of the latest computations for clarifying the nature of the low-temperature phase in four dimensions.

The replica exchange method was used in [101] to study the $4d$ spin glass model with a Gaussian bond distribution at rather low temperatures $T \sim 0.2J \sim 0.1T_c$. The zero-overlap probability $P(0)$ was measured in four dimensions as well as in three. In both cases $P(0)$ was found to be independent of the system size for a fixed temperature, and a roughly linearly dependent on the temperature for a fixed system size. The authors of [101] summarized their results as being consistent with the TNT picture mentioned above. They also estimated the exponent characterizing the size dependence of the variance of the link-overlap distribution, namely, $\theta + 2(d - d_s)$ where d_s is the fractal dimension of droplet boundaries (see the discussion in subsection 3.4). The extrapolated value to the zero temperature was $\theta + 2(d - d_s) = 0.35(6)$ while they did not rule out the possibility of this value being zero.

For the ground state properties in four dimensions, we refer the reader to [107], in which the ground states of the model in four dimensions up to $L = 7$ were computed. The stiffness exponent was estimated as $\theta_s = 0.64(5)$.

Although somewhat misplaced in this section on higher dimensional models we mention here the one-dimensional spin glass model with *long-range* interactions, i.e. $J_{ij} = c_\sigma \epsilon_{ij} / r_{ij}^\sigma$, where ϵ_{ij} is a Gaussian random number with zero mean and variance one and r_{ij} the Euclidean distance between spin i and j on a finite ring (of perimeter L) embedded in the two-dimensional space. This system, on the borderline between finite-dimensional and mean field models, was studied in [108,109] for system sizes up to $L = 512$. Finite temperature simulations as well as the study of

low-energy excitations yielded results that are inconsistent with the droplet picture but (partially) consistent with the TNT picture.

5. Aging

The out-of-equilibrium dynamics of spin glasses has become a very rich field in the recent years and an excellent review on the intensive theoretical work that has been performed on it until 1998 can be found in [110] and an overview over the experimental situation until that date can be found in [111,112]. Since then a number of interesting developments have occurred and we will focus on them with the prerequisites necessary to understand them. We start with the theoretical concept of a length scale that evolves in time and is flexible enough to account for a number of numerical and experimental results. Then we focus on two-time quantities that are typically measured experimentally and their behavior in various temperature protocols (i.e. aging histories) — showing effects like memory and rejuvenation. Finally we discuss the theory for violations of the fluctuation-dissipation theorem and the numerical and experimental evidences for it.

5.1. A Growing Length Scale During Aging?

Spin glasses have an order parameter which is (cum grano salis, i.e. disregarding the potential complications arising from a possible RSB) $q_{EA} = [\langle S_i \rangle^2]$. In comparison to structural glasses¹¹³ this is a very lucky situation, not only as a starting point for equilibrium theory, which we have discussed in last sections, but also for non-equilibrium dynamics. An example is the common picture of the dynamical evolution of a system out of equilibrium quenched into the phase with non-vanishing q_{EA} , in which larger and larger regions of space become ordered.¹¹⁴ Thus it appears natural to postulate a time-dependent length-scale $L(t)$ for these equilibrated domains for spin glasses. We choose such a picture, motivated by coarsening systems,¹¹⁴ as our starting point for reviewing the out-of-equilibrium dynamics of spin glasses.

Within the droplet theory¹¹⁵ the slow out-of-equilibrium dynamics of a finite-dimensional spin glass is due to thermally activated growth of locally equilibrated regions. The growth of such regions is supposed to happen through domain wall movements as in the context of pinned domain walls in random field systems¹¹⁶ or in elastic manifolds in a disordered environment¹¹⁷ via a thermally activated process overcoming a free energy barrier. It is assumed that the typical energy barrier $B_{L(t)}$ scales with the

typical size $L(t)$ of the domains reached after a time t as

$$B_{L(t)} \sim \Delta(L(t)/L_0)^\psi, \quad (14)$$

where ψ is the barrier exponent characteristic of the particular system under consideration and Δ is some constant. Since the dynamics is activated, the typical time to overcome a barrier B grows exponentially with B/T , T being the temperature; $t_{L,\text{activated}} \sim \exp(B_L/k_B T)$. Hence one would expect that after a time t domains of size

$$L(t) \sim \left(\frac{k_B T}{\Delta} \ln(t/\tau_0) \right)^{1/\psi} \quad (15)$$

are equilibrated (τ_0 being a microscopic time scale), i.e. the typical domain size grows logarithmically slowly with t . Numerically one can determine the typical domain size $L(t)$ directly via the spatial two-replica correlation function

$$G(r, t) = \frac{1}{N} \sum_{i=1}^N \langle S_i^a(t) S_{i+r}^a(t) S_i^b(t) S_{i+r}^b(t) \rangle, \quad (16)$$

where a and b denote two replicas of the same system (i.e. the same disorder realization). For the first time this spatial correlation function was studied numerically for the two-dimensional EA spin glass model in [118], and for the 3d EA model in [119,120,121], later also in [122,123,124,125]. The extraction of the typical time-dependent domain-size, $L(t)$, from the correlation function $G(r, t)$ given in (16) is itself a delicate issue. In the first studies in [119,118,120] the definition $L_T(t) = \int dr G_T(r, t)$ was used where the subscript T signifies the temperature dependence. This form would be justified if $G_T(r, t)$ is of a pure exponential form $G_T(r, t) \sim \exp(-r/L_T(t))$. Also a scaling form $G_T(r, t) \sim \tilde{g}(r/L_T(t))$ has been checked in these early works using the length scale obtained via the integral method and a good data collapse was obtained for all parameter values (times and temperatures) used. A more flexible functional form was assumed in [121] that was also capable of fitting more accurate estimates of $G_T(r, t)$ obtained later:^{123,126}

$$G_T(r, t) \sim r^{-\beta(T)} \tilde{g}(r/L_T(t)). \quad (17)$$

The best-fit values of temperature exponent $\beta(T)$ were found to be constant around 0.5 in three dimensions and decreasing from 1.6 to 0.9 in the temperature range 1.0 to 0.5 in four dimensions (where $T_c \approx 1.8$). In [125] only the tail of $G_T(r, t)$ was used to extract $L_T(t)$ assuming a pure exponential form for it. All in all, these different forms do not cause

large variations in the estimates of $L_T(t)$, the reason simply being that the typical domain sizes reached in the times t accessible to Monte-Carlo studies to date are only a few lattice spacings. It should be noted that these functional forms imply that $G_T(r, t)$ decays to zero with the distance r even in the limit $t \rightarrow \infty$, whereas in the droplet theory one would expect a non-vanishing large distance limit: $\lim_{r \rightarrow \infty} \lim_{t \rightarrow \infty} G_T(r, t) = q_{EA}^2(T) + \mathcal{O}(r^{-\theta})$. Functional forms respecting such an asymptotic behavior can be also devised to fit the data of $G_T(r, t)$ well.¹²⁶

Suppose that we have now estimates of $L(t)$ obtained in one way or the other from numerical simulations or from experiments. (Experimentally there is no straightforward way, by which one could possibly measure $G(r, t)$ or its space and/or time Fourier transform via scattering or similar techniques. Still there is an interesting experimental development¹²⁷ on this point which we discuss further below.) When fitted to the logarithmic growth law (15) the estimated value of ψ was approximately 0.7¹²⁰ and was only acceptable if a finite offset length was introduced. However, a power law form with a temperature dependent exponent

$$L(t) \propto t^{\alpha(T)} \quad (18)$$

fits the data well, with $\alpha(T) \approx 0.16 T/T_c$.^{120,121} This observation may indicate that we must replace the power-law length-dependence of the barriers (14) by the logarithmic dependence

$$B_{L(t)} \propto \Lambda \ln L(t) \quad (19)$$

as suggested in [128,129], or it may serve as a motivation to modify the simple domain growth picture discussed so far in a way that has been first discussed in [124], later also in [130,131,126,125]. The essential idea in these discussions is that the initial coarsening process is still influenced by critical fluctuations — which is plausible since (i) the temperature that are usually studied are not too far from the critical temperature $T/T_c \geq 0.7$ and (ii) in the initial stage the equilibrated length scales are still very small.

Close to T_c the equilibrium correlation length is given by $\xi(T) \sim L_0 |1 - T/T_c|^{-\nu}$, and even at $T < T_c$ the dynamics on length scales $L < \xi$ might be dominated by critical fluctuations rather than activated processes. Hence one might expect that as long as $L < \xi$ the typical size of equilibrated domains grows with time t as $L(t) \sim l_0(t/t_0)^{1/z}$ (l_0 and t_0 being microscopic length and time scales, respectively) and only for $L(t) > \xi$ activated dynamics obeying (15) sets in. Thus a crossover from critical to activated dynamics happens at a time of order $\tau_0(T)/t_0 \sim (\xi(T)/l_0)^z$, when

the typical domain size reaches $\xi(T)$:

$$L(t)/\xi(T) \propto g(t/\tau_0(T)) \quad \text{with} \quad g(x) \sim \begin{cases} x^{1/z} & \text{for } x \ll 1 \\ (\ln x)^{1/\psi} & \text{for } x \gg 1 \end{cases} \quad (20)$$

Thus, if one plots $L(t) \cdot (T_c - T)^\nu$ versus $t \cdot (T_c - T)^{z\nu}$ one expects a data collapse for the time dependent typical domain size at different temperatures. Indeed such a data collapse has been observed in numerical studies of the 4d EA model.¹²⁴

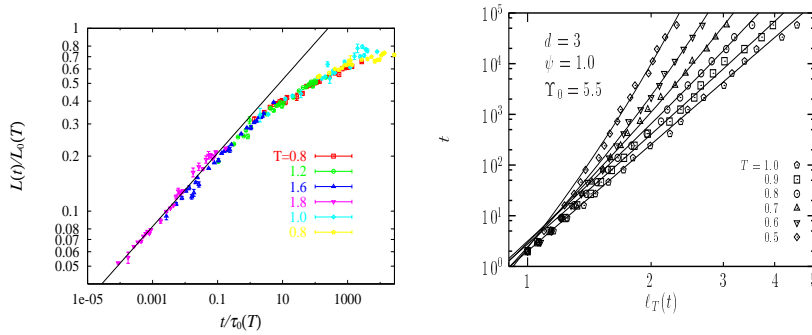


Fig. 6. **Left:** Scaling plot of $L(t)$ of the 4d EA model according to (20), where the SG transition temperature $T_c = 2.0$ and the critical exponent $\nu = 0.93$ are fixed, but the dynamical exponent z is obtained to be 4.98(5) from the best scaling. (From [125].) **Right:** Growth laws of the coherence length in the 3d EA model with fitting curves according to (21). (From [126].)

One can go one step further^{132,126} and write down a more explicit form for the relation between length and time scales, similar to (15) but now taking into account critical fluctuations:

$$t(L) \approx \tau_0 L^z \exp\left(\frac{\Delta(T)L^\psi}{k_B T}\right) \quad \text{with} \quad \Delta(T) \approx \Delta_0/\xi(T)^\psi \quad (21)$$

where Δ_0 is an energy scale of order T_c . Here, following [115], the temperature dependent free energy scale $\Delta(T)$ is assumed to vanish at T_c since one might expect that, in analogy to random bond ferromagnets, the surface tension of the domain walls vanishes at T_c . The pre-factor $\tau_0 L^z$ reflects the critical dynamics on short length scales (when the exponential term is still small) and might be interpreted as a renormalized microscopic time scale $\tilde{\tau}_0$ due to critical fluctuations. In this way, we obtain $t(L)/\tilde{\tau}_0 \approx f(L/\xi(T))$, with $f(x) = \exp(cx^\psi)$ (and $c = \Delta_0/k_B T$) in reminiscence of (20). Note, however, that now the short time critical dynamics is absorbed into $\tilde{\tau}_0$.

In [126] numerical data for the typical domain size $L(t)$ for the 3d and 4d EA model, obtained via Monte-Carlo simulations, were successfully fitted to the form (21). For the barrier exponent, $\psi = 1.0$ was obtained in three dimensions using $\nu = 1.65$ and $z = 7.0$, while in four dimensions $\psi = 2.3$ was obtained using $\nu = 0.8$ and $z = 5.9$.

As we mentioned above, experimentally it appears to be impossible to have a direct access to spatial correlations in spin glass models. However an indirect way to estimate a typical size of correlated volumes has recently been suggested in [127]. When measuring the waiting-time (t_w) dependent thermo-remnant magnetization $M_{\text{TRM}}(t, t_w)$, which is a two-time quantity discussed further below, its logarithmic derivative $S(t) = -dM_{\text{TRM}}(t, t_w)/d(\ln t)$ at the time t after the field has been switched off has a characteristic peak at an *effective* waiting time t_w^{eff} . One observes that the peak position depends on the strength of the field that is applied. Since this time scale is related, via the thermal activation $\tau_{\text{relax}} \sim \tau_0 \exp(\Delta/k_B T)$, to the typical value of the free energy barriers that can be explored over experimental time scales: $\Delta(t_w) \sim k_B T \ln(t_w/\tau_0)$, the shift in the peak position of $S(t)$ contains information on the field dependence of the free energy barriers: $\Delta(t_w) - E_z \sim k_B T \ln(t_w^{\text{eff}}/\tau_0)$, where in [127] it is assumed that E_z is the the magnetic (or Zeeman) energy associated with the change in the magnetic field. The latter is connected to the number N_s of spins that are involved in the barrier shift induced by the field change via $E_z \approx N_s \chi_{\text{fc}} H^2$, where χ_{fc} is the field cooled susceptibility per spin and H the magnetic field strength. If one assumes that the N_s spins to be effectively locked together one gets an estimate for a correlated volume $N_s \propto \xi^3$, i.e an estimate for the coherence length ξ as a function of the waiting time t_w .

By analyzing their data for the peak position of $S(t)$ to obtain $\xi(t_w)$ in the way just described the authors of [127] find that it fits to (18) with $\alpha(T) \approx 0.169 T/T_g$, in agreement with the numerical results reported in [120,121]. A fit to the logarithmic form (15) works equally well, but best-fit value of ψ turns out to be rather large (≈ 5), which does not agree with the numerical estimates cited above. These experiments probe a time window that is different from the one accessible to numerical simulations; each is roughly 6 decade wide but centered around times roughly 10 decades apart. Thus only the algebraic growth law (18), or the form (21) that interpolates between critical and activated dynamics, would consistently match the data of both time windows.

5.2. Two Time Quantities: Isothermal Aging

The out-of-equilibrium properties of glassy materials, quenched rapidly below the glass transition temperature T_g and then aged *isothermally* (i.e. at constant temperature $T < T_g$), manifest themselves most prominently in two-time quantities, typically response functions, susceptibilities or correlation functions. The magnetic response function is defined as

$$R(t + t_w, t_w) = N^{-1} \sum_i \left. \frac{\delta \langle S_i(t + t_w) \rangle}{\delta h_i(t_w)} \right|_{h_i=0} \quad (22)$$

In experiments as well as numerical simulations one usually does not apply field pulses after a waiting time but one switches a constant magnetic field on or off after a waiting time t_w — the corresponding susceptibility is then related to the response function via a time integral

$$\chi(t + t_w, t_w) = \int_{t_w}^{t+t_w} dt' R(t + t_w, t') \quad (23)$$

If one switches the field on at time t_w after the quench and measure the susceptibility, one calls it *zero-field-cooled* (ZFC), whereas if it is switched off it is called *field-cooled* (FC). In the former case the magnetization, which is within the *linear response regime* simply related to the susceptibility via $M(t, t_w) = h \cdot \chi(t, t_w)$, increases with the time t spent in the field, whereas in the latter case it decreases with the time t after the field has been switched off — it is then also called the *thermo-remnant magnetization* (TRM).

Very useful for the development of theoretical concepts is the two-time spin autocorrelation function

$$C(t + t_w, t_w) = N^{-1} \sum_i \langle S_i(t + t_w) S_i(t_w) \rangle. \quad (24)$$

In *equilibrium* it is related to the response function, the susceptibility and the ZFC/FC magnetization via a *fluctuation-dissipation theorem* (FDT). (We discuss the violation of the FDT in the subsection 5.4.) However, since we are out of equilibrium, we have first to regard C as being an independent quantity.

The huge amount of experimental data that have been collected are nicely over-viewed in [111,112]. Let us here simply state the main results. For the field cooled magnetization one observes that the remnant magnetization can be decomposed into a stationary part $M_{\text{eq}}(t)$ that depends on t only and an aging part $M_{\text{aging}}(t + t_w, t_w)$. Sometimes this decomposition is assumed to be multiplicative, $M(t + t_w, t_w) = M_{\text{eq}}(t) \cdot M_{\text{aging}}(t + t_w, t_w)$, as in the universal short time dynamics for coarsening at the critical point,^{133,134}

and sometimes additive, $M(t + t_w, t_w) = M_{\text{eq}}(t) + M_{\text{aging}}(t + t_w, t_w)$, as in coarsening dynamics of pure systems¹¹⁴ and in the out-of-equilibrium theory of mean-field spin glasses.¹¹⁰ Since $M_{\text{aging}}(t + t_w, t_w)$ is approximately constant for $t \ll t_w$ both forms usually fit the data well, although they are fundamentally different. For instance the multiplicative decomposition is incompatible with the existence of a plateau in $C(t + t_w, t_w)$ that occurs in mean-field theories of spin glasses at low temperatures for long waiting times.¹¹⁰ Analogously it is also hardly compatible with a non-vanishing long time limit of $\lim_{t_w \rightarrow \infty} C(t + t_w, t_w)$, which is, within the droplet theory, identical to the order-parameter q_{EA} .

The most remarkable feature of the aging part is that it scales to a good approximation with t/t_w

$$M_{\text{aging}}(t + t_w, t_w) \approx \tilde{M}_{\text{aging}}(t/t_w) \quad (25)$$

In ZFC experiments, instead of applying a constant field after a waiting time t_w , one usually applies a small oscillating field with frequency ω , which essentially means that one measures the t -Fourier transform $\chi(\omega, t_w)$ of $\chi(t + t_w, t_w)$. The frequency ω plays the role of an inverse observation time $1/t$, with $t \ll t_w$. The waiting time t_w is usually in the range of hours or more, while ω is in the range of 0.1Hz to 100Hz, i.e., t is less than ten seconds. Again $\chi(t + t_w, t_w)$ can be decomposed into a stationary part $\chi_{\text{eq}}(\omega)$ and an aging part $\chi_{\text{aging}}(\omega, t_w)$ that now scales to a good approximation with ωt_w :

$$\chi_{\text{aging}}(\omega, t_w) \approx \tilde{\chi}_{\text{aging}}(\omega t_w) \quad (26)$$

corresponding to the aforementioned t/t_w scaling for M_{FC} . Numerically one also has access to the spin autocorrelation function (24), which can also be decomposed into two parts. In [120] it has been shown that (i) the equilibrium part $C_{\text{eq}}(t)$ decays algebraically with a very small temperature-dependent exponent $x(T)$ and (ii) that $C_{\text{age}}(t + t_w, t_w)$ again obeys to a good approximation the t/t_w scaling:

$$C_{\text{eq}}(t) \approx A t^{-x(T)} \quad \text{and} \quad C_{\text{age}}(t + t_w, t_w) \approx \tilde{c}(t/t_w), \quad (27)$$

where the scaling function \tilde{c} behaves as $\tilde{c}(x) \propto x^{-\lambda(T)}$ with $\lambda(T)$ being a temperature-dependent exponent much larger than $x(T)$. This behavior was also found for the 4d EA model.¹⁰⁵ Later studies¹²⁶ focused on small but systematic deviations in the aging part from a simple t/t_w scaling behavior; the values of $C_{\text{age}}(t + t_w, t_w)$ for fixed ratio t/t_w show a slight tendency to decrease with increasing t_w , which is called *sub-aging* and is interpreted in

terms of an *effective relaxation time* t_{eff} that is smaller than the actual waiting time t_w . We shall return to this point later.

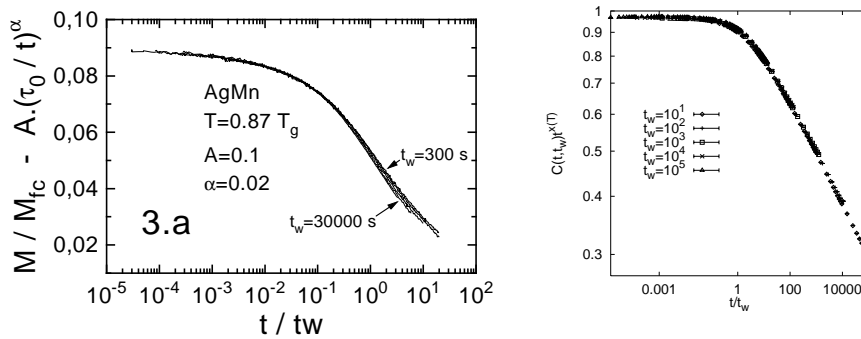


Fig. 7. **Left:** Aging part of the FC magnetization $M_{FC}(t+t_w, t_w)$ measured in an AgMn spin glass: the estimated stationary contribution $M_{eq}(t)$ has been subtracted from the full measured value. The data is plotted versus t/t_w . The deviations from perfect t/t_w scaling occur for $t \sim t_w$ (sub-aging) and can be accounted for by choosing $h(t+t_w)/h(t_w)$ with $h(t)$ given in (30) as a scaling variable. (From [111].) **Right:** Autocorrelation function $C(t+t_w, t_w)$, divided by $t^{-x(T)} \propto C_{eq}(t)$, versus t/t_w for $T = 0.4$ in the 3d EA model. (From [120].)

Within a domain growth (or droplet) picture of the out-of-equilibrium dynamics of spin glasses,¹¹⁵ only *one* characteristic length scale $L(t)$ for a given time t after the quench is assumed to exist. One would then expect that two-time quantities depend only on the ratio of the two length scales that are equilibrated within the two times t_w and $t+t_w$:

$$O_{aging}(t+t_w, t_w) \sim \tilde{o}(L(t+t_w)/L(t_w)), \quad (28)$$

where $O(t+t_w, t_w)$ is any two-time observable (such as R , χ , M or C) and \tilde{o} the corresponding scaling function. The first observation is that an algebraic growth law, (18) for instance, would then be completely compatible with the t/t_w scaling of the aging part of various observable reported so far. Note also that as long as $L(t)$ depends algebraically on t the use of the scaling variable $L(t_w)/L(t)$ is equivalent to using $L(t+t_w)/L(t_w)$, both end up to be some function of t/t_w .

In the case of logarithmic domain growth (15), on the other hand, the scaling with $L(t_w)/L(t)$ is different from the scaling with $L(t+t_w)/L(t_w)$, and one should note that droplet scaling,¹¹⁵ as it is usually applied to the experimental and numerical data, is assumed to work with

$L(t_w)/L(t)$,^{135,124,131} where $L(t_w)$ is the typical size of the domains after waiting time t_w and $L(t)$ is the typical size of the droplets being activated in the time t or being polarized by an ac field of frequency $\omega = 1/t$. The basic physical idea behind this scaling form is that the presence of a domain wall effectively reduces the excitation gap of droplets that it touches.

However, assuming the simple logarithmic growth law (15), $L(t) \approx ((k_B T/\Delta) \ln(t/\tau_0))^{1/\psi}$, the numerical as well as the experimental data turn out not to scale with $L(t_w)/L(t)$ as suggested by the droplet theory^{115,135} (it does not scale with $L(t+t_w)/L(t_w)$, either, which is incompatible with the experimental observation of sub-aging). For some time this observation was taken as an indication that the droplet theory might be inappropriate to describe the out-of-equilibrium properties of spin glasses, at least for the time scales accessible to experiments and to numerical studies. However, recently it was pointed out¹³¹ that, taking into account the crossover from critical to activated dynamics already discussed in the last subsection, the apparent inconsistency of the data with the droplet theory disappears. There experimental data for the (imaginary part of the) susceptibility $\chi(\omega, t_w)$, measured for the 3d Ising spin glass $\text{Fe}_{0.5}\text{Mn}_{0.5}\text{TiO}_3$ and the 3d Heisenberg spin glass $\text{Ag}(11\% \text{ at Mn})$, were presented. The aging part $\chi''_{\text{aging}}(\omega, t_w)$ (obtained after subtracting a fitted equilibrium part χ''_{eq}) was shown to scale as $L(t_w)/L(1/\omega)$ with $L(t)$ following the logarithmic growth law (15), where the microscopic time and energy scale τ_0 and Δ replaced by a temperature dependent characteristic time and energy scale, $\tau_c(T)$ and $\Delta(T)$. This replacement captures the features of the critical, short-time dynamics close to the critical point: $\tau_c(T) \sim \tau_m \xi^z$ and $\Delta(T) \sim \xi^{-\psi}$ ($\xi = |1 - T/T_c|^{-\nu}$ being the correlation length), which is in the same spirit as (20) and (21).

The authors of [131] found a very good data collapse when plotting their data for $(\chi''(\omega, t_w) - \chi_{\text{eq}})/\chi''(\omega, t_w)$ versus the scaling variable $\ln(t/\tau_c(T))/\ln(\omega^{-1}\tau_c(T))$ (which is $L(t)/L(1/\omega)$, since $\Delta(T)$ and $k_B T$ cancel in this ratio). Given the critical exponents ν and z from earlier studies, the fitting parameters are ψ , the whole equilibrium part χ_{eq} (for which an explicit functional form predicted by the droplet theory was used) and a microscopic time scale τ_m . They found $\psi \approx 1.9$ for the Ising spin glass, which was much larger than what had been reported before in experiments¹³⁶ (see also [130,132]) and in the numerical simulations discussed in the previous subsection, and $\psi \approx 1.3$ for the Heisenberg spin glass. The authors of [131] showed that their experimental data are also compatible to the ωt_w scaling.

So far, we have discussed the compatibility of numerical and experimental data with a simple (or simplified) domain growth picture. Mean field

models, however, show a more complicated behavior.^{110,137} The mean field theory for the out-of-equilibrium dynamics predicts “ultra-metric behavior” in the time domains^{138,139,140}:

$$O_{\text{aging}}(t + t_w, t_w) = \sum_i \mathcal{O}_i(h_i(t + t_w)/h_i(t_w)), \quad (29)$$

where the infinite sum over the index i refers to various large time sectors^{138,110} defined by the ratio of $h_i(t + t_w)/h_i(t_w)$ being of order 1, where the different (unknown) functions $h_i(t)$ represent different physical mechanisms at work during aging and need not necessarily to be related to domain sizes. They are monotonously increasing and grow differently such that when $0 < h_i(t + t_w)/h_i(t_w) < 1$ holds for an index i then $h_j(t + t_w)/h_j(t_w) = 1$ for all larger indices $j > i$ — implying that if two times t_1 and t_2 belong to the time sector defined by h_i and t_2 and t_3 to the one defined by h_j with $j > i$, then t_1 and t_3 also belong to the sector defined by h_i . One simple example for $h_i(t)$ is

$$h_i(t) = \exp\{(t/t_0)^{1-\mu_i}/(1-\mu_i)\}, \quad (30)$$

with $0 < \mu_i < 1$ ($\mu = 1$ yields a t/t_w -scaling, $\mu = 0$ time-translational invariance).

A consequence of such an Ansatz is for instance a hierarchy in these large-time sectors, called *dynamic ultrametricity*, which for the correlation function C means that in the limit of large times $t_1 < t_2 < t_3$

$$C(t_3, t_1) = \min\{C(t_2, t_1), C(t_3, t_2)\} \quad (31)$$

holds. A number of consequences can be drawn from this Ansatz.^{110,137} Among them is a particular form of the violation of the fluctuation-dissipation relation, which we discuss later. Let us here just state that mean-field theory predicts a richer scenario for glassy out-of-equilibrium dynamics than the domain growth picture with only one waiting-time-dependent length-scale. However, as rich as this scenario is, all experimental data for real spin glasses and all numerical data for spin glasses with short-range interactions obtained for isothermal aging up to now can, to our knowledge, be scaled nicely with one single large-time domain, i.e. with only one term appearing in the infinite sum (29).

For instance, the aforementioned sub-aging property of two-time quantities that has been observed in experimental data^{111,141} (and also in analytically tractable coarsening, non-spin glass, models^{142,143}) can easily be accounted for by taking only a single term in the sum (29) with $h(t)$ being the function defined in (30) and with the exponent μ now being a fitting

parameter. This form was actually used in the earliest experiments on aging in polymer glasses,¹⁴⁴ and later also in spin glass experiments.¹¹¹ The exponent μ commonly turns out to be not very different from 1, accounting for the fact that the deviations from simple t/t_w scaling are usually very small. In numerical simulations of $3d$ models the scaling with t/t_w , i.e. $\mu = 1$, is almost perfect. In four dimensions the numerical data for $C(t + t_w, t_w)$ tend to show *super-aging*,¹²⁶ i.e. the values of $C_{\text{age}}(t + t_w, t_w)$ for fixed ratio t/t_w show a slight tendency to increase with increasing t_w . This can be interpreted by an effective relaxation time that grows faster than t_w , and it can be shown that the aging part $C_{\text{age}}(t + t_w, t_w)$ scales nicely with $h(t + t_w)/h(t_w)$, when $\mu > 1$ for $h(t)$ in from (30) is chosen (which bears unfortunately mathematical inconsistencies¹⁴⁵). However, the data can also be scaled with a domain growth scaling form (21) and a non-vanishing long time limit for the equilibrium part.¹²⁶

5.3. More Complicated Temperature Protocols

From what we learned from isothermal-aging experiments described in the last subsection, it follows that the dynamics of a spin glass depends crucially on the age of the system, i.e. the time t_w that it spent in the glass phase, i.e. at $T < T_g$. Moreover, as experiments have impressively demonstrated,^{111,112} it depends sensitively on changes of temperature (and also field) *during* this waiting time t_w . A major goal of their systematic study described in this subsection is to understand the different phenomena that are measurable by applying different protocols (i.e. temperature variations during aging) and relating them to a theoretical picture, if not a theory, of the out-of-equilibrium dynamics of spin glasses.

The simplest experiments in this direction are small-temperature-shift experiments.¹⁴⁶ The protocol is as follows. First the system is rapidly quenched below T_c to a temperature T_1 where it is aged for a waiting time t_w . Then the temperature is shifted to a new temperature $T_2 = T_1 \pm \Delta T$ and the measurement is started. The first systematic numerical study of such a protocol was performed for the $3d$ EA model in [147] and a little later in [126]. It was observed that the decay of the correlation function is slower for negative shifts ($T_2 < T_1$) when compared with the same function aged isothermally at T_1 . For small shifts ΔT the functional form of $C(t + t_w, t_w)$ is the same as that for isothermal aging, and it can be matched with it using an effective waiting time $t_w^{\text{eff}} < t_w$ for $T_2 < T_1$. If one assumes that the barriers that the system can surmount during a time t_w at temperature

T_1 are of the same size as those that it can surmount during a time t_w^{eff} at temperature T_2 , one obtains a good agreement with the numerical data, only if one replaces the microscopic time τ_0 by the typical time scale for critical dynamics as in (21).¹²⁶

Obviously such an interpretation of the numerical results implies that successive aging at two different temperatures will add to each other in a full accumulative way. The effective age t_w^{eff} is a monotonically increasing function of t_w and also depends on the pair (T_1, T_2) : $t_w^{\text{eff}} = f_{T_1, T_2}(t_w)$, and t_w can be related to t_w^{eff} by the inverse: $t_w = f_{T_1, T_2}^{-1}(t_w^{\text{eff}})$. In [148] twin-experiments — negative shift from T_1 to T_2 and positive shift from T_2 to T_1 — were considered. A criterion for purely accumulative aging would be $f_{T_1, T_2}^{-1}(t) = f_{T_2, T_1}(t)$ and in contrast to the aforementioned numerical results deviations from it were observed in these experiments for $\Delta T/T_c \geq 0.01$, i.e. still very small shifts. The authors then concluded that positive and negative temperature shifts both cause a restart of aging and these findings were then interpreted as a symmetrical *temperature-chaos* effect.^{148,149,150}

The temperature chaos in spin glasses is one of the basic ingredients of the droplet theory¹¹⁵ and implies that the equilibrium configurations at two different temperatures T_1 and $T_2 = T_1 \pm \Delta T$ below T_g are uncorrelated beyond a length scale called the *overlap-length*, $l_{\Delta T} \sim (\Delta T)^{-1/\zeta}$, where ζ is the chaos exponent. A number of experimental results, in particular obtained from temperature-shift or temperature-cycling experiments,¹¹² have been interpreted within this scenario. Numerical estimates of the value of ζ are based on small variations of the *couplings* J_{ij} (via $J_{ij} \rightarrow J_{ij} + \delta_{ij}$ with δ_{ij} small and random) at $T = 0$ ^{151,152} rather than variations of the temperature, simply because ground states of spin glasses, in particular in $d = 2$ can be obtained more easily than equilibrated configurations at small T . The reported estimates are $\zeta \approx 1$ both in two and three dimensions. While the same exponent was reported for temperature chaos (via Monte-Carlo simulations) in the two dimensional case, recent large scale numerical studies of the $3d$ EA model did not show any evidence for temperature chaos in spin glasses on the length and time scales that could be probed.¹⁵³ Even if temperature-chaos exists in three dimensional spin glasses, the overlap length might be much larger than the length-scales that have been equilibrated during a particular waiting time, which then makes the chaotic rearrangements due to the temperature shift invisible. However, there still might be some effect due to dangerously irrelevant droplets whose free energy gaps are quite small, as discussed in [125,150,154].

The next temperature protocols that we discuss here are larger shifts

and cycles $T_1 \rightarrow T_2 \rightarrow T_1$.¹¹¹ The first shift experiments was reported in [155] whereas the cycle experiments can be found in [156]. The first qualitative numerical study of this kind was reported in [157]. In the theory of the asymptotic out-of-equilibrium dynamics of mean-field spin glass models one can understand these effects on the basis of infinitely many time scales organized in a hierarchical — ultra-metric — way (which we will discuss in section 5.4).

A systematic numerical study of large-shift and cycle experiments was recently performed for the 3d and 4d EA model in [126]. The basic message of large temperature shift experiments is that, independent of the sign of $T_1 - T_2$, aging is “restarted” at the new temperature. This *rejuvenation effect* can nicely be observed in experiments as well as in simulations through the measurement of the susceptibility $\chi(\omega, t_w)$. Rejuvenation after a negative temperature shift comes from fast modes^{158,159,126} which were equilibrated at T_1 , but fall out of equilibrium and are slow at T_2 . Therefore, one should expect to see this phenomenon if the spin configurations in the equilibrated regions (on length scales $\leq L_{T_1}(t_w)$) are sufficiently different at the two temperatures. This mechanism is obviously qualitatively different from the interpretation involving the notion of temperature chaos (see above), which implies that length scale smaller than the overlap length are essentially unaffected by the temperature shift, while larger length scales are completely reshuffled by the shift. In this picture, rejuvenation is thus attributed to *large* length scales and strong rejuvenation effects therefore require a very small overlap length.

No clear rejuvenation effects have ever been observed in simulations of the 3d EA model.^{157,160,161,162} This was first attributed to the fact that the overlap length was perhaps numerically large, so that no large scale reorganization could be observed on the time scale of the simulation. However, in the fast-mode mechanism mentioned above, the crucial ingredient is the small-scale reorganization due to a temperature shift. When comparing the spatial correlation function $G_T(r, t_w)$ at two different temperatures and waiting times such that the length scales $L_{T_1}(t_{w_1}) = L_{T_2}(t_{w_2})$, there is nearly no difference even for quite large $\Delta T = T_1 - T_2$ in three dimensions but significant differences in four dimensions,¹²⁶ which is compatible with the observation that the exponent $\beta(T)$ in (17) remains roughly constant for a large temperature interval in three dimensions whereas it varies significantly in four dimensions. This observation suggests that the 4d EA model should be more favorable in studying temperature shift/cycle protocols. The numerical simulations of the 4d EA model show indeed a clear reju-

venation effect in $\chi(\omega, t_w)$, increasing smoothly with ΔT , which one would not expect within the temperature chaos picture. (See Fig.8 (Right).)

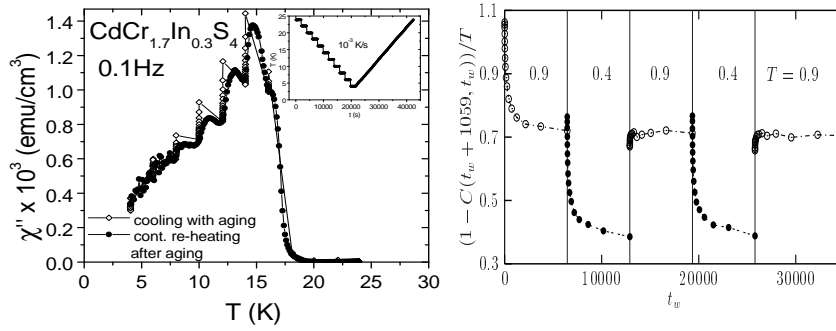


Fig. 8. **Left:** Series of ‘dip’ imprinted on the a.c. susceptibility by successive stops at different temperatures while the system is cooled. Further cooling ‘rejuvenates’ the system (i.e the susceptibility goes up). However, the dips are one by one remembered by the system when heated back. For more details, see [163]. (The figure is adopted from [132]). **Right:** Evolution of the ‘a.c.’ correlation function taken from Monte-Carlo simulations of the $4d$ EA model in the procedure $T = \infty \rightarrow T_1 = 0.9 \rightarrow T_2 = 0.4 \rightarrow T_1 \rightarrow T_2$, showing, as in experiments the coexistence of rejuvenation and memory effects (from [126]).

The experimental procedure for cycles is $T = \infty \rightarrow T_1 \rightarrow T_2 < T_1 \rightarrow T_1$. The time spent at T_1 is t_s and the time spent at T_2 is t'_s . The spectacular *memory effect* arises when the temperature is shifted back to T_1 . It is observed that although aging was fully restarted at T_2 , the system has a strong memory of the previous aging at T_1 . The dynamics at T_1 proceeds almost as if no cycle to T_2 has been performed.¹⁵⁵ The coexistence of rejuvenation and memory was made even more impressive in a multiple step, or *dip* experiment,¹⁶³ in which the temperature was decreased to T_1 , then maintained for some time, then further decreased to $T_2 < T_1$, again maintained, then further decreased to $T_3 < T_2$ etc. At some lowest temperature the sample was then re-heated with the same rate as it was cooled before, but now without the interrupts at T_1, T_2, T_3, \dots . As shown in Fig.8 (Left), on the way down to the final temperature the susceptibility $\chi(\omega)$ as a function of the temperature showed clear dips at T_1, T_2, T_3, \dots , which is the rejuvenation effect. Most remarkably the same dips reappear in $\chi(\omega)$ on the way up, which is the memory effect. The spin glass has memorized the individual temperatures at which the constant cooling was interrupted for

some time.

According to [132] the memory effect is a simple consequence of the separation of time and length scales, also observable in simpler slowly coarsening systems with activated dynamics.¹⁵⁹ When the system is at $T_2 < T_1$, rejuvenation involves very small length scales as compared to the length scales involved in the aging at T_1 . Thus when the temperature is shifted back to T_1 , the correlation of length scale $L_{T_2}(t'_s)$ nearly instantaneously re-equilibrate at T_1 . The memory is just stored in the intermediate length scales, between $L_{T_2}(t'_s)$ and $L_{T_1}(t_s)$. How such a storage mechanism actually works in a microscopic model for a finite-dimensional spin glass, like the EA model, is a challenging question. Progress has been made for simpler microscopic models, such as the $2d$ Mattis model, a simple coarsening model,¹⁶⁴ or the directed polymer in a random medium.¹⁶⁵ Also experiments on random *ferromagnetic* systems,^{166,167,168,169,170} on random *ferroelectric* systems^{171,172} and on frustrated systems without a spin glass transition at finite temperatures¹⁷³ show strong rejuvenation effects and a weak memory effect. This indicates that the existence of “many pure states” as predicted by Parisi’s equilibrium solution of the Sherrington-Kirkpatrick model and the interpretation of these non-equilibrium effects based on it (in terms of a diffusion in a hierarchical space^{174,111}) are not necessary prerequisites to observe rejuvenation and memory in the out-of-equilibrium dynamics.

Nevertheless the hierarchical picture might be relevant in more complex situations and a concrete implementation was proposed in [175] in terms of a thermally activated random energy model (for an overview see [110]). Here to each level of a hierarchical tree a transition temperature is associated, such that for each level the dynamics is stationary for higher temperatures and aging for lower temperatures. A small decrease of temperature induces some rejuvenation by driving out of equilibrium a new level of the tree, while freezing out the dynamics at the upper levels, thereby allowing the memory to be conserved. This model was recently studied further,¹⁷⁶ where it was shown numerically that the rejuvenation/memory effect is indeed already reproduced with two levels. A real space interpretation of this hierarchical tree was proposed in [175,177], and further developed in [159] in terms of a multi-scale dynamics. Low levels of the tree correspond to short wavelength modes, which are only frozen at low temperature, while large wavelength modes are frozen at a higher temperature and constitute a *backbone*, where memory is imprinted. In the context of domain walls this picture is particularly clear¹⁵⁹ and should apply directly to disordered ferromagnets

where the slow dynamics comes from the motion of these pinned domain walls.^{166,167,168,169,170}

5.4. Violation of the Fluctuation-Dissipation Theorem

In a system in equilibrium the response R to an external magnetic field (Eq.(22)) and the autocorrelation function C (Eq.(24)) depend only on the time difference t , i.e., $R(t + t_w, t_w) = R_{\text{eq}}(t)$ and $C(t + t_w, t_w) = C_{\text{eq}}(t)$, and are related to each other through the fluctuation-dissipation theorem (FDT)

$$R_{\text{eq}}(t) = -\frac{1}{T} \frac{\partial C_{\text{eq}}(t)}{\partial t}. \quad (32)$$

In a system that is out-of-equilibrium this relation is generally not valid and the violation of FDT can be parameterized through a violation factor $X(t + t_w, t_w)$:

$$R(t + t_w, t_w) = -\frac{X(t + t_w, t_w)}{T} \frac{\partial C(t + t_w, t_w)}{\partial t_w}, \quad (33)$$

where the differentiation is done with respect to t_w , not the time difference t as in (32). In analytic studies of mean-field systems it can be shown¹³⁸ that for large times ($t_w \rightarrow \infty$) X depends on t and t_w only through the value of the correlation function. Hence $X(t + t_w, t_w) = X[C(t + t_w, t_w)]$. In particular, when $C > q_{EA}$ it is $X = 1$ and the FDT is recovered. In essence, the asymptotic dependence of X on the values of C alone underlies the decomposition into asymptotic time domains discussed in subsection 5.2 under (29). It turns out¹⁷⁸ that the *effective temperature* $T_{\text{eff}}(t + t_w, t_w) = T/X(t + t_w, t_w)$ is precisely the temperature which would be read on a thermometer with response time t (or frequency $\omega \sim 1/t$) when connected to the magnetization at time t_w . A “fast” thermometer of response time $t \ll t_w$ will then probe the stationary regime for which $X = 1$ and thus measure the heat-bath temperature.

Different scenarios of the FDT violation can occur. **(A)** $X(C) = 1$ for all C implies the system is in equilibrium, e.g. in the paramagnetic phase of a spin glass. **(B)** Coarsening systems with $q_{EA} = m^2$ have $X(C) = 1$ for $C > q_{EA}$ and $X(C) = 0$ for $C < q_{EA}$. **(C)** So called *discontinuous* spin glasses, such as the spherical mean field spin glass model with p -spin interactions ($p \geq 3$),¹³⁸ have $X(C) = 1$ for $C > q_{EA}$ and $X(C) = x_1 < 1$ for $C < q_{EA}$, where x_1 is a constant. This corresponds to the existence of only *one* asymptotic time domain (see (29)), and the two-time quantities

are expected to scale with only one (possibly unknown) function $h(t)$ ¹⁷⁹ (D) So called *continuous* spin glasses, like the SK model, have $X(C) = 1$ for $C > q_{EA}$ and $X(C)$ continuously varying, non-constant function of C for $C < q_{EA}$.¹³⁸

A convenient way to extract the function $X(C)$ is to measure the auto-correlation function $C(t + t_w, t_w)$ and the susceptibility $\chi(t + t_w, t_w)$, (23), for a situation in which a (infinitesimal) small homogeneous external field h is switched on after a time t_w (in which case the induced magnetization is zero-field-cooled and $\chi(t + t_w, t_w) = \lim_{h \rightarrow 0} M_{ZFC}(t + t_w, t_w)/h$). In this case we have

$$\begin{aligned} \chi(t + t_w, t_w) &= \int_{t_w}^{t+t_w} dt' R(t + t_w, t') \\ &= \frac{1}{T} \int_{t_w}^{t+t_w} dt' X[C(t + t_w, t')] \frac{\partial C(t + t_w, t')}{\partial t'}. \end{aligned} \quad (34)$$

As long as the function $C(t + t_w, t')$ is monotonously increasing with t' for fixed time $t + t_w$, the substitution of $X(t + t_w, t')$ by $X[C(t + t_w, t')]$ is legitimate. One should keep in mind that then $X[C]$ still has a t_w -dependence (that we could indicate by $X_{t_w}[C]$), which however vanishes in the limit $t_w \rightarrow \infty$. Hence one gets (with $C(t + t_w, t + t_w) = 1$):

$$\chi(t + t_w, t_w) = \int_{C(t+t_w, t_w)}^1 dC X[C] \quad \text{or for fixed } t_w : \quad \frac{d\chi}{dC} = -\frac{X[C]}{T} \quad (35)$$

which implies that for fixed waiting time the slope of a parametric plot of $\chi(t + t_w, t_w)$ versus $C(t + t_w, t_w)$ yields $X_{t_w}[C]$. In the limit $t_w \rightarrow \infty$ one should obtain the desired FDT-violation $X[C] = \lim_{t_w \rightarrow \infty} X_{t_w}(C)$.

The first study of the FDT violation function $X(C)$ in the $3d$ EA model was performed in [180] (the first report of an FDT violation was actually already presented earlier in [181]). The non-constant part of $X(C)$ still showed a small but systematic t_w -dependence for the small- C branch of the curve $X(C)$. Since no tendency to approach a straight line (scenario B or C) could be observed the data were interpreted as an indication for scenario D, which implies that the $3d$ EA model has an out-of-equilibrium dynamics that is similar to the SK model. Later studies confirmed this result, in three dimensions¹²³ as well as in four dimensions.¹⁸² However, in [125] it was proposed that the numerical data for the FDT-violation in the $3d$ EA-model (as well as those for the spatial correlations and the two-time quantities) can be interpreted in view of an extended droplet theory and that for the $3d$ EA model scenario B (essentially slow coarsening in

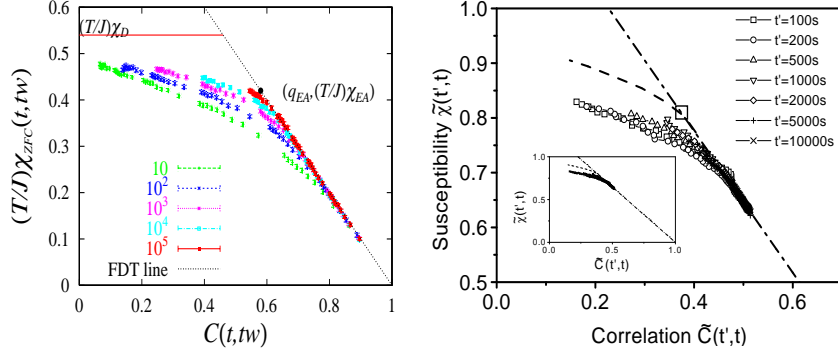


Fig. 9. **Left:** Parametric plot $(T/J)\chi_{ZFC}(t + t_w, t_w)$ vs $C(t + t_w, t_w)$ at $T/J = 1.2$ for the $4d$ EA model. The straight tangent lines represents the FDT. The convergence points of the break points of time translational invariance $(q_{EA}, (T/J)\chi_{EA})$ and the break points of FDT $(q_D, (T/J)\chi_D)$. (from [125]) **Right:** FDT-plot obtained from the experiments performed in [185]. Relaxation measurements are plotted versus correlation functions for each t' . The dot-dashed line (FDT line) is calculated for $T = 0.8T_g = 13.3K$, from a calibration obtained with a copper sample. The dashed line represents the scaling extrapolation for $t' \rightarrow \infty$. The branching point with the FDT line, corresponds to $\tilde{C} = q_{EA}$ (square symbol, with size giving the error range). In Inset, the same data in the whole range. (from [185]).

the spirit of the droplet model) is appropriate. (See Fig.9 (Left).) Since numerical simulations can cover only a few decades of the waiting time t_w and there is, as mentioned above, still a significant t_w dependence in $X(C, t_w)$ in the numerical data,^{183,184} a definite statement is hard to make.

For a clear experimental demonstration of the FDT violation one has to measure both; response and autocorrelation function (in [186] possible indications of the FDT violation based only on the response have been discussed). Such an experimental evidence of the violation of the FDT in spin glasses has been presented for the first time in [185] (for a structural glass, glycerol, it has been measured in [187], for a colloidal glass, laponite, in [188]), where autocorrelation function $C(t + t_w, t_w)$ has been measured via the magnetization fluctuations in a spin glass sample and the susceptibility $\chi(t + t_w, t_w)$ in the usual way by applying a magnetic field. (See Fig.9 (Right).) The χ versus C plots show still a strong waiting time dependence and give some room for extrapolations to the long time limit — one that is suggested by the authors has similarities to the one for the SK-model. On the other hand, the aging part of their data for C and χ scale perfectly with $h(t_w)/h(t)$ where $h(u) = \exp(u^{1-\mu}/(1-\mu))$ with $\mu = 0.85$, which would not correspond to what one expects for the SK model.

The action for the long-time asymptotic behavior of the generating functional for the correlation and response functions is invariant under a time re-parameterization $t \rightarrow h(t)$, simply because in the long-time regime a re-parameterization of time with a monotonous function does not change the ultra-metric relation in the time ordering. The global invariance under the re-parameterization group (RpG) for mean-field models was recently extended^{189,190} to its local variant for short range models to treat fluctuations. In analogy to Heisenberg magnets, where the global spin rotation invariance lead to the existence of spin waves in finite dimensional models via the Goldstone modes, the authors proposed that local time re-parameterizations play a similar role for the asymptotic dynamics of short-range spin glasses. One consequence of this observation is that one expects fluctuations in local correlation functions and local susceptibilities

$$C_r(t+t_w, t_w) = \overline{S}_r(t+t_w)\overline{S}_r(t_w), \quad \chi_r(t+t_w, t_w) = \overline{S}_r(t+t_w)|_{h_r(t)=h\theta(t)}/h, \quad (36)$$

where $\overline{S}_r(t)$ means a slightly coarse-grained spin value at position r and time t , i.e. it involves a spatial average of the spin values over a small volume centered around r and a time average over a small time window centered around t . If the volume is extended to the system size, the usual global quantities discussed above are recovered. These spatially fluctuating quantities then have a joint probability distribution $\rho(C_r, \chi_r)$ that stretches along the FDT-relation $\chi(C)$ for the global quantities χ and C , as has been shown numerically in [190].

5.5. Hysteresis in Spin Glasses

Due to the complex energy landscape of spin glasses one expects strong hysteresis effects, which were studied recently via Monte-Carlo simulations^{191,192,193,194} also using new techniques such as the recently introduced First Order Reversal Curve (FORC) method.¹⁹⁵

In [193], the zero temperature dynamics of the $2d$ EA spin glass model was simulated with a varying external field H . The procedure used there was as follows. The magnetic field is changed in small steps, first downward from positive saturation and then upward from a reversal field H_R . After each field step, the effective local field h_i of each spin S_i is calculated: $h_i = \sum_j J_{ij}S_j - H$. A spin is unstable if $h_i S_i < 0$. A randomly chosen unstable spin is flipped and then the local fields at neighboring sites are updated. This procedure is repeated until all spins become stable.

The first important observation was of a memory effect in the hysteresis

of the $2d$ EA spin glass model that emerged when the magnetic field was first decreased from its saturation value and then increased again from some reversal field H_R . It was found that the EA spin glass exhibited a singularity at the negative of the reversal field, $-H_R$, in the form of a kink in the magnetization of the reversal curve (See Fig.10).

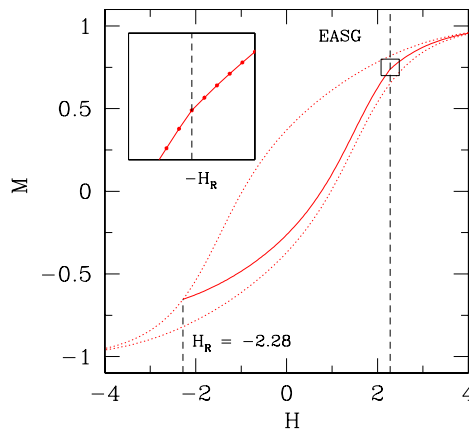


Fig. 10. Reversal curve (solid line) and major hysteresis loop (dotted line) for a two-dimensional (2D) EA spin glass with 10^4 spins and $H_R = -2.28$. In the inset a kink is seen around $-H_R$. (From [193]).

One can describe this effect within a phenomenological approach to hysteretic systems, the Preisach model.¹⁹⁶ In the Preisach model a magnetic system is described as a collection of independent two-state (± 1) switching units, or “hysteron”. Unlike Ising spins, which always align with their local field, the hysteron’s state changes from -1 to $+1$ at a field $H_b + H_c$, different from the field $H_b - H_c$, required to switch the hysteron from $+1$ to -1 . Different systems are distinguished by their different distributions $\rho(H_b, H_c)$ of hysterons of a given bias H_b and coercivity H_c . Here $\rho(H_b, H_c)$ is the so-called “Preisach function”.

This function was extracted by a tool developed for analyzing experimental data of hysteretic systems.¹⁹⁵ A family of First Order Reversal Curves (FORCs) with different H_R was generated, with $M(H, H_R)$ denoting the resulting magnetization as a function of the applied and re-

versal fields. Computing the mixed second order derivative $\rho(H, H_R) = -(1/2)[\partial^2 M / \partial H \partial H_R]$ and changing variables to $H_c = (H - H_R)/2$ and $H_b = (H + H_R)/2$, the local coercivity and bias, respectively, yielded the “FORC distribution” $\rho(H_b, H_c)$. For phenomenological Preisach models, the FORC distribution is equal to the Preisach function. However, the definition of the FORC distributions is more general, because it is extracted from numerical or experimental data, and thus is model-independent.

Fig. 11 shows the FORC diagram of the EA spin glass. The ridge along the H_c axis in the range $1.5 < H_c < 4.0$ corresponds to the kinks of Fig. 10. Thus FORC diagrams capture the reversal-field memory effect in the form of a ridge along the H_c axis. In Fig. 11 also the experimentally determined FORC diagram of thin films of well-dispersed single-domain magnetic Co- γ -Fe₂O₃ particles provided by Kodak Inc is shown. It clearly exhibits the horizontal ridge associated with the reversal-field memory effect. This striking similarity between the experimentally determined FORC diagram of the Co- γ -Fe₂O₃ films and the numerically determined FORC diagram of the EASG indicates not only that Co- γ -Fe₂O₃ films exhibit reversal-field memory but also that frustration may be a component of the physics of the Co- γ -Fe₂O₃ films. Note that for instance the 2d random field Ising model does NOT exhibit a reversal-field memory and that its FORC diagram has a vertical ridge rather than a horizontal one.¹⁹³

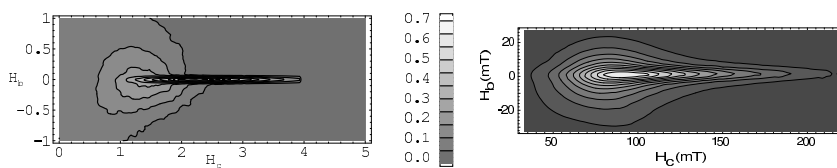


Fig. 11. **Left:** FORC Diagram of the EASG. Note the ridge along the H_c axis. **Right:** Experimental FORC diagram of a Kodak sample. Note the similarity to the FORC diagram of the EASG shown in the left diagram. (From [193]).

6. Equilibrium Properties of Classical XY and Heisenberg Spin Glasses

6.1. Continuous Spin Models in Three Dimensions

Compared to Ising spin glass models, less effort has been devoted to the models with continuous spins. One of the reasons might be that the minimal model of spin glasses, the Ising spin glass model, already shows a

highly non-trivial behavior and poses serious difficulties to reach a final conclusion. Nonetheless, the continuous spin models are worth studying for several reasons. An obvious reason is that, in many real spin glass materials such as AuFe and CuMn, the magnetic anisotropy is much smaller than the (isotropic) exchange interaction. For these materials, therefore, the Heisenberg spin glass models would be more realistic than the Ising spin glass models.

However, the continuous spin models in three dimensions had long been thought of as models without a spin glass transition, which is another reason why the continuous spin models have not been studied so extensively until recently. The scenario that seemed to explain this apparent disagreement between the models and the materials was that the anisotropy is a relevant perturbation and, no matter how small it may be, it changes the system to an Ising-like spin glass, giving rise to a finite temperature phase transition. This is quite analogous to what happens when a small amount of Ising anisotropy was introduced to the isotropic Heisenberg model (with no disorder) in two dimensions. If this scenario is valid, the critical behavior of any spin glass material should be the same and fall into the Ising-spin-glass universality class. However, there are some qualitative differences between experimental results for materials with a small anisotropy and numerical results for the Ising spin glasses. In particular in a series of recent torque experiments [197,198] of Heisenberg spin glass samples with varying degree of anisotropies indications for a freezing transition even within an external field were found (implying the applicability of a mean field or RSB scenario rather than a droplet scenario to these Heisenberg spin glass systems). More surprisingly, the transition in spin glass materials with lower anisotropy (more Heisenberg-like) appeared to be more robust against the application of an external field than those with higher anisotropy (more Ising like), which is in contrast with the traditional view that higher anisotropy implies a stronger tendency to order. These observations call for further theoretical investigations, and here we report on recent theoretical efforts to scrutinize the existence of a transition in pure Heisenberg spin glasses without anisotropy. Below we present two sets of evidences that seem to contradict each other. (The conflict has not been solved yet.) While the first set of evidences supports a novel phase transition via the chirality scenario (see below), the other suggests an apparently more familiar spin glass transition.

The first one was proposed by Kawamura and coworkers. (For a review, see [199].) It was suggested that a phase transition may exist in three dimensional Heisenberg model even if there is no anisotropy, and belong to a

new universality class different from that of the Ising spin glass model. In a series of numerical works (e.g., [71]), the origin of the disagreement between the experimental and numerical results was scrutinized by reconsidering the role of the magnetic anisotropy in the mechanism of the spin glass transition. The resulting hypothesis was that there is a phase transition already in the isotropic system but the spins do not show long-range correlations even below this critical point. It is therefore difficult, if not impossible, to detect an anomalous behavior in spin-spin correlations which had been focused on in most preceding numerical simulations. Only the anisotropy gives rise to the long range correlations in spins, not the transition itself, by coupling them to other degrees of freedom that have been already ordered. It was proposed that these degrees of freedom relevant for the transition are the chiralities defined as

$$\chi_i = \mathbf{S}_i \cdot (\mathbf{S}_{i+\delta} \times \mathbf{S}_{i+\delta'})$$

where δ and δ' are two distinct unit lattice-vectors.

The dynamical behavior of the three-dimensional Heisenberg model with and without a uni-axial spin anisotropy was studied⁷¹ and a clear aging phenomena, for both the isotropic and the anisotropic cases, was found in the autocorrelation function of the chirality at sufficiently low temperatures. For the isotropic Heisenberg spin glass model in three dimensions with the Gaussian bond distribution, the critical temperature and the exponent were estimated as

$$T_{\text{ch}} = 0.157(1), \quad \beta_{\text{ch}} = 1.1(1).$$

Such a clear aging phenomena, however, was observed in the bare spin degrees of freedom only when the anisotropy exists. It was therefore suggested⁷² that this phase transition is not accompanied by a freezing of spins in the isotropic case. As can be seen in Fig.12, the estimate of the Binder parameter for the bare spins decreases as the system size increases at any temperature and does not show any crossing. In contrast, the Binder parameter of the chirality crosses.

An evidence of a finite temperature phase transition was also found for the plane-rotator model (i.e., the XY model with two-component spins) in three dimensions. In [76] an equilibrium Monte Carlo simulation was performed and a crossing in the Binder parameter defined in terms of the chirality was observed while, again, no such crossing was observed for the Binder parameter defined with the bare spins. For the 3d plane-rotator

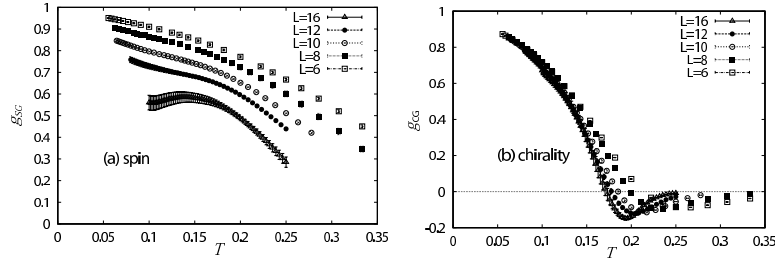


Fig. 12. The binder parameter for the $\pm J$ Heisenberg spin glass model in three dimensions. The left panel is for the spin overlap distribution and the right panel is for the chirality overlap distribution. (From [72].)

model with $\pm J$ bond-distribution their estimates are

$$T_{\text{ch}} = 0.39(3), \quad \nu = 1.2(2), \quad \eta_{\text{ch}} = 0.15(20), \quad z_{\text{ch}} = 7.4(10).$$

It was further argued that, if a small but finite anisotropy exists, the spins and the chiralities are coupled, and therefore the spin sector, being dragged by anomalies in the chirality sector, also shows anomalies at the transition point. It follows that, as a function of the anisotropy, the transition temperature continuously approaches its isotropic limit. Moreover, the singular part of dragged quantities, i.e., those which diverge when the system is anisotropic and do not diverge when it is isotropic, are proportional to the quantity that drags them, namely, the chirality. The spin glass susceptibility, for instance, is given by

$$\chi_{\text{SG}}(T, D) \sim D^4 (T - T_c)^{-\gamma_{\text{SG}}^{\text{chiral}}}$$

The exponent γ_{SG} characterizing the spin glass susceptibility is the same as the one characterizing the chiral spin glass susceptibility. Their estimates of critical indices were compared with those of real materials, and many experimental estimates are closer to those of chirality transition than the Ising spin glass transition (See, Table 1).

The second set of evidences contradicts to these findings. In a few recent reports on the XY and the Heisenberg spin glasses in three dimensions, it was suggested that spins are ordered at the same finite temperature as the chiral degrees of freedom even in the isotropic case. The first such evidence was obtained²⁰⁰ through the computation of the domain-wall energy of the XY model in two and three-dimensions. The authors of [200] computed the spin and the chiral domain-wall energies and estimated the corresponding stiffness exponents. In the three-dimensional case, they obtained a positive

value for the spin stiffness exponent,

$$\theta_S^{\text{spin}} = 0.056(11),$$

while they obtained a much larger stiffness exponent for the chiral domain-wall energy. The positivity of the stiffness exponent was reconfirmed by another computation based on the Coulomb gas representation.²⁰¹ However, since the estimated value is close to zero and the actual increase observed in the domain-wall energy was only about 10 percent for the whole range of system size explored, these results on the stiffness exponent alone could not be taken as a conclusive evidence.

Additional evidences came from Monte Carlo simulations at finite temperature,^{202,203,73} in which the Binder parameters for the magnetization and the chirality of the three-dimensional $\pm J$ Heisenberg model were computed. A common crossing of the curves for different system sizes was found in both Binder parameters. The two crossing temperatures, one for the spin and the other for the chirality, were close to each other. Based on this result, the presence of a finite temperature phase transition at which both the spin and the chiral degrees of freedom are ordered was suggested.

This result was confirmed in [74] where again the $\pm J$ Heisenberg spin glass in three dimensions was studied. There the relaxation of several quantities at temperatures close to the critical one were measured, starting from a completely random initial configuration. In the time regime where the time-dependent length scale discussed in subsection 5.1 is smaller than the system size, the size dependence was absent in the auto-correlation function and the observed time-dependence could be regarded as the one in the thermodynamic limit. Right at the critical temperature, this time dependence was well described by an algebraic function for diverging quantities. For example, for the spin glass susceptibility, we have

$$\chi_{\text{SG}} \propto t^\lambda \tag{37}$$

with $\lambda = \gamma_{\text{SG}}/z\nu$.²⁰⁴ Using this asymptotic form, the critical temperature as well as the critical exponents (divided by $z\nu$) can be determined through the observation of the time dependence of some quantity. The exponent $z\nu$ can be obtained from the temperature dependence of the characteristic time

$$\tau(\Delta T) \propto (\Delta T)^{-z\nu},$$

where $\Delta T \equiv T - T_{\text{sg}}$. In addition, z was estimated from the results of relatively small system sizes for which the correlation length was larger than

the system size. In such a setting, the size dependence of the correlation time near the critical point should be described by

$$\tau(\Delta T = 0) \propto L^z.$$

The estimated critical temperature and exponents for the Heisenberg spin glass model with $\pm J$ bond-distribution in three dimensions were

$$T_{\text{sg}}/J = 0.21^{+0.01}_{-0.03}, \quad \gamma_{\text{sg}} = 1.9(4), \quad \nu = 1.1(2), \quad \beta = 0.72(6).$$

It should be noted that this estimate of ν agrees with some of the experiments on spin glass materials that appear not to be in the Ising universality class.

A clearer demonstration of the existence of the spin ordering was presented in [75], in which an equilibrium Monte Carlo simulation was performed covering not only the critical point but also a fairly large region in the low temperature phase. Instead of the Binder parameter, which is an indirect probe of the presence of the long range order, they used the correlation length itself as in the estimation of the transition temperature of the Ising spin glass model⁵¹ (See Fig.3). For both the XY and the Heisenberg spin glass with the Gaussian bond distribution in three dimensions, a clear crossing in the correlation length divided by the system size as a function of the temperature was observed (Fig.13). The critical indices were estimated as

$$T_{\text{sg}} = 0.34(2), \quad \nu = 1.2(2) \quad (\text{XY})$$

and

$$T_{\text{sg}} = 0.16(2), \quad \nu = 1.1(2) \quad (\text{Heisenberg}).$$

It is rather puzzling to have two conflicting sets of numerical evidences, represented, e.g., by Fig.12 and Fig.13, each would pass as a convincing evidence if the other did not exist. This puzzling situation has not been resolved yet. It is at least clear that there is an unexpectedly large correction to scaling and that we need to answer why one of the seemingly legitimate methods for detecting the long-range order failed in the present case.

6.2. *Continuous Spin Models in Higher Dimensions*

The Heisenberg spin glass model with Gaussian couplings was studied in four and in five dimensions via equilibrium Monte Carlo simulations in

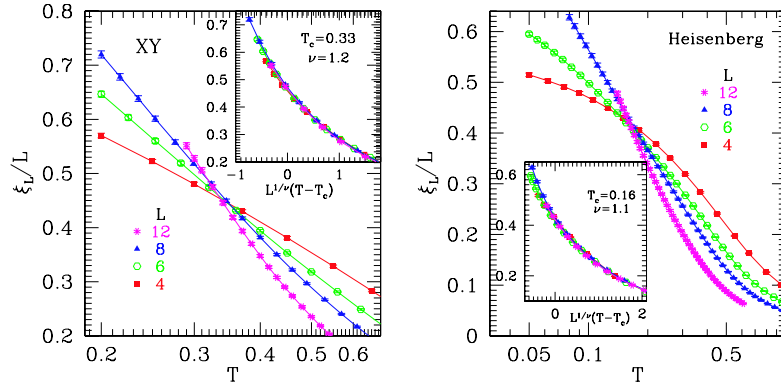


Fig. 13. Correlation lengths of bare spins of the XY model (left) and of the Heisenberg model (right) divided by the system size. (From [75].)

[205]. As in the study of the three-dimensional case⁷² the Binder parameter for spins and chiralities was calculated. In the four dimensional case, it was found that the spin Binder parameters for various system sizes do not intersect while the chirality Binder parameters do. In contrast, in the five dimensional case, both kinds of the Binder parameters intersect. Based on these results it was suggested that the spin chirality separation occurs only in four or lower dimensions while in five or higher dimensions an ordinary phase transition, at which both degrees of freedom freeze, takes place. In five dimensions, the transition temperature was estimated as $T_c = 0.60(2)$ and the critical indices as

$$\alpha = -1.0(3), \beta_{SG} = 0.7(3), \gamma_{SG} = 1.7(2), \nu_{SG} = 0.6(2).$$

Indications were found that the chiral order phase is characterized by one-step replica symmetry breaking unlike the mean-field model. The findings for the four dimensional model were not as clear as those for the five dimensional model. In four dimensions, the chiral transition temperature was estimated to be $T_c = 0.38(2)$ but no reliable estimates for the critical indices for the four dimensional model could be obtained. This may be because four dimensions is marginal or nearly marginal and the critical region is rather narrow.

For these numerical evidences based on the Binder parameters, however, one has to be aware that the same ambiguities might be present in four and five dimensions as in the three-dimensional case discussed in the previous subsection. Therefore, while the existence of a phase transition has been

established in four and five dimensions as well as in three, we still cannot make a conclusive statement concerning the nature of the phase transition in continuous spin models for the same reason as in the three-dimensional case.

6.3. Potts Spin Glasses

Potts spin variables are discrete variables that can take on q different states $S_i \in \{1, 2, \dots, q\}$ and that interact with one another in such a way that only two cases are discriminated: either both interacting spins are in the same state or they are in different states. The Hamiltonian of the q -state Potts glass is given by

$$H = - \sum_{(i,j)} J_{ij} (q\delta_{S_i, S_j} - 1), \quad (38)$$

where the coupling constants J_{ij} are quenched random variables and the sum runs over all interacting spin pairs (i.e., all possible spin pairs in a mean-field model).

The q -state infinite range Potts glass with $q > 4$ ^{206,207} displays a dynamical phase transition at a temperature T_d , where the dynamics freezes and, for instance, the spin auto-correlations do not decay any more (i.e. they reach asymptotically a non-vanishing plateau value). The second, static, transition takes place at a lower temperature T_c , below which the EA spin glass order parameter has a non-vanishing value and the replica symmetry is broken. On the mean-field level there is a close connection between Potts glasses for $q \geq 4$, and Ising spin glass models with p -spin interactions for $p \geq 3$, which again display similar self-consistency equations as the mode-coupling equations describing structural glasses above the glass transition temperature.^{208,209} Therefore Potts spin glasses can also be regarded as simple prototypical models for structural glasses.

The question unanswered to date is, whether this analytically well-established mean-field scenario with the two separate transitions is also valid in finite-dimensional models with short range interactions. Recently, the q -state Potts glass was thoroughly investigated via Monte Carlo simulations in three dimensions,^{210,211} on the simple cubic lattice, with $q = 10$ for a discrete, bimodal bond-distribution as well as a Gaussian distribution. In both cases, the first two moments of the distribution were chosen such that no ferromagnetic ordering of the Potts spins could occur. It was found that for all temperatures investigated the spin glass susceptibility remained finite, the spin-glass order-parameter remained zero, and that the

specific heat had only a smooth Schottky-like peak. These results could be understood quantitatively by considering small but independent clusters of spins. These observations imply that there is no static phase transition at any nonzero temperature. Consistent with these findings, only very minor size effects were observed, which implied that all correlation lengths of the models remained very short.

Moreover, the auto-correlation function $C(t)$ of the Potts spins was computed. While in the Gaussian model $C(t)$ shows a smooth uniform decay, the correlation for the $\pm J$ model has several distinct steps. These steps correspond to the breaking of bonds in small clusters of ferromagnetically coupled spins (dimers, trimers, etc.). The relaxation times follow simple Arrhenius laws, with activation energies that are readily interpreted within the cluster picture, giving an evidence that the system does not have a dynamic transition at a finite temperature. Hence one can conclude that all the transitions known for the mean-field version of the model are completely wiped out in three dimensions.

It should also be mentioned that the mean-field model of the Potts spin glass was studied numerically via Monte-Carlo simulations.^{212,213,214} It turned out that it is extremely difficult to control the finite size effects in the mean-field model and that the fourth order cumulant $g_4(N, T)$ and the Guerra parameter $G(N, T)$ could not be used to locate the static transition temperature for the system sizes investigated. Also the spin-autocorrelation function $C(t)$ showed strong finite size effects and did not display a plateau even for temperatures around the dynamical critical temperature T_d .

7. Weak Disorder

While there are only very few exactly known facts about spin glass models, they serve as helpful guides to numerical studies. This is particularly the case in the study of random spin system with weak disorder. An example is the findings based on the gauge invariance (a brief review can be found in [215]). A line in the phase space, commonly referred to as the Nishimori line (simply N-line, hereafter), was found on which the free energy can be computed exactly. The line is associated with the crossover from the high-temperature ferromagnetic region to the low-temperature disorder-dominated region. The results derived from the gauge invariance seem to have a close connection to a number of renormalization group studies. In the following, we present a gross survey of these findings and related works.

7.1. Phase Diagram of the Discrete Spin Models

It was pointed out²¹⁶ that the gauge invariance of the partition function under the transformation $S_i \rightarrow \sigma_i S_i$ (with an arbitrary choice of $\sigma_i \in \{-1, +1\}$ for every site) can be used to derive a number of exact relations among various quantities in spin glass models. This gauge transformation relates thermal fluctuations to the geometrical properties of the bond configurations. Consequently, a *geometric temperature*, T_p , can be defined that depends only on the bond distribution. This temperature appears in various exact relationships derived from this gauge invariance. An example is the identity for correlation functions in $\pm J$ models:

$$[\langle S_i S_j \rangle_T] = [\langle S_i S_j \rangle_T \langle S_i S_j \rangle_{T_p}] \quad (39)$$

where $\langle \dots \rangle_T$ is the thermal average at temperature T . In particular, $\langle \dots \rangle_{T_p}$ means the thermal average with the real temperature and the geometrical temperature being equal to each other. The symbol $[\dots]$ denotes, as usual, the bond-configuration average. The geometric temperature T_p is defined as

$$p = (1 + \tanh(J/T_p)) / 2, \quad \text{or} \quad T_p = \frac{2J}{\log \frac{p}{1-p}}$$

where p is the concentration of the ferromagnetic bonds. The higher the randomness ($p \rightarrow 1/2$), the higher the geometric temperature ($T_p \rightarrow \infty$). The line in the $p - T$ phase diagram defined by $T_p = T$ is the N-line. Along this line, (39) infers $m = q$, i.e., the spin-glass order is always accompanied by the ferromagnetic order. Therefore, no part of the line lies inside the pure spin-glass phase. (Here, we define the spin-glass phase by the conditions $m = 0$ and $q > 0$.) Another consequence of (39) is that the ferromagnetic long-range order is absent at any temperature if the concentration p is such that the point (p, T_p) falls in the paramagnetic region in the $p - T$ plane. This can be understood by an inequality directly derived from (39):

$$|[\langle S_i S_j \rangle_T]| \leq [|\langle S_i S_j \rangle_{T_p}|]. \quad (40)$$

If the point (p, T_p) belongs to the paramagnetic region, the right hand side of the inequality is zero in the limit of $R_{ij} \rightarrow \infty$, which makes the left hand side also zero, meaning the absence of ferromagnetic order at (p, T) . Assuming that the topology of the $T - p$ phase diagram is as depicted in Fig.14(a), this fact implies that any phase in the region $p < p_N$ (or $T_p > T_N$) cannot have a ferromagnetic long-range order where p_N is the ferromagnetic bond concentration at the N-point. Here the N-point (p_N, T_N) is defined as

the point at which the paramagnetic phase boundary intersect with the N-line. It follows that the phase boundary separating the ferromagnetic phase from the other low-temperature phase (paramagnetic or spin-glass) must be strictly vertical or bend toward the ferromagnetic side. (See Fig.14.)

The inequality (40) also means that the ferromagnetic order is maximal on the N-line when p is fixed. When $T_p < T_N$, as we decrease the temperature departing from the N-line, the magnetization decreases and the spin glass order parameter becomes larger than the square of the magnetization squared. This hints a cross-over from the purely ferromagnetic region to the randomness-dominating region at the temperature $T = T_p$.

It was further argued²¹⁷ that the phase boundary below the N-line is strictly vertical. The argument is based on the fact that the free energy on the N-line is the same as the geometric entropy, i.e., the entropy of the frustration distribution at p :

$$S(p) \equiv - \sum_F P(F) \log P(F)$$

where F is a configuration of frustrated plaquettes and $P(F)$ is the probability of F being realized. Since the free energy (or its derivative with respect to some external field) must have some singularity at the N-point when one moves along the N-line, so does the geometric entropy. The latter singularity is, however, solely due to the geometric properties of the bond configuration, in which the temperature does not play any role. Therefore, it is reasonable to suspect that the same singularity with the geometric origin may affect the spin system defined on it at $p = p_N$ regardless of the temperature. This leads to a temperature-independent transition point, i.e., the strictly vertical phase boundary (See Fig.14). Note that the argument applies also to models with continuous degrees of freedom, such as the XY model and the Heisenberg model, if the ferromagnetic phase exists in the pure model. It was claimed²¹⁷ that the vertical phase boundary between the ferromagnetic phase and the other is universal.

In order to substantiate this argument, the authors of [218] considered the random Z_q model with gauge symmetry, $\mathcal{H} = - \sum_{\langle ij \rangle} V(S_i - S_j + J_{ij})$ with S_i, S_j, J_{ij} takes on a value $0, 1, 2, \dots$ or $q-1$, and $V(\dots)$ is a periodic function of the period q . This model includes the $\pm J$ Ising spin glass model as a special case. The sample-to-sample fluctuations of the energy along the N-line was computed via the exact relationship between the sample-to-sample fluctuations and the thermal fluctuations:

$$[(\Delta E)^2] \equiv [E^2] - [E]^2 = N_B(\{V^2\} - \{V\}^2) - [\langle H^2 \rangle - \langle H \rangle^2].$$

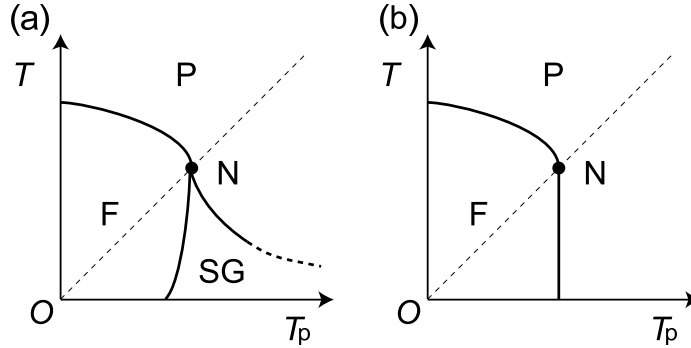


Fig. 14. The schematic $p - T$ phase diagram the $\pm J$ Ising model for (a) the generic case and (b) the two-dimensional case. The thin dashed lines represent the N-line.

Here, $E \equiv \langle \mathcal{H} \rangle$, N_B the number of nearest-neighbor pairs, and $\{\dots\}$ denotes a single-bond average defined by $\{Q(l)\} \equiv \sum_{l=0}^{q-1} \exp(-\beta V(l))Q(l) / \sum_{l=0}^{q-1} \exp(-\beta V(l))$. The sample-to-sample fluctuations are proportional to the ‘geometric specific heat’, i.e., the energy differentiated by $K_p \equiv 1/T_p$. The results showed that $[(\Delta E)^2]$ takes its maximum at the N-point. The authors of [218] argued that this indicates the existence of a singularity in the geometric nature of the system at the N-point, though the nature of the singularity is not known possibly because of the size limitation in their calculation.

It is interesting to note that the correlation length exponent ν at the zero-temperature phase transition from the paramagnetic phase to the ferromagnetic phase in two dimension was found^{219,31} to be very close to (or perhaps exactly equal to) the one for two-dimensional percolation. This fact, together with the geometric mechanism of the transition, makes it very attractive to speculate that the transition is due to a percolation of something that is defined geometrically. However, this “something” has not yet been identified.

7.2. Dynamical Properties

Based on the gauge invariance of the model, several interesting exact relations were derived²²⁰ for the dynamics. Particularly important is the one that relates the auto-correlation function with the totally aligned initial state and that with the initialization at $T = T_p$. Specifically,

$$[\langle S_i(t + t_w) S_i(t_w) \rangle_T^{(F)}] = [\langle S_i(t + t_w) S_i(T_w) \rangle_T^{T_p}]. \quad (41)$$

The superscripts specify the initial spin configurations: “(F)” indicates that the initial state is the totally aligned ferromagnetic state, and “ T_p ” an equilibrium spin configuration at T_p . The left hand side is the autocorrelation function of a spin S_i at the t_w -th Monte Carlo step (MCS) after the initialization (at $t = 0$) and itself at the $(t + t_w)$ -th step. At $t > 0$ the system evolves with the dynamics of a finite temperature T . The right hand side is the autocorrelation function after a quenching from the temperature T_p to T (or a sudden heating up, depending upon whether $T > T_p$ or $T < T_p$). Of particular interest is the relation obtained by setting $t_w = 0$ and $T = T_p$ in the above

$$[\langle S_i(t) \rangle_{T_p}^{(F)}] = [\langle S_i(t) S_i(0) \rangle_{T_p}^{T_p}].$$

This indicates the equivalence of the equilibrium auto-correlation function on the N-line to the non-equilibrium relaxation of the single-spin expectation value starting from the all-aligned condition. By using this relation, we can simply measure the value of a spin without equilibrating at all to obtain the equilibrium autocorrelation function. This is a considerable advantage from the computational point of view.

7.3. The Renormalization Group Approach for the Discrete Models

The Harris criterion²²¹ is well-known as the criterion by which one can decide whether introduction of a weak disorder to a pure system is relevant or irrelevant: If the specific heat diverges at the critical point of the pure system, i.e., the specific heat exponent α is positive, the universality class of the transition in the disordered system will be different from the one of the pure system. In particular, it was argued that if the disorder is relevant the specific heat divergence is smeared out by the effect of the quenched disorder.

The argument was elaborated further with the help of the renormalization group theory.²²² The analysis of the randomly diluted m -vector model showed that the quenched disorder is relevant around the “pure” fixed point (denoted as “P” hereafter), if the specific exponent α is positive at P. As a result, the existence of another fixed point, called the random fixed point (denoted as “R”), was suggested, and the renormalization group flow leads the system to R when starting in the vicinity of P. However, because of the small cross-over exponent, i.e., α in this case, the critical region where the true critical behavior of R can be observed may be very narrow in many

cases, such as the random Ising model in three dimensions ($\alpha \sim 0.11$). For instance results of Monte Carlo simulations of the site-disordered Ising system²²³ were interpreted in terms of a non-universal behavior, i.e., continuously varying critical exponent depending on the strength of the disorder. It was argued that this apparent non-universal behavior can be interpreted as a cross-over from P to R.

As for the critical indices at R, the following values for three dimensional systems were reported²²⁴ based on the four-loop order field-theoretic renormalization group calculation:

$$\beta = 0.348, \gamma = 1.321, \nu = 0.671, \eta = 0.032. \quad (42)$$

In [225] the role of the gauge invariance in the renormalization group method was scrutinized. It was found that the defining condition of the N-line, $T_p = T$ is invariant under a certain renormalization group transformation. More specifically, in an extended phase space an invariant manifold exists that intersects with the $p - T$ plane with the intersection being the N-line. A fixed point is located on this manifold and can be identified with the one corresponding to the multi-critical point that is shared by three phases: paramagnetic, ferromagnetic and spin-glass. One of the directions of the two scaling axes is also found to be parallel to the temperature axis while the other is tangent to the N-line. The fixed point is unstable in both directions.

The authors of [226] studied the site-diluted Ising model with Monte Carlo simulation. Their estimates for the critical indices were

$$\beta = 0.3546(18), \gamma = 1.342(5), \nu = 0.6837(24), \eta = 0.0374(36).$$

These are very close to the corresponding estimates of the indices for the pure model such as:²²⁷

$$\beta = 0.3250(15), \gamma = 1.241(2), \nu = 0.6300(15).$$

Therefore it is technically rather difficult to discriminate a critical point corresponding to the random fixed point from the pure fixed point.

The numerical renormalization group approach based on Monte Carlo simulation²²⁸ suggested the simplest flow diagram consistent with all of these predictions. The variance and the mean of the domain wall free energy were computed and analyzed with the method of the domain-wall renormalization group.²⁸ For the randomly diluted spin systems in three dimensions the flow diagram turned out to be the simplest one consistent with preceding theoretical predictions (see Fig.15). The RG flow diagram

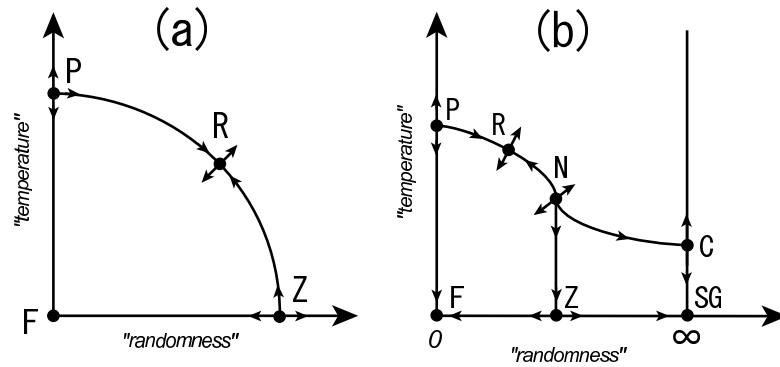


Fig. 15. A schematic RG flow diagram for (a) non-frustrated models (e.g., the randomly diluted ferromagnet) and (b) frustrated models (e.g., the $\pm J$ model) in three dimensions.

for the bond-diluted model consists of two finite temperature fixed points (the pure fixed point (P) and the random fixed point (R)) together with two zero-temperature fixed points (the ferromagnetic fixed point (F) and the zero-temperature percolation fixed point (Z)). The two eigen values of the linearized RG transformation were evaluated at R. The positive one turned out to be

$$y_1 = 1.47(4)$$

which is consistent with the previous estimates of $\nu = 1/y \sim 0.68$ mentioned above. The other negative one was

$$y_2 = -1.3(4).$$

A similar calculation for the site-diluted system yielded the result consistent with these.

When in addition the system is randomly frustrated, the simplest flow diagram must contain at least three more fixed points: the multi-critical or Nishimori fixed point (N), the spin-glass critical fixed point (C), and the spin-glass zero-temperature fixed point (SG). The findings in [228] were indeed consistent with this simplest flow diagram (Fig.15). In this case the exponent at R was estimated as

$$y_1 = 1.52(2), \quad \text{and} \quad y_2 = -0.42(13).$$

While the positive one agrees with the estimate for the non-frustrated system, the other does not agree. The reason for this has not been clarified yet.

7.4. The Location of the Multi-Critical Point

For the location of the multi-critical point, or the N-point, of the $\pm J$ model, there are a number of numerical estimates. In particular, the non-equilibrium simulation was employed effectively to deduce the equilibrium properties. The basic idea of the method can be traced back to the dynamical scaling hypothesis.^{229,230} Various scaling relations, such as (37), can be derived from it. It is assumed that a generating function, which is an extension of the equilibrium free energy, exists and that the time-dependence of various quantities can be obtained as its derivatives. The hypothetical generating function has the form

$$f(\Delta T, h, L, t) = L^{-d} \tilde{f}(\Delta T L^y, h L^{y_h}, t L^{-z}) \quad (43)$$

analogous to the ordinary form of the finite size scaling. While this form is presumably valid in the near-equilibrium time regime, it was suggested¹³³ that there exists an initial time regime where the dynamics is governed by another critical exponent independent of those which appear in (43).

Using the scaling relations derived from (43), the non-equilibrium relaxation of the system was studied. The authors of [231] measured the magnetization $m(t) \equiv [\langle S_i(t) \rangle_T^{(F)}]$ on the N-line, which is proved to be the same as the equilibrium autocorrelation function $q(t)$ as mentioned above (see subsection 7.2). Then they used the following scaling form

$$m(t) = L^{-\beta y} \tilde{q}((T - T_N) L^y, t L^{-z})$$

that can be derived from (43). In particular, the long-time asymptotic form at $T = T_N$

$$m(t) \sim t^{-\beta y/z}$$

was used to obtain the effective exponent at a finite time,

$$\lambda(t) \equiv -\frac{d \log m(t)}{d \log t},$$

which should converge to $\lambda \equiv \beta y/z$ as $t \rightarrow \infty$ at the critical point. A good convergence to a finite value was observed around the N-point for the two and three dimensional models, although the convergence in the latter case seemed more unstable. They quoted the values

$$p_N = 0.8872(8), \quad \lambda = 0.021(1) \quad (44)$$

for the two dimensional model and

$$p_N = 0.7673(3), \quad \lambda = 0.090(3) \quad (45)$$

for the three dimensional model.

In two dimensions, the exact location of the N-point was predicted by [232]. The authors studied the duality transformation formulated in [233], applying it to a random model with Z_q symmetry. The model is defined in terms of variables, ξ_i , each taking one of q values ($\xi = 0, 1, 2, \dots, q - 1$). The partition function is defined as

$$Z = \sum_{\{\xi_i\}} e^{\sum_{\langle ij \rangle} V(\xi_i - \xi_j + J_{ij})}$$

where $V(l)$ is a periodic function defined on integers with the period q and J_{ij} is a quenched random variable that takes on $0, 1, 2, \dots, q - 1$. They obtained an equation that yields a (possibly exact) value of the critical concentration p_c . The resulting values of p_c agreed with numerical estimates for various models such as the $\pm J$ Ising model and the three state Potts gauge glass. In addition, a similar equation derived for the random Ising model with Gaussian bond distribution yielded a value very close to the numerically obtained critical value of $J/\Delta J$ where J and ΔJ are the mean and the standard deviation of the bond distribution, respectively.

The replica method was employed in the derivation of the key equation; the duality relation of the n replica system was considered. As reported in [234], a quantity, which we denote as α , defined with the physical parameters, such as p and T for the Ising model, has a very simple transformation rule under the duality transformation:

$$\alpha \rightarrow q^n / \alpha,$$

Therefore, $\alpha = q^{n/2}$ defines a manifold that is invariant under the duality transformation. The virtue of this equation is that we can explicitly take its $n \rightarrow 0$ limit, resulting in

$$\sum_{l=0}^{q-1} p_l \log \left(\sum_{\eta=0}^{q-1} e^{V(\eta+l) - V(l)} \right) = \frac{1}{2} \log q, \quad (46)$$

where p_l is the probability of J_{ij} being l . If a well-defined duality equation in the $n \rightarrow 0$ limit exists and if a self-dual point lies on our real $p-T$ plane, the condition (46) must be satisfied on it. The problem is that we do not know what the $n \rightarrow 0$ self-dual equation is nor whether a self-dual point lies on our $p-T$ phase diagram.

However, with the assumption that a self-dual point coincides with the N-point, it becomes possible to obtain a number, which may be an exact

value of p_c . Specifically, the intersection of the N-line and the line defined by (46) for the $\pm J$ Ising model is located at

$$p_c = 0.889972 \dots$$

which agrees with preceding numerical estimates of the N-point such as

$$p_c = 0.8905(5)$$

in [235]. This remarkable agreement, together with similar agreements for a few other models, seems a little too much to regard as a mere coincidence; the exact transition points of these models may have been derived from the duality.

7.5. Phase Diagram of the Random XY Model in Two Dimensions

The effect of weak randomness in the XY model in two dimensions is of special relevance due to its relationship to various other models, such as the Coulomb gas and Josephson junction arrays. The model discussed most frequently is the random phase XY model

$$\mathcal{H} = - \sum_{\langle ij \rangle} J_{ij} \cos(\theta_i - \theta_j - \phi_{ij})$$

with J_{ij} being a uniform constant $J > 0$ and ϕ_{ij} a quenched random variable. However, other models, such as the one with random J_{ij} and uniform ϕ_{ij} , most likely have essentially the same property.

In an early study²³⁶ the random phase model was studied and it was suggested that a sufficiently strong disorder destroys the quasi-long-range order of the pure XY model. More strikingly, the amount of the disorder sufficient to destroy the quasi-order is vanishing as we approach the zero temperature. Consequently, the system undergoes a re-entrant phase transition as the temperature is lowered with the magnitude of the disorder being fixed at a sufficiently small value.

The latter prediction concerning the re-entrance phase transition was corrected later by a number of groups.^{237,238,239,240,241} Here we follow the heuristic argument given by the authors of [238]. They argued that there is a disorder induced phase transition at zero temperature in the two-dimensional XY model. Generalizing the Kosterlitz argument for the KT transition, they considered the balance between the energy-cost for creating a topological excitation (vortex) and the energy-gain due to the interaction of the vortex with the disordered potential. They estimated the probability

p_{defect} of creating a vortex on a given site being energetically favored. It depends algebraically on the area of the system A with an exponent α :

$$p_{\text{defect}} \sim A^{-\alpha}$$

where α depends on the magnitude of the disorder and the temperature. The ordered phase is stable against the introduction of disorder when the total number of sites on which the creation of the vortex is favored is zero in the thermodynamic limit. That is, $Ap_{\text{defect}} \rightarrow 0$. Therefore, $\alpha = 1$ defines the phase boundary. This result contradicts preceding studies such as the one mentioned above^{236,242} that suggest that the ground state of the pure system is unstable at any finite disorder.

They argued that the preceding renormalization group theories failed to capture the correct physics because they neglected the fluctuation in the local energy gain due to disorder potential, which can be very large with a small but finite probability. In particular, we cannot neglect such a fluctuation when it exceeds the thermal fluctuation. This means that the previous argument may fail near and below the N-line because the N-line can be regarded as the cross-over line below which the geometrical fluctuation dominates (see subsection 7.1).

They also discussed a finite temperature phase diagram introducing the thermal fluctuations in their argument. This yields another interesting feature of their results; the straight phase boundary between the ordered phase and the disordered phase in the $T - T_p$ phase diagram, in agreement with the Nishimori's claim (see subsection 7.1). Generalizing the simple argument based on the energy-balance, they computed the exponent α for finite temperature:

$$\alpha = \begin{cases} \frac{T^*}{T_p} & (T_p > \lambda T) \\ \frac{T^*}{T_p} \left(\frac{T_p}{\lambda T} \left(2 - \frac{T_p}{\lambda T} \right) \right) & (T_p < \lambda T) \end{cases} \quad (47)$$

where T^* and λ are model-dependent parameters. The phase boundary is again given by $\alpha = 1$. Therefore, for the region where the disorder fluctuation dominates, ($T_p > \lambda T$), the phase boundary is $T_p = T^*$, independent of the temperature, whereas it depends on the temperature in the region where the thermal fluctuation dominates ($T_p < \lambda T$). If one identifies, quite naturally, the line $T_p = \lambda T$ with the N-line, the result is perfectly in parallel with Nishimori's picture based on the gauge invariance.

In fact, the gauge invariance can be used for deriving exact results for continuous spin models, such as the XY models and the Heisenberg models. In [215], the author derived a number of exact equations for the Villain

model on the N-line. For example, the exact solution for the energy along the N-line was obtained. As we have seen in subsection 7.1 for the discrete models, one can argue, based on the exact results, that the N-line ($T = T_p$) is the cross-over line separating the purely ferromagnetic region and the disorder dominant region. Interestingly, the renormalization group theory on the XY model²³⁷ indicates that there is a freezing transition or a cross-over at $T = 2T_p$ with the difference of a factor 2 from the N-line. It is plausible that this difference is only due to the approximation involved in the renormalization group theory, and they both reflect the same physics.

8. Quantum Spin Glasses

A quantum spin glass is a magnetic system that can be described by a quantum mechanical Hamiltonian with spin-glass like features (randomness and frustration). In such a system, a spin glass phase may exist while at the same time quantum fluctuations play an important role, possibly a dominant role, in particular, in the absence of thermal fluctuations at zero temperature. Such a Hamiltonian is, for instance, the spin-1/2 Heisenberg spin glass

$$H = \sum_{(ij)} J_{ij} (\sigma_i^x \sigma_j^x + \sigma_i^y \sigma_j^y + \sigma_i^z \sigma_j^z), \quad (48)$$

where $\sigma^{x,y,z}$ are Pauli spin-1/2 operators, J_{ij} random exchange interactions (e.g., Gaussian), and the sum runs over all nearest neighbors on some d -dimensional lattice. Another example is the Ising spin glass in a transverse field

$$H = - \sum_{(ij)} J_{ij} \sigma_i^z \sigma_j^z + \Gamma \sum \sigma_i^x, \quad (49)$$

where Γ denotes the transverse field strength. This Hamiltonian becomes diagonal if Γ is zero, in which case it reduces simply to the classical Ising spin glass that we have discussed in the previous sections. Thus the role of the parameter Γ is to tune the strength of quantum fluctuations, they do not play a role in the equilibrium statistical physics of a diagonal Hamiltonian. An important experimental realization of this model Hamiltonian is the system $\text{LiHo}_x\text{Y}_{1-x}\text{F}_4$,²⁴³ an insulating magnetic material in which the magnetic ions (Ho) are in a doublet state due to crystal field splitting. The interactions between Ho ions can be described by an Ising model with dipolar couplings. For $x = 1$ the system is a ferromagnet with a critical temperature of $T_c = 1.53$ K at $\Gamma = 0$ and as x is reduced the critical

temperature decreases. For concentrations below 25% Ho and above 10% Ho a thermal phase transition to a spin glass phase occurs indicated by a diverging nonlinear susceptibility (for instance at $x = 0.167$ the spin glass transition temperature is $T_g = 0.13\text{K}$ at $\Gamma = 0$). If a transverse field is applied ($\Gamma > 0$) the spin glass transition temperature decreases monotonically to zero (see Fig. 16). This particular point, at zero temperature and at a critical field strength is what we denote as a quantum-phase-transition point.²⁴⁴

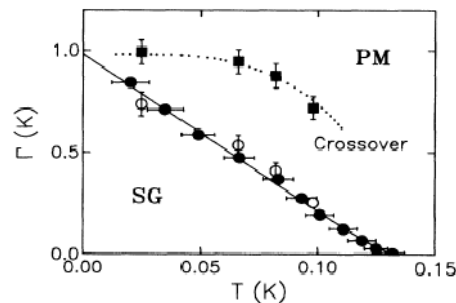


Fig. 16. Phase diagram of $\text{LiHo}_{0.167}\text{Y}_{0.833}\text{F}_4$ according to the measurement of the nonlinear susceptibility. From [243].

Earlier reviews on quantum spin glasses and in particular the Ising spin glass in a transverse field can be found in [245,246,247]. Here we try to focus on a number of new developments that have been made since then.

8.1. Random Transverse Ising Models

The generic phase diagram for the EA Ising spin glass model in a transverse field Γ is shown in Fig. 17 for two dimensions and for three dimensions. In the three-dimensional case, starting from the classical spin glass transition temperature T_c for $\Gamma = 0$ the critical temperature decreases monotonically with increasing transverse field strength Γ until it reaches $T = 0$. One expects that the universality class of the transition at any non-vanishing temperature is the same as the one of the classical Ising spin glass transition at T_c . The zero-temperature quantum phase transition, however, establishes a new universality class. This transition exists in any dimension, including one and two dimensions. A critical value Γ_c for the transverse field strength separates a disordered or paramagnetic phase for $\Gamma > \Gamma_c$ from an ordered

phase for $\Gamma < \Gamma_c$. This transition is characterized by a diverging length scale $\xi \sim |\Gamma - \Gamma_c|^{-\nu}$ and a vanishing characteristic frequency $\omega \sim \Delta E \sim \xi^{-z}$. The latter is the quantum analog of “critical slowing-down” in the critical dynamics of classical, thermally driven transitions. The new and most important property occurring at zero temperature in the random transverse Ising model is the *infinite randomness fixed point* (IRFP) that governs the quantum critical behavior at the critical value Γ_c of the transverse field.²⁴⁸ One feature of the IRFP is that the dynamical exponent z is formally infinite, the relation between length and energy scales is not algebraic but exponential: $\Delta E \sim \exp(-A\xi^\psi)$.

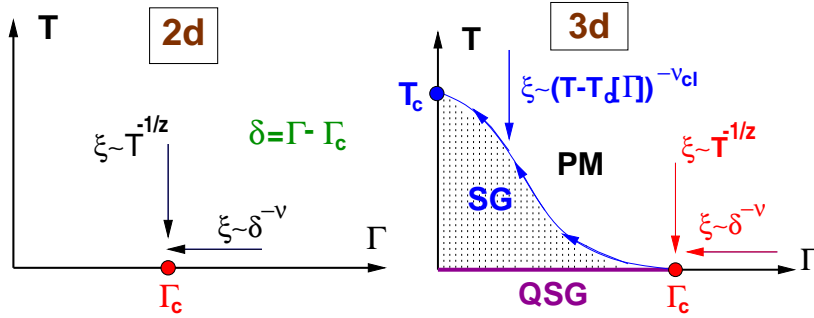


Fig. 17. **Left:** Generic phase diagram for the two-dimensional Ising spin glass in a transverse field Γ . Since no spin glass phase is present in $d = 2$ for $T > 0$, only a quantum spin glass phase and a quantum phase transition at $T = 0$ exists. Approaching the quantum critical point at Γ_c by decreasing the temperature T , the correlation length diverges like $T^{-1/z}$, where z is the dynamical critical exponent (if z is formally infinite, it increases logarithmically). **Right:** Generic phase diagram of a three-dimensional Ising spin glass in a transverse field. The classical transition temperature (at $\Gamma = 0$) is T_c and the corresponding classical correlation length exponent is ν_{cl} .

To describe this scenario we generalize the discussion of the transverse Ising spin glass by including also random *ferromagnetic* interactions $J_{ij} > 0$, because many more analytical and numerical results are available for the ferromagnetic rather than the spin glass case and the same main features are expected to hold in both cases.

Let us start with a review of the one-dimensional case, in which the sign (if it can be negative) of the nearest neighbor couplings can be gauged away so that all interactions are ferromagnetic and the resulting model is the random Ising chain in a transverse field or a random transverse-field

Ising model (RTIM) in one dimension:

$$\mathcal{H} = - \sum_i J_i \sigma_i^z \sigma_{i+1}^z + \sum_i h_i \sigma_i^x. \quad (J_i > 0) \quad (50)$$

A uniform transverse field is represented by $h_i = \Gamma$ for all sites. Since this case and the case of random transverse fields turn out to belong to the same universality class, we also consider random transverse field here. The couplings J_i and the transverse fields h_i are random variables with distributions $\pi(J)$ and $\rho(h)$, respectively. The Hamiltonian in (50) is closely related to the transfer matrix of a classical two-dimensional layered Ising model, which was first introduced and studied by McCoy and Wu.²⁴⁹ Extensive researches on this model were initiated by D. Fisher²⁵⁰ with an application of the Ma-Dasgupta-Hu renormalization group scheme,²⁵¹ followed by numerical and analytical work.^{252,253,254,255,256,257,258,259} We briefly summarize the results. The quantum control-parameter of the model is given by

$$\delta = \frac{[\ln h]_{av} - [\ln J]_{av}}{\text{var}[\ln h] + \text{var}[\ln J]}. \quad (51)$$

For $\delta < 0$ the system is in the ordered phase with a non-vanishing average magnetization, whereas the region $\delta > 0$ corresponds to the disordered phase. There is a phase transition in the system at $\delta = 0$ with rather special properties, which differs in several respects from the usual second-order phase transitions of pure systems. One of the most striking phenomena is that some physical quantities are not self-averaging, which is due to very broad, logarithmic probability distributions. As a consequence the *typical value* (which is the value in an frequent event) and the *average value* of such quantities can be drastically different. Thus the critical behavior of the system is primarily determined by rare events that give dominating contributions to the averaged values of various observables.

The average bulk magnetization is characterized by an exponent β , which is $\beta = 2 - \tau$ where $\tau = (1 + \sqrt{5})/2$ is the golden-mean. The average spin-spin correlation function $C(r) = [\langle \sigma_i^z \sigma_{i+r}^z \rangle]_{av}$ involves the average correlation length ξ , which diverges at the critical point as $\xi \sim |\delta|^{-\nu_{av}}$, and $\nu_{av} = 2$. On the other hand, the typical correlations have a faster decay, since $\xi_{typ} \sim |\delta|^{-\nu_{typ}}$ with $\nu_{typ} = 1$.

Close to the critical point the relaxation time t_r is related to the correlation length as $t_r \sim \xi^z$, where z is the dynamical exponent. The random transverse-field Ising spin chain is strongly anisotropic at the critical point,

since according to the RG-picture²⁵⁰ and to numerical results²⁶⁰

$$\ln t_r \sim \xi^{1/2}, \quad (52)$$

which corresponds to $z = \infty$. On the other hand the relaxation time is related to the inverse of the energy-level spacing at the bottom of the spectrum $t_r \sim (\Delta E)^{-1}$. Then, as a consequence of (52), some quantities (such as specific heat, bulk and surface susceptibilities, etc.) have an essential singularity at the critical point, and the correlation function of the critical energy-density has a stretched exponential decay, in contrast to the usual power law behavior.

Away from the critical point in the disordered phase the rare events with strong correlations still play an important role, up to the point, $\delta = \delta_G$. Above this point, all transverse-fields are bigger than the interactions. In the region $0 < \delta < \delta_G$, which is called the Griffiths-McCoy phase, the magnetization is a singular function of the uniform longitudinal field H_z as $m_{\text{sing}} \sim |H_z|^{1/z}$, where the dynamical exponent z varies with δ . At the two borders of the Griffiths-McCoy phase it behaves as $z \approx 1/2\delta \times (1 + \mathcal{O}(\delta))$ ²⁵⁰ as $\delta \searrow 0$ and $z = 1$ as $\delta \nearrow \delta_G$, respectively.

All these results could be obtained and understood by the application of a Ma-Dasgupta-Hu renormalization group scheme,²⁵⁰ in which strong bonds or fields are successively decimated either by elimination of spins (in case of large transverse fields) or formation of strongly coupled clusters (in case of large ferromagnetic bonds). With decreasing energy scale Δ of the bonds and fields to be decimated the typical size L of these strongly coupled clusters increases as

$$L \sim |\ln \Delta|^{1/\psi} \quad (53)$$

defining an exponent ψ that is $1/2$ in the random transverse-field Ising chain. Such a cluster typically contains

$$\mu \sim L^{\phi\psi} (= |\ln \Delta|^\phi) \quad (54)$$

spins that essentially behave collectively (for instance in response to the application of a longitudinal magnetic field H — and thus generating a huge contribution to the spin susceptibility). This defines another exponent ϕ , which is $(1 + \sqrt{5})/2$ in the RTIM. Finally there is the correlation length exponent ν that defines the characteristic length scale of spin-spin correlations away from the critical point.

The RG runs into a fixed point that is fully determined by the geometrical features of the clusters that are generated asymptotically — very much

in reminiscence of the percolation fixed point in conventional percolation. This picture is expected to hold also for higher-dimensional RTIMs, and even for the spin glass case. Therefore we summarize its essence here. The distribution of the random bonds and fields not yet decimated during the RG procedure becomes broader and broader. Hence the name, *infinite randomness fixed point* (IRFP). It is characterized by the three exponents ψ , ϕ and ν and the critical behavior of the physical observables is determined by them. For instance the correlation function (at criticality) for two spins at site i and j with a distance r from each other is simply given by their probability to belong to the same cluster of size r : $[C_{ij}]_{\text{av}} \sim |\mathbf{r}_i - \mathbf{r}_j|^{-2(d-\phi\psi)}$. Other relations follow straightforwardly from this scheme²⁴⁸:

lowest energy scale:	$-\ln \Delta$	\sim	L^ψ
magnetic moment:	μ	\sim	$(-\ln \Delta)^\phi$
average correlations:	$[C_{ij}]_{\text{av}}$	\sim	$ \mathbf{r}_i - \mathbf{r}_j ^{-2(d-\phi\psi)}$
typical correlations:	$-\ln [C_{ij}]_{\text{av}}$	\sim	$\kappa_{ij} \mathbf{r}_i - \mathbf{r}_j ^\psi$
finite T -susceptibility:	χ	\sim	$T^{-1}(-\ln T)^{2\phi-d/\psi}$
finite H -magnetization:	M	\sim	$(-\ln H)^{-\phi+d/\psi}$

Away from the critical point ($\delta \neq 0$) the correlation length is finite and its average and typical value scale differently:

average correlation length:	ξ_{av}	\sim	$\delta^{-\nu}$
typical correlation length:	ξ_{typ}	\sim	$\xi_{\text{av}}^{1-\psi}$
spontaneous magnetization:	M_0	\sim	$(-\delta)^{\nu(d-\phi\psi)}$

In spite of the finiteness of the average correlation length away from the critical point still arbitrarily large strongly-coupled clusters exist — though with an exponentially small probability — leading to algebraically decaying correlations in imaginary time. Phenomenologically, one can see that as follows.^{261,262} Let L be the size of a region of *strongly coupled* spins. In a random system in the paramagnetic phase they occur with an exponentially small probability $P(L) \propto \exp(-\lambda L^d)$. For instance in the diluted ferromagnet strongly coupled regions are connected clusters and their probability is p^V , where V is the region's volume and p is the site occupation probability ($0 < p < 1$). Then, λ is given by $\lambda = |\ln p| > 0$. The special feature of transverse-field Ising systems is that in first order perturbation theory the gap of a finite system containing L^d spins is exponentially small: $\Delta_0 \sim \exp(-sL^d)$. An exponentially small gap means an exponentially large tunneling time, and combining the two observations on cluster probability and relaxation time one obtains an algebraical decay for the

spin-spin correlation function: $C(\tau) = [\langle \sigma_i(\tau) \sigma_i(0) \rangle]_{\text{av}} \sim \tau^{-\lambda/s} = \tau^{-d/z(\delta)}$. The parameter $z(\delta) = s/d\lambda$ is called the *dynamical exponent* in the Griffiths phase and it varies continuously with the distance from the critical point. The consequences, e.g., for the susceptibility are dramatic: $\chi(\omega = 0) = \int_0^{1/T} d\tau C(\tau) \propto T^{-1+d/z(\delta)}$ which implies that for $z > d$ the susceptibility diverges for $T \rightarrow 0$ even away from the critical point. Since in random transverse-field Ising system $z(\delta)$ grows without bounds for $\delta \rightarrow 0$ (and thus merging with the critical dynamical exponent at $\delta = 0$, which is infinite), there is always a region around the critical point, where the susceptibility diverges.

In general the dynamical exponent $z(\delta)$ introduced above is expected to determine all singularities occurring in the Griffiths-McCoy phase close to an IRFP²⁴⁸:

dynamical exponent:	$z(\delta)$	\propto	$\delta^{-\psi\nu}$
lowest energy scale:	Δ	\sim	$L^{-z(\delta)}$
finite H -magnetization:	M	\sim	$H^{1/z(\delta)}$
susceptibility:	$\chi(\omega = 0)$	\sim	$T^{-1+d/z(\delta)}$
nonlinear susceptibility:	$\chi_{nl}(\omega = 0)$	\sim	$T^{-1+d/3z(\delta)}$
specific heat:	c	\sim	$T^{d/z(\delta)}$

The last three tables summarize the scaling predictions at and close to a IRFP and in $1d$ they have been confirmed many times, analytically and numerically.^{252,253,254,255,256,257,258,259} In higher dimensions $d \geq 2$ the randomly diluted Ising-ferromagnet in a transverse field is a show-case for a quantum phase transition governed by an IRFP. The site diluted model is defined by the Hamiltonian

$$H = -J \sum_{(ij)} \varepsilon_i \varepsilon_j \sigma_i^z \sigma_j^z - \Gamma \sum_i \varepsilon_i \sigma_i^x \quad (55)$$

and the bond diluted model by

$$H = -J \sum_{(ij)} \varepsilon_{ij} \sigma_i^z \sigma_j^z - \Gamma \sum_i \sigma_i^x \quad (56)$$

where ε_i and ε_{ij} are random variables that take on the values 1 with probability p and 0 with probability $1 - p$. Its phase diagram is depicted in Fig. 18

Along the vertical line starting from the point $(p, \Gamma) = (p_c, 0)$ up to the multi-critical point the transition from the paramagnetic to the ferromagnetic phase is a *classical percolation transition*.^{263,264} Denoting the distance from the critical point with $\delta = p_c - p$ the connectivity correlation length

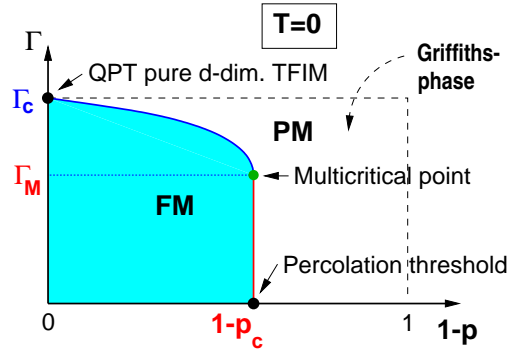


Fig. 18. Phase diagram of the diluted Ising ferromagnet in a transverse field Γ at zero temperature $T = 0$.

diverges upon approaching the percolation point $1 - p_c$ as $\xi \sim |\delta|^{-\nu_{\text{perc}}}$. The number of spins M in the percolating cluster at $p = p_c$ scales with the linear system-size L as $M \sim L^{D_{\text{perc}}}$, where D_{perc} is the fractal dimension of the percolating clusters. For small values of the transverse field Γ one expects the percolating cluster to be fully magnetized, which implies that the gap scales as $\Delta \sim \exp(-L^{D_{\text{perc}}})$. This means that $\psi = D_{\text{perc}}$ in the IRFP scenario described above. Moreover, the connectivity correlation function at the percolation threshold p_c decays as $C(r) \sim r^{-(d-2+\eta_{\text{perc}})}$, which means that the exponent ϕ is given by the relation $2(d - \psi\phi) = (d - 2 + \eta_{\text{perc}})$. To summarize the exponents characterizing the IRFP in the randomly diluted ferromagnet in a transverse field are related to the classical percolation exponents (which are exactly known in dimensions $d = 2$ and in $d > 6$) via:

$$\nu = \nu_{\text{perc}}, \quad \psi = D_{\text{perc}}, \quad \phi = (d + 2 - \eta_{\text{perc}}) / D_{\text{perc}}. \quad (57)$$

For the random bond ferromagnet in a transverse field in dimensions $d \geq 2$ one has to rely only on numerical calculations: In the $2d$ ferromagnetic case quantum Monte-Carlo simulations^{265,266} provided an evidence for an infinite randomness fixed point with $\psi \approx 0.42$ and $\phi \approx 2.1$. Later a numerical implementation of the Ma-Dasgupta-Hu RG scheme indeed provided another evidence for an infinite randomness fixed point²⁶⁷ with $\psi = 0.42 \pm 0.06$, $\phi = 2.5 \pm 0.4$, which agrees with the QMC estimate within the error bars, and $\nu = 1.07 \pm 0.15$. For random Ising ferromagnets in a transverse field the existence of the IRFP dominating the quantum critical behavior thus appears to be confirmed for finite dimensions. Strictly speak-

ing detailed numerical studies have only been performed for $d = 1$ and $d = 2$ up to now, but there seems to be no strong argument against the existence of the IRFP also in higher, finite, dimensions although one expects the numerical and experimental visibility of the IRFP to diminish for increasing dimension d . In the mean field limit ($d \rightarrow \infty$) the quantum phase transition is *not* described by an IRFP and obeys conventional scaling laws. In particular z is finite and Griffiths-McCoy singularities are absent.

What about the spin glass case? Quantum Monte Carlo simulations on the Ising spin glass with a transverse-field have been performed for the cases $d = 2$ ^{268,262} and $d = 3$,^{269,270} they are reviewed in [246,247]. The main result is that the numerical data appeared to be compatible with a finite value for the dynamical exponent in $d = 2$ and 3 and that the critical behavior can be described by conventional scaling laws. However, the existence of a Griffiths-McCoy phase away from the critical point has been uncovered, with a continuously varying dynamical exponent describing the singularities of the susceptibility and non-linear susceptibility. In contrast to the quantum Monte-Carlo simulations of the random bond ferromagnets no cluster-algorithm could be used in the quantum spin glass case, which restricted the system sizes and in particular the temperatures to rather small values (note that anisotropic finite size scaling demands that the temperature has to decrease exponentially with the system size at a quantum critical point described by an IRFP). In addition a homogeneous rather than a random transverse field has been used, which causes strong cross-over effects and the true asymptotic scaling behavior might be more difficult to extract. Therefore it might very well be that the indications found for the absence of a IRFP in the $2d$ and $3d$ quantum spin glass are still pre-asymptotic and that studies using larger system sizes and more sophisticated simulation methods could detect evidence for the IRFP also here.

Finally a word about the consequences of the aforementioned theoretical developments for the experiments. There it was observed that upon approaching the quantum critical point the divergence of the non-linear susceptibility was drastically suppressed indicating even the absence of a divergence at zero temperature. The numerical results, on the other hand, hint at a strong divergence of the non-linear susceptibility at the quantum critical point — even more than the IRFP scenario. Up to now no clear reason for the discrepancy has been pinned down. The possibility of a second-order transition turning a first-order one at low temperatures has been raised,²⁷¹ but this possibility can definitely be ruled out for a sys-

tem that can be described by the Hamiltonian (50) that we discussed here. We do not think that dipolar interactions of a magnetically diluted system cause substantial modifications of the picture that emerged for short range interactions. At this point one cannot rule out the possibility that the transverse field Ising Hamiltonian with quenched disorder is simply not a sufficiently detailed description of $\text{LiHo}_{0.167}\text{Y}_{0.833}\text{F}_4$.

8.2. Mean-Field Theory

As a mean-field model of quantum Ising spin glass, we consider the Sherrington-Kirkpatrick model in a transverse field

$$H = - \sum_{(i,j)} J_{ij} \sigma_i^z \sigma_j^z - \Gamma \sum_i \sigma_i^x. \quad (58)$$

The first sum is over all pairs of spins and the couplings J_{ij} are quenched random variables that obey the Gaussian distribution with zero mean and variance J^2/N , where N is the number of spins. Γ is the strength of the transverse field. Although no exact solution has been found for finite Γ , the phase diagram of this model has been well delineated. At zero transverse field the transition is the well-known classical transition of the SK model at $T_c(\Gamma = 0) = J$. For sufficiently high temperature and/or sufficiently large Γ , thermal and/or quantum fluctuations destroy the spin glass order, yielding a paramagnet.²⁷² For low T and small Γ one finds a SG ordered phase, apparently with broken replica symmetry.²⁷³ Monte Carlo calculation, numerical spin summation²⁷⁴ and perturbation expansion²⁷⁵ in $1/\Gamma$ have determined the phase boundary to some precision. As in the classical model, the infinite range interactions apparently wipe out the Griffiths singularities discussed in the last subsection. The critical behavior along the line $T_c(\Gamma)$ is expected to be the same as the classical critical behavior, i.e., the non-linear susceptibility diverges as $\chi_{nl} \sim (T - T_c(\Gamma))^{-\gamma}$ with $\gamma = 1$, the specific heat exponent is $\alpha = 0$, etc.

The zero temperature quantum critical point $\Gamma_c(T = 0)$ is in a different universality class and has been studied in [276,277,278]. The static approximation — the approximation usually applied to small field values in which the imaginary time correlation function $C(\tau) = \langle \sigma_i(\tau) \sigma_i(0) \rangle$ is assumed to be time independent — is not valid at $T = 0$ (large fields) and the full functional form of $C(\tau)$ has to be explored. The dynamical self-consistency equations obtained via standard manipulations^{272,279} was analyzed at $T = 0$ at the quantum critical point in [276,277,278], and it turned out that the quantum critical point is located at $\Gamma_c \approx 0.7J$. At $\Gamma > \Gamma_c$ (and

zero temperature) $C(\tau)$ decays exponentially with τ as $\tau \rightarrow \infty$, indicating a gap Δ in the corresponding spectral density; at $\Gamma = \Gamma_c$, $C(\tau)$ decays as $1/\tau^2$, and in the ordered phase, $C(\tau) \rightarrow q_{\text{EA}}$. The Fourier transform of $C(\tau)$ has the form $C(\omega) \sim \text{const.} \cdot \sqrt{\omega^2 - \Delta^2}$ for $\Gamma \geq \Gamma_c$, which is responsible for the $1/\tau^2$ behavior at Γ_c and it turned out that the correlation time diverges as $\xi_\tau \sim 1/\Delta \sim [(\Gamma - \Gamma_c)^{-1} \ln(\Gamma - \Gamma_c)]^{1/2}$. Thus we can define an exponent $z\nu$, anticipating anisotropic scaling in space and time in the short range model, which takes the value $z\nu = 1/2$ in the infinite-range model. Since $C(\tau \rightarrow \infty) = q_{\text{EA}}$ is the Edwards-Anderson order parameter, we may also define $q_{\text{EA}} = (\Gamma_c - \Gamma)^\beta$ and it was found that $\beta = 1$. At $\Gamma = \Gamma_c$ one expects $C(\tau) \sim \tau^{-\beta/z\nu}$, which is satisfied with the values obtained. The non-linear susceptibility diverges as $1/\Delta$, which implies with $\chi_{nl} \sim (\Gamma - \Gamma_c)^{-\gamma}$ that $\gamma = 1/2$. Studying Gaussian fluctuations around the saddle-point solution valid for infinite range one finds²⁷⁸ for the correlation length exponent above the upper critical dimension (i.e. $d \geq 8$) that $\nu = 1/4$ and therefore $z = 2$. Moreover $\eta = 0$ in mean field theory. The complete collection of critical exponents obtained so far in comparison with the classical model ($T > 0$, where we assume to cross the phase boundary under a non-vanishing angle) are as follows:

	β	γ	ν	z
quantum ($T = 0$)	1/2	1/2	1/4	2
classical ($T = 0$)	1	1	1/2	–

(59)

Note that as a consequence of the absence of Griffiths-singularities in mean-field models the dynamical exponent z is finite in contrast to the IRFP scenario that is supposedly valid for the finite-dimensional models. In a longitudinal field one obtains, in analogy to the classical case, an AT manifold in the T, Γ, h phase diagram below which replica symmetry is broken and the system is in the SG phase.

The dynamics of the model (58) in the paramagnetic phase has been studied in [280], where the dynamical single-site self-consistency equations have been iteratively solved using a quantum Monte Carlo scheme developed in [281]. They mapped the spin-glass transition line in the Γ - T plane using the stability criterion $1 = J\chi_{\text{loc}}$, where $\chi_{\text{loc}} = \int_0^\beta d\tau C(\tau)$ is the local susceptibility. They found a second-order transition line ending at a quantum critical point at $T = 0$ in agreement with the argument presented above. Going down in temperature to $T \sim 0.01J$ and extrapolating the results to $T = 0$ they determined a precise value for the critical field $\Gamma_c = 0.76 \pm 0.01$, which lies between previous estimates.^{273,276} The asymp-

otic form of $C(\tau) \sim \tau^{-2}$ found in [276] was also confirmed. A comparison of the results for the low-frequency susceptibility with the experimental curves obtained for $\text{LiHo}_{0.167}\text{Y}_{0.833}\text{F}_4$ in [243] yields a good agreement.

A different class of mean-field spin-glass models has been studied in [271] — simplified in so far as spherical spins rather than Ising spins were considered and more general in so far as p -spin interactions were considered. The quantum fluctuations are introduced via a kinetic energy rather than the transverse field. The corresponding quantum spherical p -spin-glass Hamiltonian is defined by

$$H = \frac{1}{2M} \sum_{i=1}^N \hat{p}_i^2 - \sum_{i_1, \dots, i_p} J_{i_1, \dots, i_p} s_{i_1} \cdots s_{i_p} \quad (60)$$

where s_i are “soft-spins” fulfilling the spherical constraint $\sum_{i=1}^N s_i(t)^2 = N$ for all times t . Quantum mechanics is introduced into the classical p -spin glass via the canonical momenta \hat{p}_i that fulfill the commutation relation $[\hat{p}_i, s_j] = -i\hbar\delta_{ij}$. The multi-spin coupling constants are taken from a Gaussian distribution with zero mean and variance $\tilde{J}p!/(2N^{p-1})$ with \tilde{J} being a constant of $\mathcal{O}(1)$.

Before we discuss this model we want to clarify the connection to the SK model in a transverse field discussed above. The replacement of Ising spins $S_i = \pm 1$ by continuous spins $s_i \in [-\infty, +\infty]$ is often performed in the theory of critical phenomena — the discrete symmetry is then enforced by a quartic term $\sum_i s_i^4$ in the Hamiltonian (this is just the usual Φ^4 Ginzburg-Landau theory for critical phenomena with a discrete symmetry), which also restricts automatically the spin length. Analytically the quartic term causes extra complications in all computations, saddle point evaluations, RG calculations, dynamical formalism etc. — for which reason one often skips it and replaces it by a spherical constraint (either strictly or via a Lagrangian parameter having the same effect as a chemical potential). Unfortunately the classical spherical mean-field spin-glass model with the usual 2-spin interactions does not have a non-trivial spin glass phase. Therefore, generalizations to p -spin interactions are sometimes considered.¹³⁸ At this point a clear connection to the original magnetic system of interest is already lost. Nevertheless, one might expect that one can learn something about possible scenarios.

Finally spherical spins cannot be quantized in the same way as Ising spins via the application of a transverse field. Therefore they are usually quantized via the introduction of a kinetic energy term as in (60). In addi-

tion, various analytical techniques available for interacting soft spins with kinetic energy, such as the Schwinger-Keldysh formalism,²⁸² are not available for spin operators. The microscopic details of the quantum dynamics described by either a transverse field or a kinetic energy term might be very different, on large timescales, however, one expects a similar behavior for the following reason. To see this, let us consider a model that consists of two terms; an arbitrary classical Hamiltonian, H_{cl} , that is diagonal in the z -representation of the spins, and the transverse-field term. Performing a Trotter decomposition of the partition function of this model, one obtains

$$\begin{aligned} \text{Tr} e^{-\beta(\Gamma\sigma^x + H_{\text{cl}}(\sigma^z))} &= \lim_{\Delta\tau \rightarrow 0} \prod_{\tau=1}^{L_\tau} \langle S_\tau | e^{-\Delta\tau[\Gamma\sigma^x + H_{\text{cl}}(\sigma^z)]} | S_{\tau+1} \rangle \\ &\propto \lim_{\Delta\tau \rightarrow 0} \sum_{S_1, \dots, S_{L_\tau}} \exp \left(-\Delta\tau \left[\sum_{\tau=1}^{L_\tau} K(S_\tau - S_{\tau+1})^2 + H_{\text{cl}}(S_\tau) \right] \right) \end{aligned} \quad (61)$$

where L_τ is the number of Trotter slices in the imaginary time direction, $\Delta\tau = \beta/L_\tau$ and K given by $e^{-2K} = \tanh(\Delta\Gamma)$. For $\Delta\tau \ll 1$ it is $K = |\ln(\Delta\tau\Gamma)|/2$. In the last step we neglected a constant factor $\cosh(\Delta\tau\Gamma)^{L_\tau}$. If we choose $\Delta\tau$ as a small time cut-off (representing the typical spin flip time) we can approximate the last Trotter sum as the imaginary time path integral

$$Z \approx \int \mathcal{D}S(\tau) \exp \left(\int_0^\beta d\tau \left[\frac{M}{2} \left(\frac{\partial S}{\partial \tau} \right)^2 + H_{\text{cl}}(S(\tau)) \right] \right) \quad (62)$$

where $M = 2K\Delta\tau = \Delta\tau |\ln(\Gamma\Delta\tau)|$. The first term in the integral of the action is identical to what one would obtain for the kinetic energy if one writes down the imaginary time path integral for the partition sum of the Hamiltonian (60). In this way, the transverse-field term and the kinetic-energy term are related.

In [271] the equilibrium properties of the model were obtained using a replicated imaginary-time path integral formalism²⁷⁹ and analyzing the dynamical self-consistency equations for the spin auto-correlation function $C(\tau)$ arising in the limit $N \rightarrow \infty$ from a saddle point integration. The result for the phase diagram, EA order-parameter and linear susceptibility in the case $p = 3$ are depicted in Fig. 19, where the parameter $\Gamma = \hbar^2/(JM)$ has been used — resembling the transverse field strength (since for $\Gamma \rightarrow 0$ one recovers the classical case). Above a temperature T^* one has a continuous transition at a critical point $\Gamma = \Gamma_c(T)$ from a paramagnetic phase with

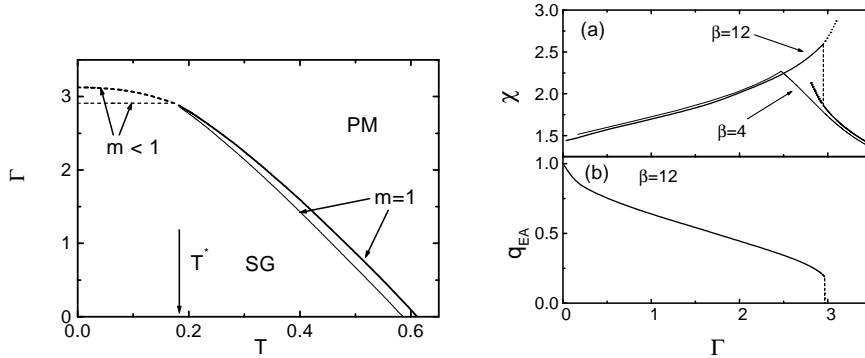


Fig. 19. **Left:** Static (thin lines) and dynamic (thick lines) phase diagrams of the p -spin model for $p = 3$. Solid and dashed lines represent second and first order transitions, respectively. **Right:** Magnetic susceptibility (a) and Edwards-Anderson order parameter (b) of the $p=3$ model. (From [271]).

vanishing EA order parameter to a spin glass phase with $q_{EA} \neq 0$ and one-step replica-symmetry-breaking (1RSB). Although the EA order-parameter jumps discontinuously the transition is second order: there is no latent heat (as in the classical case $\Gamma = 0$) and the susceptibility has only a cusp. This is due to the fact that the parameter m characterizing the Parisi order parameter function $q(x)$ (which is a step function with a single step at $x = m$) is unity at the transition. However, for temperatures below T^* this parameter jumps at the transition, too, and the transition becomes discontinuous; for $T < T^*$ the transition is of the first order with latent heat and a discontinuous susceptibility (see Fig. 19).

8.3. Mean-Field Theory — Dissipative Effects

An important question that arises for interacting quantum spins at low temperatures are the effects of a dissipative environment.^{283,284} This is usually described in terms of its collective excitations, lattice vibrations, spin or charge fluctuations, etc., which may be thought of as an ensemble of independent quantum harmonic oscillators.^{285,286,287,288,289} A concrete example of a single quantum degree of freedom, a spin-1/2 or a so-called two-level-system (TLS), coupled to a bath of bosons is the well-known spin-boson-model.^{283,284}

$$H = H_S + H_B + H_{SB} \quad (63)$$

where H_S , H_B and H_{SB} denote the Hamiltonian of the system, the bath and their coupling, respectively. These are given by

$$\begin{aligned} H_S &= -\Gamma\sigma^x \\ H_B &= \frac{1}{2} \sum_n (p_n^2/m_n + m_n\omega_n^2 x_n^2) \\ H_{SB} &= - \sum_n c_n x_n \sigma^z \end{aligned} \quad (64)$$

where Γ is the transverse field (or tunneling matrix element in the context of TLSs), n the index enumerating an infinite number of harmonic oscillators with coordinates and momenta, x_n and p_n , and mass and frequency, m_n and ω_n , respectively. The constant c_n is the coupling between oscillator n and the spin. The spectral density of the environment, $I(\omega) = \pi \sum_n (|c_n|^2 / (m_n \omega_n)) \delta(\omega - \omega_n)$, is commonly assumed to take the standard form²⁸⁴

$$I(\omega) = 2\alpha\hbar(\omega/\omega_{\text{ph}})^{s-1}\omega e^{-\omega/\omega_c}, \quad (65)$$

where α is a dimensionless coupling constant, ω_c a high frequency cut-off (which can be set to $\omega_c = \infty$ if $0 < s < 2$), and ω_{ph} a phonon frequency necessary in the non-ohmic ($s \neq 1$) case to keep α dimensionless.

With standard techniques^{290,283} one can integrate out the oscillator degrees of freedom to express the partition function of the system solely in terms of the spin variables

$$Z = \text{Tr} e^{-\beta H} = \int \mathcal{D}\sigma(\tau) \mathcal{T} \exp(-S/\hbar), \quad (66)$$

where $\int \mathcal{D}\sigma(\tau)$ denotes a path integral over all spin configurations (in time), \mathcal{T} is the imaginary time ordering operator and the action is

$$S = - \int_0^{\beta\hbar} d\tau \Gamma \sigma^x(\tau) - \frac{1}{2} \int_0^{\beta\hbar} d\tau \int_0^{\beta\hbar} d\tau' K(\tau - \tau') \sigma^z(\tau) \sigma^z(\tau'). \quad (67)$$

The kernel $K(\tau)$ is related to the spectral density $I(\omega)$ and is for the ohmic case ($s = 1$) essentially an inverse square $K(\tau - \tau') \propto \alpha / (\tau - \tau')^2$. The effect of the dissipative environment is therefore a long range interaction of the quantum spin in imaginary time. In analogy to the Ising model with inverse square interactions²⁹¹ depending on the strength of the coupling constant α , the system is ferromagnetically ordered or paramagnetic in the imaginary time direction; for large α the spin is frozen and for small α the spin will tunnel.

Indeed, for the ohmic case, at zero temperature, there is a phase transition at $\alpha = 1$.^{286,287} For $\alpha < 1$ there is tunneling and two distinct regimes

develop. If $\alpha < 1/2$, the system relaxes with damped coherent oscillations; in the intermediate region $1/2 < \alpha < 1$ the system relaxes incoherently. For $\alpha > 1$ quantum tunneling is suppressed and $\langle \sigma^z \rangle \neq 0$, signaling that the system remains localized in the state in which it was prepared. These results also hold for sub-Ohmic baths while weakly damped oscillations persist for super-Ohmic baths.²⁸³ At finite temperatures (but low enough such that thermal activation can be neglected) there is no localization but the probability of finding the system in the state it was prepared decreases slowly with time for $\alpha > \alpha_c$.

These conclusions hold for a single spin interacting with a bath. The question then arises as to which are the effects of the interplay between the spin-spin interactions and the spin-noise coupling in the physics of the interacting system. In [282] the effect of a dissipative bath on a mean-field spin glass model with p -spin interactions has been investigated. They studied the dissipative spin-boson system (64) for N interacting spins $H = H_S + H_B + H_{SB}$, where the bath Hamiltonian is the same, the coupling Hamiltonian gets an additional sum over the spin index i and H_S is now the p -spin Hamiltonian with transverse field

$$H_S = -\Gamma \sum_{i=1}^N \sigma_i^x - \sum_{i_1, \dots, i_p} J_{i_1, \dots, i_p} \sigma_{i_1}^z \cdots \sigma_{i_p}^z. \quad (68)$$

The second term, namely, the multi-spin interaction term is the same as the one in (60). For the reason explained in the last section it is analytically easier to study spherical spins instead of quantum spin-1/2 degrees of freedom and the quantization of the spherical spins is done via the introduction of a kinetic energy term. The partition function then reads

$$Z = \int \mathcal{D}\sigma(\tau) \exp(-S/\hbar), \quad (69)$$

with the action

$$S = \int_0^{\hbar\beta} d\tau \left[\frac{M}{2} \sum_i \left(\frac{\partial s_i(\tau)}{\partial \tau} \right)^2 - \sum_{i_1 < \dots < i_p} J_{i_1, \dots, i_p} s_{i_1}(\tau) \cdots s_{i_p}(\tau) \right. \\ \left. + z \sum_i [s_i^2(\tau) - 1] \right] - \int_0^{\hbar\beta} d\tau \int_0^{\hbar\beta} d\tau' K(\tau - \tau') s_i(\tau) s_i(\tau'), \quad (70)$$

where the first term is the kinetic-energy term already motivated in (61-62) replacing the transverse-field term, the second is the p -spin interaction term, the third a term with the Lagrangian multiplier z enforcing the spherical

constraint and the last term is the long range interaction imaginary time (67) that is generated by the integration over the bath variables.

Starting from (70) the saddle point equations for the self-consistent single-spin dynamics were derived²⁸² and the phase diagram computed. Analogous to the non-dissipative case discussed in the previous subsection a critical line with a second-order section (close to the classical critical point $(T_d, \Gamma = 0)$) and a first-order section (close to the quantum critical point $(T = 0, \Gamma_d)$) was obtained in the presence of a dissipative environment. The second order critical line is determined by the condition $m = 1$, the first order critical line is defined as the locus of the points where a marginally stable solution first appears with decreasing Γ for T fixed. For each Γ and α this defines a *dynamic* transition temperature $T_d(\Gamma, \alpha)$. The qualitative features of the phase diagram, similar to those found for the isolated system, see the discussion in the previous section. Notice that the line $T_d(\Gamma, \alpha)$ lies always *above* $T_s(\Gamma, \alpha)$, the static critical line that we shall discuss below.

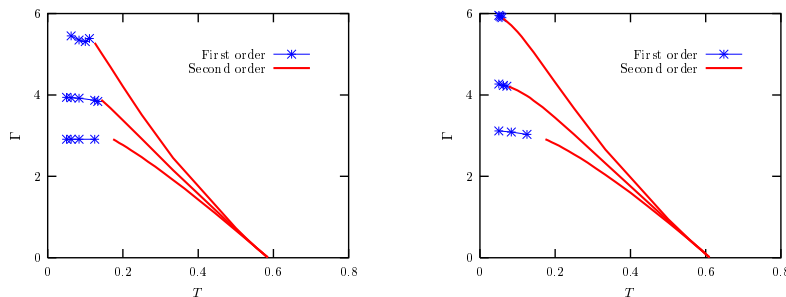


Fig. 20. Static (left) and dynamic (right) phase diagrams for the $p = 3$ spin model coupled to an Ohmic bath ($s = 1$). The couplings to the bath are $\alpha = 0, 0.25$, and 0.5 from bottom to top. The solid line and line-points represent second and first order transitions, respectively. (From [282]).

On the right side of Fig. 20 the dynamic phase diagrams obtained for $p = 3$ and three values of the coupling to an Ohmic bath, $\alpha = 0, 0.25, 0.5$ is shown. The full line and the line-points represent second and first order transition, respectively.

The first observation that can be made is that in the limit $\Gamma \rightarrow 0$ the transition temperature is independent of the strength of the coupling to the bath. This is a consequence of the fact that in the limit $\Gamma \rightarrow 0$ the partition

function is essentially determined by the zero-frequency components of the pseudo-spin which are decoupled from the bath. This result is however non-trivial from a dynamical point of view, since it implies that the dynamic transition of a classical system coupled to a colored classical bath is not modified by the latter.

The second observation is that the size of the region in the phase space where the system is in the ordered state increases with α . Coupling to the dissipative environment thus stabilizes this state. This follows from simple physical considerations. The interaction term in the action favors spin-glass order. Coupling to the bath favors localization and its effect is to reduce the effective tunneling frequency. Therefore, in the presence of the bath, the value of the bare tunneling frequency needed to destroy the ordered state must increase with α . Even if the localized state and the glassy state may seem superficially similar, they are indeed very different. In the former, the correlation function $C(t + t_w, t_w)$ approaches a plateau as a function of t and never decays toward zero while in the latter the relaxation first approaches a plateau but it eventually leaves it to reach zero for $t \gg t_w$. The fact that the coupling to the environment favors the ordered state also reflects itself in the value taken by the order parameters $C(\tau)$ and q_{EA} . As α increases, $q_d(\tau)$ reaches a higher plateau level at long imaginary times.

8.4. Mean-Field Theory — Dynamics

The out-of-equilibrium dynamics in real time of the quantum spherical p -spin glass model coupled to a dissipative environment, which was discussed in the last subsection, was actually studied earlier²⁹² than the equilibrium properties. The response and correlation function are defined in analogy to the classical case; $C(t + t_w, t_w) = N^{-1} \sum_i (s_i(t + t_w)s_i(t_w) + s_i(t_w)s_i(t + t_w))$ (note that the time evolution is now governed by the quantum dynamics and C has to be symmetrized in the operators $s_i(t + t_w)$ and $s_i(t_w)$) and $R(t + t_w, t_w) = N^{-1} \sum_i \delta s_i(t + t_w) / \delta h_i(t_w)$.

In equilibrium the quantum FDT relates $R(t)$ and $C(t)$:

$$R(t) = \frac{2i}{\hbar} \theta(t) \int \frac{d\omega}{2\pi} e^{-i\omega t} \tanh(\beta\hbar\omega/2) C(\omega) \quad (71)$$

Away from the critical line, C and R decay to zero very fast with oscillations. Approaching the critical line $T_d(\alpha)$, the decay slows down and if $T_d > 0$ a plateau develops in C . At the critical line the length of the plateau tends to infinity.

In the glassy phase (below the transition) the system does not reach equilibrium. For small time differences the dynamics is stationary and time translational invariance as well as the QFDT holds: $\lim_{t_w \rightarrow \infty} C(t+t_w, t_w) = q + C_{\text{eq}}(t)$. For large times the dynamics is non-stationary, time translational invariance nor the QFDT does not hold, and the correlations decay from q to 0. The decay of C becomes monotonic in the aging regime, which implies $C_{\text{aging}}(t+t_w, t_w) = c(h(t_w)/h(t+t_w))$ (see subsection 5.2). One can generalize the QFDT in the same spirit as the classical FDT was generalized (see subsection 5.4):

$$R(t+t_w, t_w) = \frac{2i}{\hbar} \theta(t) \int \frac{d\omega}{2\pi} e^{-i\omega t} \tanh(X(t+t_w, t_w)\beta\hbar\omega/2) C(t+t_w, \omega) \quad (72)$$

with $C(t, \omega) = 2\text{Re} \int_0^t ds \exp[i\omega(t-s)] C(t, s)$. Again, as in the classical case (see subsection 5.4), $T_{\text{eff}} \equiv T/X(t+t_w, t_w)$ acts as an effective temperature in the system. For a model with two time-sectors it is proposed

$$X(t+t_w, t_w) = \begin{cases} X_{\text{st}} = 1 & \text{if } t \leq \mathcal{T}(t_w) \\ X_{\text{age}}(\hbar, T) & \text{if } t > \mathcal{T}(t_w) \end{cases} .$$

with X_{age} a non-trivial function of \hbar and T and $\mathcal{T}(t_w)$ is a certain time-scale that separates the stationary and aging time-regimes. When t and t_w are widely separated, the integration over ω in (72) is dominated by $\omega \sim 0$. Therefore, the factor $\tanh(X_{\text{age}}(t+t_w, t_w)\beta\hbar\omega/2)$ can be substituted by $X_{\text{age}}\beta\hbar\omega/2$ (even at $T = 0$ if $X_{\text{age}}(\hbar, T) = x(\hbar)T$ when $T \sim 0$). Hence,

$$R_{\text{age}}(t+t_w, t_w) \sim \theta(t) X_{\text{age}} \beta \partial_{t_w} C_{\text{age}}(t+t_w, t_w) \quad (73)$$

and one recovers, in the aging regime, the *classical* modified FDT.^{138,293}

The self-consistency equations for $C(t+t_w, t_w)$ and $R(t+t_w, t_w)$ were evaluated numerically in [292]. An example of the solution is shown in Fig. 21 for $p = 3$. In all figures the following parameters have been chosen: zero temperature $T = 0$, the width of the coupling distribution $J = 1$, the frequency cut-off for the oscillator bath set to $\omega_c = 5$, the mass in the kinetic energy term $M = 1$, and the strength of the quantum fluctuations $\tilde{\hbar} = \alpha\hbar$ (where α is the spin-bath coupling strength) is $\tilde{\hbar} = 0.1$.

These plots demonstrate the existence of the stationary and aging regimes. For $t < \mathcal{T}(t_w)$ (e.g. $\mathcal{T}(40) \sim 5$) time translational invariance and fluctuation dissipation theorem are established while beyond $\mathcal{T}(t_w)$ they break down. For $\tilde{\hbar} = 0.1$ the plateau in C is at $q \sim 0.97$. C oscillates around q but is monotonous when it goes below it. In the inset the dependence of q_{EA} on $\tilde{\hbar}$ for $T = 0$ is presented. Quantum fluctuations generate

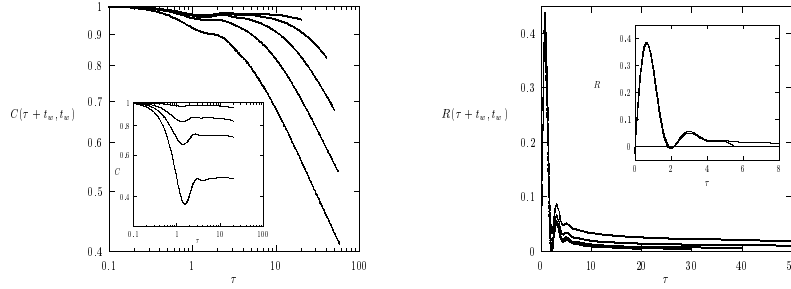


Fig. 21. **Left:** The correlation function $C(\tau + t_w, t_w)$ vs τ for the $p = 3$ quantum spherical p -spin SG model. The waiting times are, from bottom to top, $t_w = 2.5, 5, 10, 20, 40$. $q_{EA} \sim 0.97$. In the inset, the same curves for $t_w = 40$ and, from top to bottom, $\tilde{h} = 0.1, 0.5, 1, 2$. **Right:** The response function for the same model as in the left part. The waiting-times increase from top to bottom. In the inset, check of FDT in the stationary regime. The full line is $R(t + t_w, t_w)$ for $t + t_w = 40$ fixed and $t_w \in [0, 40]$. The dots are obtained from Eq.(72) with $X_{st} = 1$, using the numerical data for $C_{stat}(t) = C(t + t_w, t_w) - q$ ($q_{EA} \sim 0.97$, see left part). In both cases the response is plotted against t . (From [292]).

a $q_{EA} < 1$ such that the larger \tilde{h} the smaller q_{EA} . The addition of thermal fluctuations has a similar effect, the larger T , the smaller q_{EA} . In order to check the FDT in the stationary regime, in the inset of the right part of Fig. 21 a comparison is shown of $R(t + t_w, t_w)$ from the numerical algorithm for $t + t_w = 40$ fixed and $t_w \in [0, 40]$ (full line) with $R(t + t_w, t_w)$ from Eq.(72) with $X = 1$ using $C_{stat}(t) = C(t + t_w, t_w) - q$, $q \sim 0.97$ obtained from the algorithm (dots). The accord is very good if $t \leq \mathcal{T}(t_w) \sim 5$. Finally, when one plots parametrically the integrated response χ vs. C one finds that for $C < q \sim 0.97$ the χ vs C curve approaches a straight line of *finite* slope $1/T_{eff} = X_{age}/T \sim 0.60$.

8.5. Heisenberg Quantum Spin Glasses

The spin-1/2 Heisenberg quantum spin glass is defined by the Hamiltonian (48) where the random exchange interactions J_{ij} can be ferromagnetic and anti-ferromagnetic. The system cannot be studied efficiently with quantum Monte-Carlo methods, due to the sign problem arising from the frustration. Therefore, not much is known about these models in finite dimensions, and also the mean field theory becomes tractable only in certain limits and approximations.

8.5.1. Finite Dimensions

In [294] and later in [295] small clusters of the two-dimensional Heisenberg quantum spin glass were studied using exact diagonalization. The average total spin in the ground state turned out to scale as $S \propto \sqrt{N}$, where N is the number of sites. The spin glass order parameter in the ground state extrapolates to a small but non-vanishing value in the thermodynamic limit and the spin stiffness does not scale to zero either in the thermodynamic limit. Ma-Dasgupta-Hu renormalization group studies^{251,296} were performed for randomly frustrated spin-ladders²⁹⁷ and in $d = 2$ and 3 ²⁹⁸ for various lattices and spin-values. The general idea of this RG procedure was already described in subsection 8.1; large energies (in the form of exchange interactions) are successively decimated, ferromagnetic bonds lead to large spin formation and anti-ferromagnetic bonds to a spin reduction or even elimination in case of equal effective spins connected by the bond to be decimated. In two and three dimensions, it was also observed that the final magnetic moment to be eliminated increased with system size as \sqrt{N} , which corresponds to the aforementioned observation for the ground state spin in small clusters. In addition the Ma-Dasgupta-Hu RG calculations in [298] showed that the probability distribution of the low energy excitations scales as $P(\Delta) \sim \Delta^\omega$ with $\omega = 0$ for $2d$ and $3d$ and that the dynamical critical exponent is $z = 2$ in $d = 2$ and $z = 3/2$ in $d = 3$.

8.5.2. Mean-Field Model

The first analytical treatment of the mean-field model of the Heisenberg quantum spin glass was performed in [279] applying the replica theory. Although the solution was confined to the paramagnetic state, the arguments for the existence of a low-temperature spin-glass phase were given and the critical temperature was estimated.

Later a Landau theory for quantum rotors on a regular d -dimensional lattice was studied in [278], which is defined by the Hamiltonian

$$H = \frac{g}{2} \sum_i \hat{\mathbf{L}}_i^2 - \sum_{\langle ij \rangle} J_{ij} \hat{\mathbf{n}}_i \hat{\mathbf{n}}_j, \quad (74)$$

where $\hat{\mathbf{n}}_i$ are M -component vectors of unit length ($\hat{\mathbf{n}}_i^2 = 1$) and represent the orientation of the rotors on the surface of a sphere in M -dimensional rotor space. The operators $\hat{\mathbf{L}}_{i\mu\nu}$ ($\mu < \nu$, $\mu, \nu = 1, \dots, M$) are the $M(M-1)/2$ components of the angular momentum $\hat{\mathbf{L}}_i$ of the rotor: the first term in H is the kinetic energy of the rotor with $1/g$ the moment of inertia.

The different components of $\hat{\mathbf{n}}_i$ constitute a complete set of commuting observables and the state of the system can be described by a wave function $\Psi(n_i)$. The action of $\hat{\mathbf{L}}_i$ on Ψ is given by the usual differential form of the angular momentum $\hat{\mathbf{L}}_{i\mu\nu} = -i(n_{i\mu}\partial/\partial_{i\nu} - n_{i\nu}\partial/\partial_{i\mu})$. The difference between rotors and Heisenberg-Dirac quantum spins is that the components of the latter at the same site do not commute, whereas the components of the $\hat{\mathbf{n}}_i$ do.

In [278] a Landau theory for this model is derived and it is shown that for a suitable distribution of exchange constants J_{ij} this model displays spin-glass and quantum paramagnetic phases and a zero-temperature quantum phase transition between them. The mean-field phase diagram near the $T = 0$ critical point is mapped out as a function of T , the strength of the quantum coupling g and applied fields. The spin glass phase has replica symmetry breaking. Moreover, the consequences of fluctuations in finite dimensions are considered and above $d = 8$ the transition turned out to be controlled by a Gaussian fixed point with mean-field exponents. Below $d = 8$ a runaway RG flow to strong coupling was found.

Recently the mean-field Heisenberg quantum spin glass model was generalized from the $SU(2)$ spin algebra to an $SU(N)$ symmetry and solved in the limit $N \rightarrow \infty$.²⁹⁹ Certain universal critical properties are shown to hold to all orders in $1/N$. A spin-glass transition was found for all values of the spin S and the phase diagram as a function of the spin S and temperature T was described. The quantum critical regime associated with the quantum transition at spin value $S = 0$ and the various regimes in the spin-glass phase at high spin are analyzed. The specific heat is shown to vanish linearly with temperature.

The out-of-equilibrium dynamics of the the same model in the same limit $N \rightarrow \infty$, but coupled to a thermal bath, was studied in [300]. It was found that the model displays a dynamical phase transition between a paramagnetic and a glassy phase. In the latter, the system remains out-of-equilibrium and displays an aging phenomenon, which we characterize using both analytical and numerical methods. In the aging regime, the quantum fluctuation-dissipation relation is violated and replaced over a very long time-range by its classical generalization, as in models involving simple spin algebras studied previously.

In the context of Heisenberg spin glasses also the work on metallic spin glasses should be mentioned, which were first considered in [301] and later more extensively in [302], [303] and [304]. The main ingredient of a metallic spin glass is an itinerant electron systems with random (and frustrated)

exchange interactions between the electron spins. Thus in contrast to the spin glass systems discussed so far the spins are not fixed to particular sites but can diffuse (quantum mechanically) from site to site. These systems are motivated by experiments on heavy-fermion compounds such as $Y_{1-x}U_xPd_3$,³⁰⁵ which appear to show a paramagnetic to spin-glass transition with increasing doping, x , in a metallic regime. To be concrete the Hamiltonian studied in [303] is

$$H = - \sum_{i<j,\alpha} t_{ij} c_{i\alpha} c_{j\alpha} - \sum_{i<j,\mu} J_{ij} S_{i\mu} S_{j\mu} + H_{\text{int}}, \quad (75)$$

where $c_{i\alpha}$ annihilates an electron on site i with spin $\alpha = \uparrow, \downarrow$, and the spin operator is given by $S_{i\mu} = \sum_{\alpha\beta} c_{i\alpha}^+ \sigma_{\alpha\beta}^\mu c_{i\beta} / 2$, with σ^μ the Pauli spin matrices. The sites i, j lie on a d -dimensional lattice, the hopping matrix elements t_{ij} are short-ranged and possibly random, and the J_{ij}^μ are Gaussian random exchange interactions, possibly with spin-anisotropies. The remainder H_{int} includes other possible short-range interactions between the electrons, and the resulting total Hamiltonian H has a metallic ground state.

Starting from this Hamiltonian, in [303], an effective field theory for the vicinity of a zero temperature quantum transition between a metallic spin glass (“spin density glass”) and a metallic quantum paramagnet was introduced. Following a mean-field analysis, a perturbative renormalization-group study was performed and it was found that critical properties are dominated by static disorder-induced fluctuations, and that dynamic quantum-mechanical effects are dangerously irrelevant. A Gaussian fixed point was found to be stable for a finite range of couplings for spatial dimensionality $d > 8$, but disorder effects always lead to runaway flows to strong coupling for $d \leq 8$. Moreover, scaling hypotheses for a *static* strong-coupling critical field theory were proposed. The non-linear susceptibility has an anomalously weak singularity at such a critical point.

In [304] the competition between the Kondo effect and RKKY interactions near the zero-temperature quantum critical point of an Ising-like metallic spin-glass was studied. In the ‘quantum-critical regime,’ non-analytic corrections to the Fermi liquid behavior were found for the specific heat and uniform static susceptibility, while the resistivity and NMR relaxation rate have a non-Fermi liquid dependence on temperature.

9. Summary and Remaining Problems

In this review we have tried to provide an overview on the recent developments in spin glasses. We concentrated on the topics to which substantial

efforts have been devoted in recent years and for which, in our view, the most significant progress has been achieved: 1) The numerical investigation of the equilibrium thermodynamics of finite-dimensional spin glass models with short range interactions using new and powerful methods, such as combinatorial optimization for ground state calculations (through which excited states can also be studied) and extended-ensemble Monte Carlo methods (e.g., the replica exchange method) for the location and characterization of the phase transition. The most challenging task remaining here is still the unification of the two paradigmatic pictures: the droplet picture and the mean-field scenario. Although being unsolved for several decades now, we see promising steps toward the unification of these two approaches. 2) The experimental and theoretical investigation of non-equilibrium dynamics and aging phenomena in spin glasses, especially the study of fluctuation-dissipation-theorem violations in the glassy phase and the concept of an effective (non-equilibrium) temperature. Still a lot of work has to be done, experimentally in particular, in order to put the fascinating theoretical ideas on a firm and consistent experimental ground. 3) The theoretical exploration of quantum effects in spin glasses, statically and dynamically, for mean-field models as well as finite dimensional models. Here the most demanding challenge appears to be handling the *real* time quantum dynamics at low temperatures for realistic (i.e. finite dimensional short-range interacting) models.

Unfortunately, we could not cover in this review many “glassy” topics related to and inspired by the spin-glass world. First and most actively pursued in recent years is the theory of the structural glass transition and the glass “phase”. A lot of progress has been made to make contact between spin glasses and structural glasses, the main difference being that the disorder is self-induced in the latter during the freezing process, whereas spin glasses live with frozen, time-independent disorder. Recently, it was discussed extensively that this might not be a major obstacle in relating the two systems. From a theoretical point of view, a more substantial difference between them with concrete experimental consequences is that spin glasses have a well-defined order parameter. A diverging correlation length and a divergent susceptibility defined in terms of this order parameter signify the transition. In the theory of structural glasses, apparently one cannot depend on these helpful vehicles.

Other related issues are vortex, gauge and Bragg glasses. All three appear in the context of disordered superconductors. The gauge glass model is essentially an XY spin-glass model with a random (quenched) vector poten-

tial, originally devoted for describing amorphous granular superconductors but later also taken as a paradigmatic model for amorphous high- T_c superconductors. It can be analyzed in the same way as XY spin glasses and also has the same order parameter. The major questions concern the existence of a finite-temperature phase transition with or without screening effects. The vortex-glass model is a model of interacting, elastic magnetic flux lines in a random potential, which freezes at low temperatures into a glassy phase (which however escapes a clean theoretical description, since an order parameter is hard to define). If the disorder is weak, topological defects can be neglected and an elastic description is possible, starting from the Abrikosov flux line lattice and taking into account its small elastic deformation via thermal fluctuations and disorder. For such weakly disordered elastic systems a Bragg glass phase is predicted in which the true long-range order of the Abrikosov flux line lattice is transformed into a quasi long-range order. This glassy phase manifests itself also via an extremely sluggish dynamics. Upon increasing the strength of the disorder or the density of the lines (via an increased magnetic field), topological defects will proliferate, the quasi long-range order of the Bragg glass phase vanishes and the system becomes a vortex glass.

Finally one should mention Bose, Fermi and Coulomb glass models, which occur in the context of the low-temperature physics of quantum-mechanical, disordered, electronic or bosonic systems. The origin of the interesting physics is the competition between the quenched random potential and the interactions between particles, usually long ranged as in the Coulomb case. The major issues concern the phase transition between conducting (metallic or superconducting) and insulating phases, in which the particles are localized. Again the name “glass” for the low-temperature phases is justified by the anomalously slow dynamics present here.

To conclude this tour through the glass zoo we hope to have demonstrated that a review on spin glasses should not only be useful for people working in the field of frustrated magnets, but also for those encountering strong disorder and strong interactions at low temperatures in other fields of condensed matter physics.

Acknowledgments

N.K.’s work was supported by the grant-in-aid (Program No.14540361) from Monka-sho, Japan. H.R. acknowledges financial support from the Deutsche Forschungsgemeinschaft (DFG) and from the European Commu-

nity's Human Potential Programme under contract HPRN-CT-2002-00307, DYGLAGEMEM, and thanks the KITP at UC Santa Barbara for its hospitality, where he composed large parts of this review. The authors are indebted to H. E. Castillo, C. Chamon, L. Cugliandolo, K. Hukushima, H. Kawamura, J. Kurchan, C. M. Newman, D. L. Stein, and A. P. Young for useful comments.

References

1. J. L. van Hemmen and I. Morgenstern, Lecture Notes in Physics 192: *Heidelberg Colloquium on Spin Glasses* (Springer, 1983).
2. J. L. van Hemmen and I. Morgenstern, Lecture Notes in Physics 275: *Heidelberg Colloquium on Spin Glasses* (Springer, 1986).
3. K. H. Fischer and J. A. Hertz, *Spin Glasses* (Cambridge, 1991).
4. J. A. Mydosh, *Spin Glasses: An Experimental Introduction*, Taylor and Francis (London · Washington, DC, 1993).
5. A. P. Young (editor), *Spin Glasses and Random Fields* (World Scientific, 1998).
6. P. E. Jönsson, H. Yoshino and P. Nordblad, Phys. Rev. Lett. **89** (2002) 097201.
7. K. Binder and A. P. Young, Rev. Mod. Phys. **58** (1986) 801.
8. M. Mézard, G. Parisi and M. A. Virasoro, *Spin Glass Theory and Beyond* (World Scientific, Singapore, 1987).
9. E. Marinari *et al.*, J. Stat. Phys. **98** (2000) 973.
10. C. M. Newman and D. L. Stein, J. Phys.: Condens. Matter **15** (2003) R1319.
11. G. Parisi, Phys. Rev. Lett. **43** (1979) 1754.
12. G. Parisi, J. Phys. A: Math. Gen. **13** (1980) 1101.
13. G. Parisi, J. Phys. A: Math. Gen. **13** (1980) 1887.
14. G. Parisi, Phys. Rev. Lett. **50** (1983) 1946.
15. D. Sherrington and S. Kirkpatrick, Phys. Rev. Lett. **35** (1975) 1792.
16. M. Mezard, G. Parisi, N. Sourlas, G. Toulouse and M. Virasoro, Phys. Rev. Lett. **52** (1984) 1156.
17. M. Mezard, G. Parisi, N. Sourlas, G. Toulouse and M. Virasoro, J. Phys. (Paris) **45** (1984) 843.
18. D. J. Thouless, P. W. Anderson and R. G. Palmer, Phil. Mag. **35** (1977) 593.
19. J. R. L. de Almeida and D. J. Thouless, J. Phys. A: Math. Gen. **11** (1978) 983.
20. F. Guerra and F. L. Toninelli, J. Math. Phys. **43** (2002) 3704; J. Math. Phys. **43** (2002) 6224; Commun. Math. Phys. **230** (2002) 71; cond-mat/0205123, cond-mat/0208579.
21. C. M. Newman and D. L. Stein, Phys. Rev. Lett. **76** (1996) 515.
22. M. A. Moore and A. J. Bray, J. Phys. C **17** (1984) L613.
23. A. J. Bray and M. A. Moore, in *Heidelberg Colloquium on Spin Glasses* eds. J. L. van Hemmen and I. Morgenstern, Springer (1986) p.121.

24. D. S. Fisher and D. A. Huse, Phys. Rev. Lett. **56** (1986) 1601.
25. D. S. Fisher and D. A. Huse, Phys. Rev. B **38** (1988) 373.
26. D. S. Fisher and D. A. Huse, Phys. Rev. B **38** (1988) 386.
27. B. Drossel, H. Bokil, M. A. Moore, and A. J. Bray, Eur. Phys. J. B **13** (2000) 369.
28. W. L. McMillan, Phys. Rev. B **29** (1984) 4026.
29. W. L. McMillan, Phys. Rev. B **30** (1984) 476.
30. A. K. Hartmann and A. P. Young, Phys. Rev. B **64** (2001) 180404.
31. N. Kawashima and H. Rieger, Europhys. Lett. **39** (1997) 85.
32. C. Amoruso, E. Marinari, O. C. Martin, A. Pagnani, Phys. Rev. Lett. **91** (2003) 087201.
33. T. Shirakura and F. Matsubara, J. Phys. Soc. Jpn. **65** (1996) 3138.
34. N. Kawashima and M. Suzuki, J. Phys. A **25** (1992) 4985.
35. N. Kawashima, H. Hatano and M. Suzuki, J. Phys. A: Math. Gen. **25** (1992) 4985.
36. S. Liang, Phys. Rev. Lett. **69** (1992) 2145.
37. Y.-C. Lin, N. Kawashima, F. Iglói and H. Rieger, Prog. Theor. Phys. Suppl. **138** (2000) 479.
38. H. Rieger et al, J. Phys. A **30** (1997) 3939.
39. M. Ney-Nifle, A. P. Young, J. Phys. A **30** (1997) 5311.
40. N. Kawashima and T. Aoki, Int. J. Mod. Phys. C **10** (1999) 1453.
41. N. Kawashima, J. Phys. Soc. Jpn. **69** (2000) 987.
42. A. K. Hartmann and M. A. Moore, Phys. Rev. Lett. **90** (2003) 127201.
43. A. A. Middleton, Phys. Rev. Lett. **83**, (1999) 1672.
44. M. Palassini and A. P. Young, Phys. Rev. B **60** (1999) R9919.
45. T. Shirakura and F. Matsubara, Phys. Rev. Lett. **79** (1997) 2887.
46. R. N. Bhatt and A. P. Young, Phys. Rev. Lett. **54** (1985) 924.
47. A. T. Ogielski, Phys. Rev. B **32** (1985) 7384.
48. E. Marinari, G. Parisi and F. Ritort, J. Phys. A: Math. Gen. **27** (1994) 2687.
49. N. Kawashima and A. P. Young, Phys. Rev. B **53** (1996) R484.
50. M. Palassini and X. Caracciolo, Phys. Rev. Lett. **82** (1999) 5128.
51. H. G. Ballesteros *et al*, Phys. Rev. B **62** (2000) 14237.
52. M. Tesi, E. J. van Resburg, E. Orlandini and S. G. Whillington, J. Stat. Phys. **82** (1996) 155.
53. K. Hukushima and K. Nemoto, J. Phys. Soc. Jpn. **65** (1996) 1604.
54. F. Cooper, B. Freedman and D. Preston, Nucl. Phys. B **210** (1989) 210.
55. E. Marinari *et al.*, Phys. Rev. Lett. **81** (1998) 1698.
56. K. Gunnarsson, P. Svedlindh, P. Nordblad, L. Lundgren, H. Aruga and A. Ito, Phys. Rev. B **43** (1991) 8199.
57. R. R. P. Singh and S. Chakravarty, Phys. Rev. B **36** (1987) 559.
58. R. N. Bhatt and A. P. Young, Phys. Rev. B **37** (1988) 5606.
59. D. Iñigues, G. Parisi and J. J. Ruiz-Lorenzo, J. Phys. A **29** (1996) 4337.
60. E. Marinari and G. Parisi and J. J. Ruiz-Lorenzo, Phys. Rev. B **58** (1998) 14852.
61. B. A. Berg and W. Janke, Phys. Rev. Lett. **80** (1998) 4771.

62. P. O. Mari and I. A. Campbell, *Phys. Rev. E* **59** (1999) 2653.
63. P. O. Mari and I. A. Campbell, *Phys. Rev. B* **65** (2002) 184409.
64. T. Nakamura, S. Endoh and T. Yamamoto, *J. Phys. A: Math. Gen.* **36** (2003) 10895.
65. N. de Courtenary, H. Bouchiat, H. Hurdequint and A. Fert, *J. Phys. (Paris)* **47** (1986) 71.
66. H. Bouchiat, *J. Physique* **47** (1986) 71.
67. L. P. Levy and A. T. Ogielsky, *Phys. Rev. Lett.* **57** (1986) 3288.
68. M. Simpson, *J. Phys. F* **9** (1979) 1377.
69. B. R. Coles and G. Williams, *J. Phys. F* **18** (1988) 1279.
70. E. Vincent and J. Hammann, *J. Phys. C:Solid State Phys.* **20** (1987) 2659.
71. H. Kawamura, *Phys. Rev. Lett.* **24** (1998) 5421.
72. K. Hukushima and H. Kawamura, *Phys. Rev. E* **61** (2000) 1008(R).
73. F. Matsubara, T. Shirakura and S. Endoh, *Phys. Rev. B* **64** (2001) 092412.
74. T. Nakamura and S. Endoh, *J. Phys. Soc. Jpn.* **71** (2002) 2113.
75. L. W. Lee and A. P. Young, *Phys. Rev. Lett.* **90** (2003) 227203.
76. H. Kawamura and M. S. Li, *Phys. Rev. Lett.* **29** (2001) 187204.
77. M. Palassini and A. P. Young, *Phys. Rev. B* **63** (2001) 140408(R).
78. F. Krzakala and O. C. Martin, *Europhys. Lett.* **53** (2001) 749.
79. A. K. Hartmann, *Europhys. Lett.* **45** (1999) 619.
80. B. A. Berg, U. E. Hansmann, and T. Celik, *Phys. Rev. B* **50** (1994) 16444.
81. A. K. Hartmann, *Europhys. Lett.* **40** (1997) 429.
82. A. K. Hartmann, *Europhys. Lett.* **44** (1998) 249.
83. A. K. Hartmann and H. Rieger, *Optimization Algorithms in Physics*, (Wiley, Berlin 2002).
84. A. K. Hartmann, *Euro. Phys. B* **13** (2000) 539.
85. A. Sandvik, *Europhys. Lett.* **45** (1999) 745.
86. M. Palassini and A. P. Young, *Phys. Rev. Lett.* **83** (1999) 5126.
87. M. Palassini and A. P. Young, *Phys. Rev. Lett.* **85** (2000) 3017.
88. A. A. Middleton, *Phys. Rev. B* **63** (2001) 060202(R).
89. M. A. Moore, *cond-mat/0203469*.
90. J. Lamacq, J.-P. Bouchaud, O. C. Martin and M. Mézard, *Europhys. Lett.* **58** (2002) 321.
91. M. Palassini, F. Liers, M. Jünger and A. P. Young, *Phys. Rev. B* **68** (2003) 064413.
92. M. Jünger, G. Reinelt and S. Thienel, in *DIMACS Series in Discrete Mathematics and Theoretical Computer Science*, Volume 20, W. Cook, L. Lovasz and P. Seymour eds. (American Mathematical Society, 1995)
93. E. Marinari and G. Parisi, *Phys. Rev. Lett.* **85** (2000) 3332.
94. E. Marinari and G. Parisi, *Phys. Rev. B* **62** (2000) 11677.
95. E. Marinari and G. Parisi, *Phys. Rev. Lett.* **86** (2001) 3887.
96. M. Palassini and A. P. Young, *Phys. Rev. Lett.* **85** (2000) 3333.
97. F. Krzakala, J. Houdayer, E. Marinari, O. C. Martin, and G. Parisi, *Phys. Rev. Lett.* **87** (2001) 197204.
98. J. Houdayer and O. C. Martin, *Europhys. Lett.* **49** (2000) 794.
99. F. Krzakala and O. C. Martin, *Phys. Rev. Lett.* **85** (2000) 03013.

100. J. Houdayer, F. Krzakala, and O. C. Martin, *Eur. Phys. J. B* **18** (2000) 467.
101. H. G. Katzgraber, M. Palassini, and A. P. Young, *Phys. Rev. B* **63** (2001) 184422.
102. D. Huse and D. Fisher, *J. Phys. A* **20** (1987) L997.
103. E. Marinari and G. Parisi and J. J. Ruiz-Lorenzo, in *Spin Glasses and Random Fields* (ed. A. P. Young, World Scientific, 1998).
104. R. R. P. Singh and S. Chakravarty, *Phys. Rev. Lett.* **57** (1986) 245.
105. G. Parisi, F. Ricci-Tersenghi, and J. J. Ruiz-Lorenzo, *J. Phys. A* **29** (1996) 7943.
106. J. D. Reger, R. N. Bhatt and A. P. Young, *Phys. Rev. Lett.* **64** (1990) 1859.
107. A. K. Hartmann, *Phys. Rev. E* **60** (1999) 05135.
108. H. G. Katzgraber and A. P. Young, *Phys. Rev. B* **67** (2003) 134410.
109. H. G. Katzgraber and A. P. Young, *Phys. Rev. B* **68** (2003) 224408.
110. J.-P. Bouchaud, L. F. Cugliandolo, J. Kurchan, and M. Mézard, in *Spin glasses and Random Fields*, ed. A. P. Young (World Scientific Singapore, 1998), pp. 161-224.
111. E. Vincent, J. Hamman, M. Ocio, J.-P. Bouchaud, and L. F. Cugliandolo, in *Complex Behaviour of Glassy Systems*, Lecture Notes in Physics **492**, ed. M. Rubi (Springer-Verlag, Berlin, 1997), pp. 184-219.
112. P. Nordblad and P. Svedlindh, in *Spin glasses and Random Fields*, ed. A. P. Young (world Scientific Singapore, 1998), pp. 1-28.
113. C. A. Angell, *Science* **267** (1995) 1924.
114. A. J. Bray, *Adv. Phys.* **43** (1994) 357.
115. D. S. Fisher and D. A. Huse, *Phys. Rev. B* **38** (1988) 373; **38** (1988) 386.
116. For a review see T. Natterman, in *Spin glasses and Random Fields*, ed. A. P. Young (world Scientific Singapore, 1998).
117. D. S. Fisher and D. A. Huse, **43** (1991) 10728.
118. H. Rieger, B. Steckemetz and M. Schreckenberg, *Europhys. Lett.* **27** (1994) 485.
119. H. Rieger, *Annual Review of Computers and Physics II*, edited by D. Stauffer (World Scientific, Singapore, 1995).
120. J. Kisker, L. Santen, M. Schreckenberg and H. Rieger, *Phys. Rev. B* **53** (1996) 6418.
121. E. Marinari, G. Parisi, F. Ritort, and J. J. Ruiz-Lorenzo, *Phys. Rev. Lett.* **76** (1996) 843.
122. T. Komori, H. Yoshino, and H. Takayama, *J. Phys. Soc. Jpn.* **68** (1999) 3387.
123. E. Marinari, G. Parisi, F. Ricci-Tersenghi, and J. J. Ruiz-Lorenzo, *J. Phys. A* **33** (2000) 2373.
124. K. Hukushima, H. Yoshino, and H. Takayama, *Prog. Theor. Phys. Suppl.* **138** (2000) 568.
125. H. Yoshino, K. Hukushima, H. Takayama, *Phys. Rev. B* **66**, (2002) 064431.
126. L. Berthier and J.-P. Bouchaud, *Phys. Rev. B* **66** (2002) 054404.
127. Y. G. Joh, R. Orbach, G. G. Wood, J. Hamman, E. Vincent, *Phys. Rev. Lett.* **82** (1999) 438.
128. G. J. Koper and H. J. Hilhorst, *J. Phys. (France)* **49** (1988) 429.

129. H. Rieger, *J. Phys. A* **26** (1993) L615.
130. V. Dupuis, E. Vincent, J.-P. Bouchaud, J. Hammann, A. Ito, and H.A. Katori, *Phys. Rev. B* **64** (2001) 174204.
131. P.E. Jönsson, H. Yoshino, P. Nordblad, H. Aruga Katori, and A. Ito, *Phys. Rev. Lett.* **88** (2002) 257204.
132. J.-P. Bouchaud, V. Dupuis, J. Hamman, and E. Vincent, *Phys. Rev. B* **65** (2001) 024439.
133. H. K. Janssen, B. Schaub, and B. Schmittmann, *Z. Phys. B.* **73** (1989) 539.
134. D. Huse, *Phys. Rev. B* **40** (1989) 304.
135. A. G. Schins, A. F. M. Arts, and H. W. de Wijn, *Phys. Rev. Lett.* **70** (1993) 2340.
136. J. Mattson, T. Jönsson, P. Nordblad, H. Aruga Katori, *Phys. Rev. Lett.* **74** (1995) 4305.
137. For a comprehensive review over the various analytical predictions of mean field theory for glassy dynamics see: L. F. Cugliandolo, eprint cond-mat/0210312.
138. L. F. Cugliandolo and J. Kurchan, *J. Phys. A* **27** (1994) 5749.
139. L. Berthier, J.-L. Barrat, and J. Kurchan, *Phys. Rev. E* **63** (2001) 016105.
140. E. Bertin and J. P. Bouchaud, *J. Phys. A* **35** (2002) 3039.
141. M. Picco, F. Ricci-Tersenghi, and F. Ritort, *Eur. Phys. J. B* **21** (2001) 211.
142. L. Berthier, *Eur. Phys. J. B* **17** (2000) 689.
143. D. S. Fisher, P. Le Doussal, and C. Monthus, *Phys. Rev. E* **64** (2001) 066107.
144. L. C. E. Struik, *Physical Aging in Amorphous Polymers and Other Materials* (Elsevier, Amsterdam, 1978).
145. J. Kurchan, *Phys. Rev. E* **66** (2002) 017101.
146. J. Hamman, M. Lederman, M. Ocio, R. Orbach, and E. Vincent, *Physica A* **185** (1992) 278.
147. T. Komori, H. Yoshino, and H. Takayama, *J. Phys. Soc. Jpn.* **69** Suppl. A (2000) 228.
148. P. E. Jönsson, H. Yoshino, and P. Nordblad, *Phys. Rev. Lett.* **89** (2002) 097201.
149. Ludovic Berthier et al., *Phys. Rev. Lett.* **90** (2003) 059701.
150. P. E. Jönsson, H. Yoshino and P. Nordblad, *Phys. Rev. Lett.* **90** (2003) 059702.
151. A. J. Bray and M. A. Moore, *Phys. Rev. Lett.* **58** (1987) 57.
152. H. Rieger, L. Santen, U. Blasum, M. Diehl, and M. Jünger, *J. Phys. A* **29** (1996) 3939.
153. A. Billoire and E. Marinari, *J. Phys. A* **33** (2000) L265.
154. H. Yoshino, K. Hukushima, and H. Takayama, cond-mat/0202110.
155. P. Réfrégier, E. Vincent, J. Hamman, and M. Ocio, *J. Phys. (France)* **48** (1987) 1533 .
156. L. Lundgren, P. Svedlindh, and O. Beckman, *J. Magn. Magn. Mat.* **31-34** (1983) 1349.
157. H. Rieger, *J. Physique I* **4** (1994) 883.
158. L. F. Cugliandolo and J. Kurchan, *Phys. Rev. B* **60** (1999) 922 .
159. J. P. Bouchaud, in *Soft and Fragile Matter*, ed. M. E. Cates and M. R. Evans

- (Institute of Physics, Bristol, 2000), e-print cond-mat/9910387.
160. H. Takayama, H. Yoshino, and T. Komori, cond-mat/9909228.
 161. M. Picco, F. Ricci-Tersenghi, and F. Ritort, Phys. Rev. B **63**, (2000) 174412.
 162. L. W. Bernardi, H. Yoshino, K. Hukushima, H. Takayama, A. Tobo, and A. Ito, Phys. Rev. Lett. **86** (2001) 720.
 163. K. Jonason, E. Vincent, J. Hamman, J.-P. Bouchaud, and P. Nordblad, Phys. Rev. Lett. **81** (1998) 3243.
 164. H. Yoshino, A. Lemaitre, and J. P. Bouchaud, Eur. Phys. J. B **20** (2001) 367.
 165. M. Sales and H. Yoshino, Phys. Rev. E **65** (2002) 066131.
 166. K. Jonason, J. Mattsson, and P. Nordblad, Phys. Rev. Lett. **77** (1996) 2562.
 167. K. Jonason and P. Nordblad, Europ. Phys. J. B **10** (1999) 23.
 168. E. Vincent, V. Dupuis, M. Alba, J. Hammann, and J.-P. Bouchaud, Europhys. Lett. **50** (2000) 674.
 169. J. Hamman, E. Vincent, V. Dupuis, M. Alba, M. Ocio, and J.-P. Bouchaud, J. Phys. Soc. Jap. **69** Suppl. A (2000) 296.
 170. E. Vincent, F. Alet, J. Hamman, M. Ocio, and J. P. Bouchaud, Europhys. Lett. **50** (2000) 674.
 171. P. Doussineau, T. de Lacerda-Aroso, A. Levelut, Europhys. Lett. **46** (1999) 401.
 172. J.-P. Bouchaud, P. Doussineau, T. de Lacerda-Aroso, and A. Levelut, Eur. Phys. J B **21** (2001) 335.
 173. A.V. Kityk, M.C. Rheinstädter, K. Knorr, and H. Rieger, Phys. Rev. B **65** (2002) 144415.
 174. E. Vincent, J. Hamman, M. Ocio, in *Recent Progress in Random Magnets* (World Scientific, Singapore, 1992).
 175. J.-P. Bouchaud and D. S. Dean, J. Phys. I (France) **5** (1995) 265.
 176. M. Sasaki and K. Nemoto, J. Phys. Soc. Jpn. **69** (2000) 2283; **69** (2000) 2642.
 177. L. Balents, J.-P. Bouchaud, and M. Mézard, J. Phys. I (France) **6** (1996) 1007.
 178. L. F. Cugliandolo, J. Kurchan, and L. Peliti Phys. Rev. E **55** (1997) 3898.
 179. L. F. Cugliandolo and J. Kurchan, Phys. Rev. Lett. **71** (1993) 173.
 180. S. Franz and H. Rieger, J. Stat. Phys. **79** (1995) 749.
 181. J. O. Andersson, J. Mattsson, and P. Svedlindh, Phys. Rev. B **46** (1992) 8297.
 182. E. Marinari, G. Parisi, F. Ricci-Tersenghi, and Juan J. Ruiz-Lorenzo, J. Phys. A **31** (1998) 2611 .
 183. L. Berthier, J.-L. Barrat and J. Kurchan, Eur. Phys. J. B **11** (1999) 635.
 184. A. Barrat and L. Berthier, Phys. Rev. Lett. **87** (2001) 087204.
 185. D. Herisson and M. Ocio, Phys. Rev. Lett. **88** (2002) 257202.
 186. L. F. Cugliandolo, D. R. Grempel, J. Kurchan, and E. Vincent, Europhys. Lett. **48** (1997) 699 .
 187. T. S. Grigera and N. E. Israeloff , Phys. Rev. Lett. **83** (1999) 5038 .
 188. L. Bellon and S. Ciliberto, preprint cond-mat/0201224.
 189. C. Chamon, M. P. Kennett, H. E. Castillo, and L. F. Cugliandolo, Phys.

- Rev. Lett. **89** (2002) 217201.
190. H. E. Castillo, C. Chamon, L. F. Cugliandolo, M. P. Kennett, Phys. Rev. Lett. **88** (2002) 237201 .
 191. F. Pazmandi, G. Zarand, G. T. Zimanyi, Phys. Rev. Lett. **83** (1999) 1034.
 192. G. Zaránd, F. Pázmándi, K. F. Pál, and G. T. Zimányi, Phys. Rev. Lett. **89** (2002) 150201.
 193. H. G. Katzgraber, F. Pazmandi, C. R. Pike, Kai Liu, R. T. Scalettar, K. L. Verosub, and G. T. Zimanyi, Phys. Rev. Lett. **89** (2002) 257202.
 194. H. G. Katzgraber, Gary Friedman, and G. T. Zimanyi, Physica B **343**, (2004) 10; cond-mat/0307178.
 195. C. R. Pike, A. P. Roberts, and K. Verosub, J. Appl. Phys. **85** (1999) 6660.
 196. F. Preisach, Z. Phys. **94** (1935) 277.
 197. D. Petit, L. Fruchter, and I. A. Campbell, Phys. Rev. Lett. **83**, (1999) 5130.
 198. D. Petit, L. Fruchter, and I. A. Campbell, Phys. Rev. Lett. **88**, (2002) 207206.
 199. H. Kawamura, Can. J. Phys. **79** (2001) 1447.
 200. J. Maucourt and D. R. Grempel, Phys. Rev. Lett. **80** (1998) 770.
 201. N. Akino and J. M. Kosterlitz, Phys. Rev. B **66** (2002) 054536.
 202. F. Matsubara, S. Endoh and T. Shirakura, J. Phys. Soc. Jpn. **69** (2000) 1927.
 203. S. Endoh, F. Matsubara and T. Shirakura, J. Phys. Soc. Jpn. **70** (2001) 1543.
 204. A. Sadic and K. Binder, J. Stat. Phys. **35** (1984) 517.
 205. D. Imagawa and H. Kawamura, Phys. Rev. B **67** (2003) 224412.
 206. T. R. Kirkpatrick and D. Thirumalai, Phys. Rev. B **36** (1987) 8552.
 207. T. R. Kirkpatrick and D. Thirumalai, Phys. Rev. B **37** (1988) 5342.
 208. U. Bengtzelius, W. Götze, and A. Sjölander, J. Phys. C **17** (1984) 5915.
 209. W. Götze, *Liquids, freezing and the glass transition*, ed. J. P. Hansen, D. Levesque, and J. Zinn-Justin (Amsterdam, North Holland, 1990), p.287.
 210. C. Brangian, W. Kob, and K. Binder, Europhys. Lett. **59**, 546 (2002); J. Phys. A in press; cond-mat/0211195.
 211. C. Brangian, W. Kob, and K. Binder, J. Phys. A: Math. Gen. **36** (2003) 10847.
 212. C. Brangian, W. Kob, and K. Binder, J. Phys. A : Math. Gen. **35** (2002) 191.
 213. C. Brangian, W. Kob, and K. Binder, Phil. Mag. B **82** (2002) 663.
 214. C. Brangian, W. Kob, and K. Binder, Europhys. Lett. **53** (2001) 756.
 215. H. Nishimori, Physica A **306** (2002) 68.
 216. H. Nishimori, Prog. Theor. Phys. **66** (1981) 1169.
 217. H. Nishimori, J. Phys. Soc. Jpn. **55** (1986) 3305.
 218. H. Nishimori, C. Falvo and Y. Ozeki, J. Phys. A: Math. Gen. **39** (2002) 8171.
 219. R. R. P. Singh and J. Adler, Phys. Rev. B **54** (1996) 364.
 220. Y. Ozeki, J. Phys.: Condens. Matter **9** (1997) 11171.
 221. A. B. Harris, J. Phys. C **7** (1974) 1671.
 222. G. Grinstein and A. Luther, Phys. Rev. B **13** (1976) 1329.

223. H.-O. Heuer, J. Phys. A: Math. Gen. **26** (1993) L333.
224. I. O. Mayer, J. Phys. A: Math. Gen. **22** (1989) 2815.
225. P. Le Doussal and A. B. Harris, Phys. Rev. Lett. **61** (1988) 625.
226. H. G. Ballesteros *et al*, Phys. Rev. B **58** (1998) 2740.
227. J. C. LeGuillow and J. Zinn-Justin, Phys. Rev. B **21** (1980) 3976.
228. K. Hukushima, J. Phys. Soc. Jpn. **69** (2000) 631.
229. M. Suzuki, Prog. Theor. Phys. **58** (1977) 1142.
230. M. Suzuki, Phys. Lett. A **58** (1978) 435.
231. Y. Ozeki and N. Ito, J. Phys. A: Math. Gen. **31** (1998) 5451.
232. H. Nishimori and K. Nemoto, Physica A **321** (2003) 108.
233. F. Y. Wu and Y. K. Wang, J. Math. Phys. **17** (1976) 439.
234. H. Nishimori, J. Phys. C **12** (1979) L905.
235. F. D. A. Araao Reis, S. L. A. de Queiroz and R. R. dos Santos, Phys. Rev. B **60** (1999) 6740.
236. M. Rubinstein, B. Shraiman and D. R. Nelson, Phys. Rev. B **27** (1983) 1800.
237. T. Nattermann, S. Scheidl, S. E. Korshunov and M. S. Li, J. Phys. (France) I **5** (1995) 565.
238. M.-C. Cha and H. A. Fertig, Phys. Rev. Lett. **74** (1995) 4867.
239. L.-H. Tang, Phys. Rev. B **54** (1996) 3350.
240. S. Scheidl, Phys. Rev. B **55** (1997) 457.
241. D. Carpentier and P. Le Doussal, Nuc. Phys. B **588** (2000) 565.
242. D. R. Nelson, Phys. Rev. B **27** (1983) 2902.
243. W. Wu, B. Ellmann, T. F. Rosenbaum, G. Aeppli, and D. H. Reich, Phys. Rev. Lett. **67** (1991) 2076; W. Wu, D. Bitko, T. F. Rosenbaum, and G. Aeppli, Phys. Rev. Lett. **71** (1993) 1919.
244. S. Sachdev: *Quantum Phase Transitions* (Cambridge University Press, 1999).
245. B. K. Chakrabarti, A. Dutta, and P. Sen, *Quantum Ising Phases and Transitions in Transverse Ising Models*, (Springer, Heidelberg, 1996).
246. H. Rieger and A. P. Young: *Quantum Spin Glasses*, Lecture Notes in Physics **492** “Complex Behaviour of Glassy Systems”, p. 254, ed. J.M. Rubi and C. Perez-Vicente (Springer Verlag, Berlin-Heidelberg-New York, 1997).
247. R. N. Bhatt in *Spin glasses and Random Fields*, ed. A. P. Young (World Scientific, Singapore, 1998).
248. D. S. Fisher, Physica A **263** (1999) 222.
249. B.M. McCoy and T.T. Wu, Phys. Rev. **176** (1968) 631; **188** (1969) 982; B.M. McCoy, Phys. Rev. **188** (1969) 1014.
250. D.S. Fisher, Phys. Rev. Lett. **69** (1992) 534; Phys. Rev. B **51** (1995) 6411.
251. S. K. Ma, C. Dasgupta, and C.-K. Hu, Phys. Rev. Lett. **43** (1979) 1434; C. Dasgupta and S. K. Ma, Phys. Rev. B **22** (1980) 1305.
252. F. Iglói and H. Rieger, Phys. Rev. Lett. **78** (1997) 2473.
253. F. Iglói and H. Rieger, Phys. Rev. B **57** (1998) 11404.
254. H. Rieger and F. Iglói, Europhys. Lett. **39** (1997) 135.
255. F. Iglói, D. Karevski and H. Rieger, Europ. Phys. J. B **1** (1998) 513; **5** (1998) 613.
256. F. Iglói and H. Rieger, Phys. Rev. E **58** (1998) 4238.

257. F. Iglói, R. Juhász and H. Rieger, *Phys. Rev. B* **59** (1999) 11308.
258. H. Rieger and F. Iglói, *Phys. Rev. Lett.* **83** (1999) 3741.
259. F. Iglói, R. Juhász und H. Rieger, *Phys. Rev. B* **61** (2000) 11552.
260. A. P. Young and H. Rieger, *Phys. Rev. B* **53** (1996) 8486.
261. M. J. Thill and D. A. Huse, *Physica A* **214**, (1995) 321.
262. H. Rieger and A. P. Young, *Phys. Rev. B* **54** (1996) 3328.
263. T. Senthil and S. Sachdev, *Phys. Rev. Lett.* **77**, (1996) 5292.
264. T. Ikegami, S. Miyashita and H. Rieger, *J. Phys. Soc. Jap.* **67** (1998) 2761.
265. C. Pich, A. P. Young, H. Rieger and N. Kawashima, *Phys. Rev. Lett.* **81** (1998) 5916.
266. H. Rieger and N. Kawashima, *Europ. Phys. J. B* **9** (1999) 233.
267. O. Motrunich, S.-C. Mau, D. A. Huse, D. S. Fisher, *Phys. Rev. B* **61** (2000) 1160.
268. H. Rieger and A. P. Young, *Phys. Rev. Lett.* **72** (1994) 4141.
269. M. Guo, R. N. Bhatt, and D. A. Huse, *Phys. Rev. Lett.* **72** (1994) 4137.
270. M. Guo, R. N. Bhatt, and D. A. Huse, *Phys. Rev. B* **54** (1996) 3336.
271. L. F. Cugliandolo, D. R. Grempel, and C. A. da Silva Santos, *Phys. Rev. Lett.* **85** (2000) 2589; *Phys. Rev. B* **64** (2001) 014403.
272. Y. V. Fedorov and E. F. Shender, *Zh. Eksp. Teor. Fiz.* **43** (1986) 526 [*JETP Lett.* **43** (1986) 681].
273. Y. Y. Goldschmidt and P. Y. Lai, *Phys. Rev. Lett.* **64** (1990) 2467.
274. K. D. Usadel and B. Schmidt, *Solid State Comm.* **64** (1987) 975.
275. T. Yamamoto and H. Ishii, *J. Phys. C* **20** (1987) 6053.
276. J. Miller and D. A. Huse, *Phys. Rev. Lett.* **70** (1993) 3147.
277. J. Ye, S. Sachdev, and N. Read, *Phys. Rev. Lett.* **70** (1993) 4011.
278. N. Read, S. Sachdev, and J. Ye, *Phys. Rev. B* **52** (1995) 384.
279. A. J. Bray and M. A. Moore, *J. Phys. C* **13** (1980) L655.
280. M. J. Rozenberg and D. R. Grempel, *Phys. Rev. Lett.* **81** (1998) 2550.
281. D. R. Grempel and M. J. Rozenberg, *Phys. Rev. Lett.* **80** (1998) 389.
282. L. F. Cugliandolo, D. R. Grempel, G. Lozano, H. Lozza, and C. A. da Silva Santos, *Phys. Rev. B* **66** (2002) 014444.
283. A. J. Leggett et al., *Rev. Mod. Phys.* **59** (1987) 1; **67** (1995) 725.
284. U. Weiss, in *Series Modern Condensed Matter Physics Vol. 2.* (World Scientific, Singapore, 1993).
285. A. O. Caldeira and A. J. Leggett, *Phys. Rev. Lett.* **46** (1981) 211; *Ann. Phys. N.Y.* **149** (1983) 374.
286. A. J. Bray and M. A. Moore, *Phys. Rev. Lett.* **49** (1982) 1545.
287. S. Chakravarty, *Phys. Rev. Lett.* **49** (1982) 681; S. Chakravarty and A. J. Leggett, *ibid.* **52** (1984) 5.
288. R. P. Feynman and F. L. Vernon, Jr., *Ann. Phys. N.Y.* **24** (1963) 118.
289. N. V. Prokof'ev and P. C. E. Stamp, *Phys. Rev. Lett.* **80** (1998) 5794.
290. H. Grabert, P. Schramm, and G-L. Ingold, *Phys. Rep.* **168** (1988) 115.
291. P. W. Anderson and G. Yuval, *Phys. Rev. Lett.* **32**, (1969) 89; *J. Phys. C* **4** (1971) 607; P. W. Anderson, G. Yuval, and D. R. Hammann, *Phys. Rev. B* **1** (1970) 4464.
292. L. F. Cugliandolo and G. Lozano, *Phys. Rev. Lett.* **80** (1998) 4979.

293. T. Giamarchi and P. Le Doussal, Phys. Rev. **B53** (1996) 15206.
294. Y. Nonomura and Y. Ozeki, J. Phys. Soc. Jpn., **64** (1995) 2710.
295. J. Oitmaa and O. P. Sushkov, Phys. Rev. Lett. **87** (2001) 167206.
296. D. S. Fisher, Phys. Rev. B **50** (1994) 3799.
297. R. Mélin, Y.-C. Lin, P. Lajkó, H. Rieger and F. Iglói, Phys. Rev. B **65** (2002) 104415.
298. Y.-C. Lin, R. Mélin, H. Rieger and F. Iglói, Phys. Rev. B **68** (2003) 024424.
299. A. Georges, O. Parcollet, and S. Sachdev, Phys. Rev. Lett. **85** (2000) 840; Phys. Rev. B **63** (2001) 134406.
300. G. Biroli and O. Parcollet, Phys. Rev. B **65** (2002) 094414.
301. J. A. Hertz, Phys. Rev. B **19** (1979) 4796.
302. R. Oppermann and M. Binderberger, Ann. Phys. (N.Y.) **3** (1994) 494.
303. S. Sachdev, N. Read, and R. Oppermann, Phys. Rev. B **52** (1995) 10286.
304. A. Sengupta and A. Georges, Phys. Rev. B **52** (1995) 10295.
305. W. D. Wu et al., Phys. Rev. Lett. **72** (1994) 3722.